Light Emitting Diodes

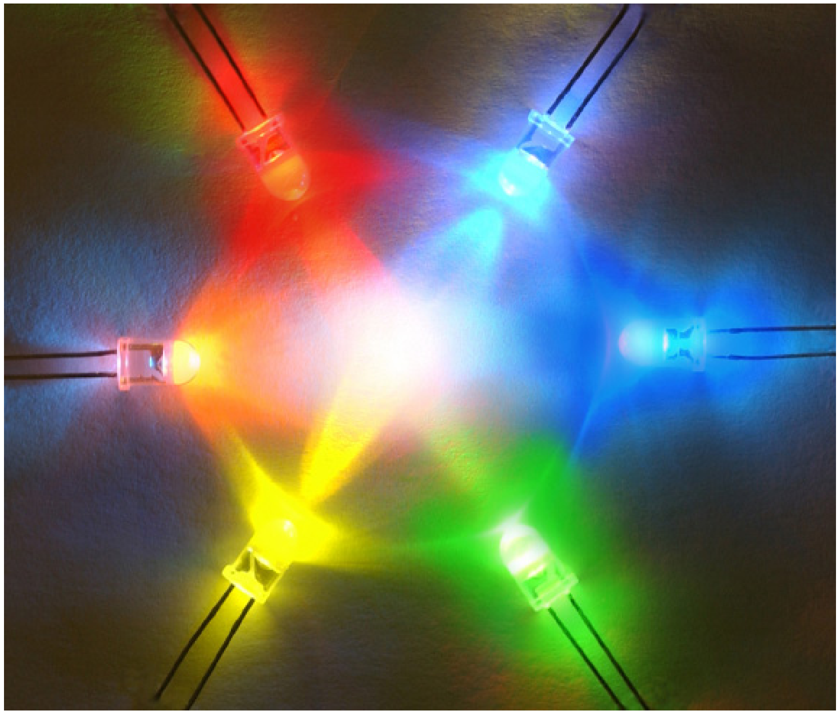

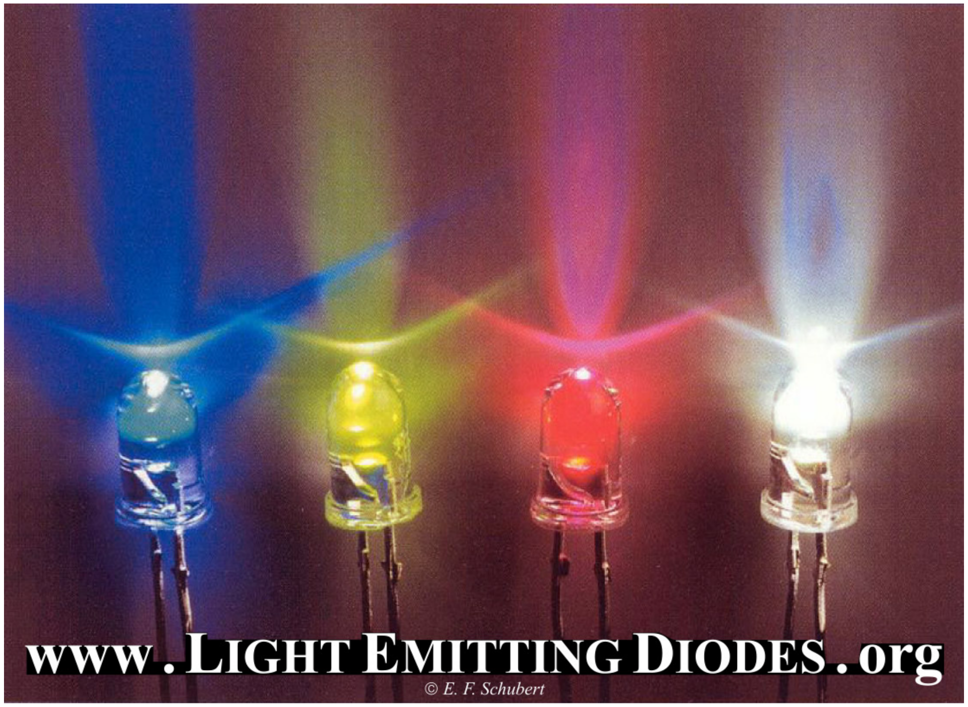

1

History of LEDs

A Note on Carborundum.

To the Editors of Electrical World:

SIRS:—During an investigation of the unsymmetrical passage of current through a contact of carborundum and other substances a curious phenomenon was noted. On applying a potential of 10 volts between two points on a crystal of carborundum, the crystal gave out a yellowish light. Only one or two specimens could be found which gave a bright glow on such a low voltage, but with 110 volts a large number could be found to glow. In some crystals only edges gave the light and others gave instead of a yellow light green, orange or blue. In all cases tested the glow appears to come from the negative pole. a bright blue-green spark appearing at the positive pole. In a single crystal, if contact is made near the center with the negative pole, and the positive pole is put in contact at any other place, only one section of the crystal will glow and that the same section wherever the positive pole is placed.

There seems to be some connection between the above effect and the e.m.f. produced by a junction of carborundum and another conductor when heated by a direct or alternating current; but the connection may be only secondary as an obvious explanation of the e.m.f. effect is the thermoelectric one. The writer would be glad of references to any published account of an investigation of this or any allied phenomena.

NEW YORK, N. Y. H. J. ROUND.

Fig. 1.1. Publication reporting on a "curious phenomenon", namely the first observation of electroluminescence from a SiC (carborundum) light-emitting diode. The article indicates that the first LED was a Schottky diode rather than a pn-junction diode (after H. J. Round, *Electrical World* Vol. **49**, p. 309, 1907)

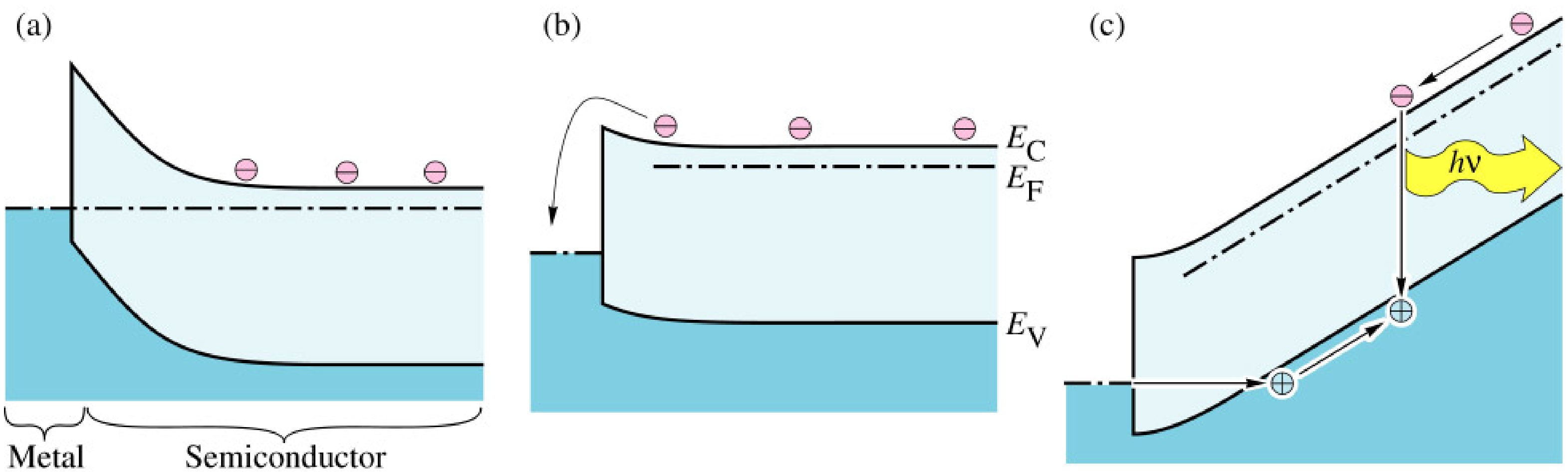

Fig. 1.2. Band diagram of Schottky diode under (a) equilibrium conditions, (b) forward bias, and (c) strong forward bias. Under strong forward bias, minority carrier injection occurs making possible near-bandgap light emission.

Origins of GaAs and AlGaAs infrared and red LEDs

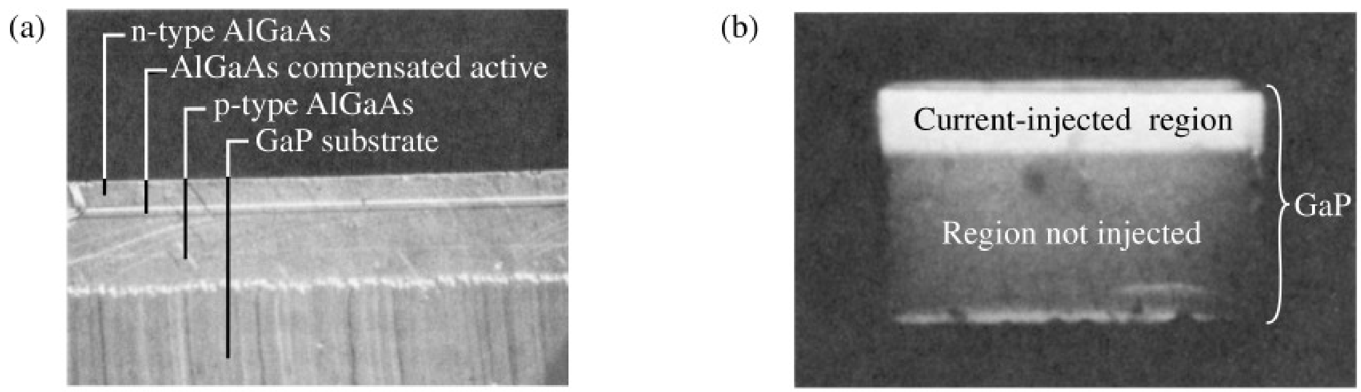

Fig. 1.3. (a) Cross section micrograph of a an AlGaAs LED grown on a transparent GaP substrate. (b) Electroluminescence originating from a current-injected region located under a stripe-shaped contact viewed through the transparent GaP substrate (after Woodall *et al*., 1972).

Fig. 1.4. This classic 1964 main-frame computer IBM System 360 used high-voltage gas-discharge lamps to indicate the status of the arithmetic unit. In later models, the lamps were replaced by LEDs. The cabinet-sized 360 had a performance comparable to a current low-end laptop computer.

Origins of GaP red and green LEDs

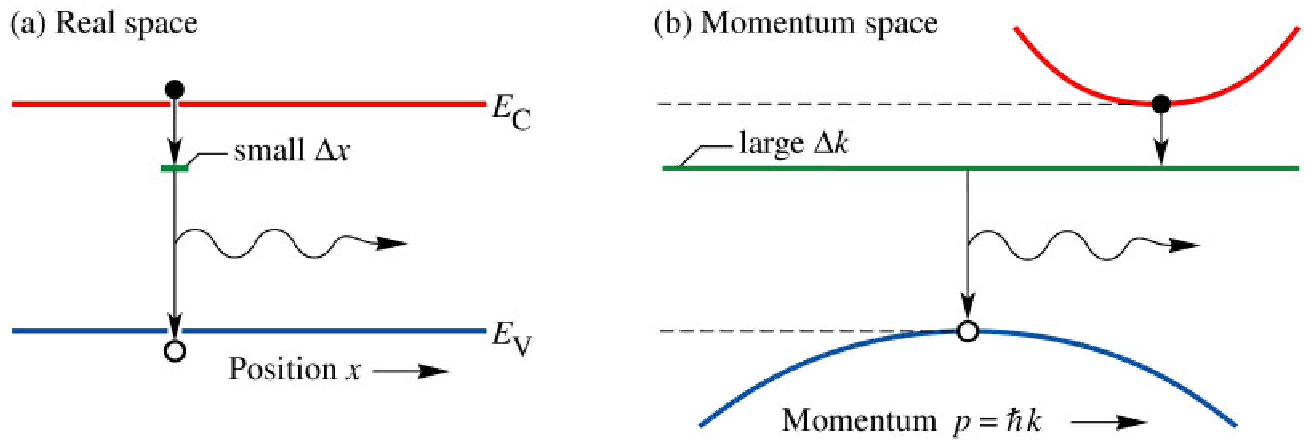

Fig. 1.5. (a) real-space and (b) momentum-space illustration of optical transitions in GaP doped with an optically active impurity level such as O or N, emitting in the red and green, respectively. GaP LEDs employ the *uncertainty principle* ($\Delta x \; \Delta p \geq \hbar$) which predicts that an electron wave function localized in real space is delocalized in momentum space thereby making possible momentum-conserving (vertical) transitions.

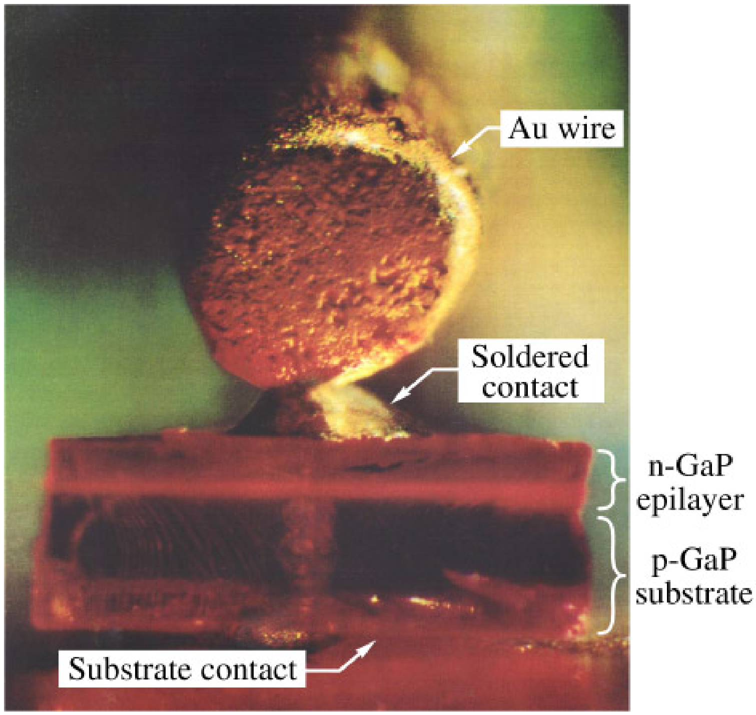

Fig. 1.6. GaP light-emitting diode grown by liquid-phase epitaxy (LPE) emitting "brilliant red light" from the Zn and O doped pn junction region (courtesy of Professor Manfred Pilkuhn, 2000).

Fig. 1.7. AT&T telephone set ("Trimline" model) with dial pad illuminated by two green N-doped GaP LEDs. The illuminated dial pad was one of the first applications of green GaP:N LEDs.

Fig. 1.8. Programmable pocket calculators Model SR-56 of the Texas Instruments Corporation and Model HP-67 of the Hewlett-Packard Corporation both manufactured starting in 1976. Seven-segment numeric characters composed of GaAsP LEDs were used in the display. The SR-56 came with a "huge" program memory of 100 steps. The HP-67 came with a magnetic card reader and had several freely programmable keys.

Early history of GaN blue light emitters

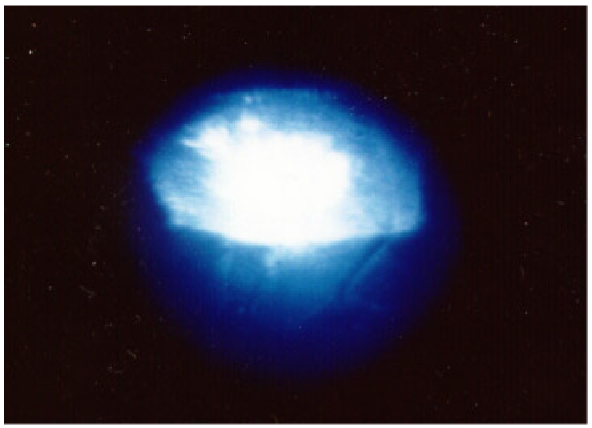

Fig. 1.9. Blue light emission found in 1972 caused by recombining electron-hole pairs created in a highly resistive GaN structure doped with Si and Mg (courtesy of Dr. Paul Maruska, 2000)

History of blue, green, and white LEDs based on GaInN

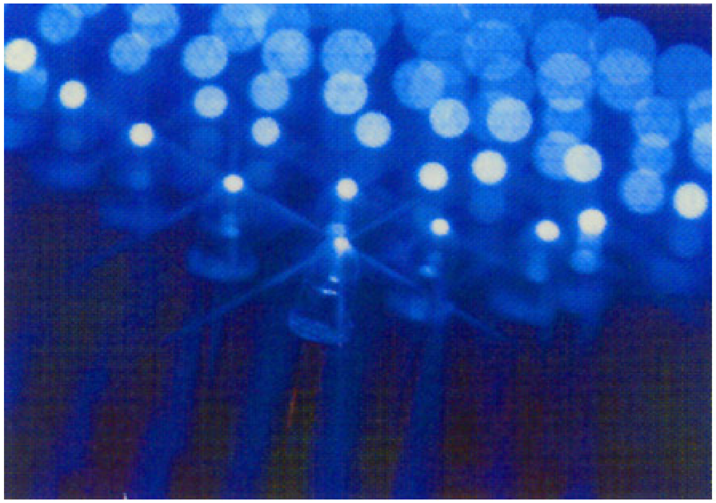

Fig. 1.10. Array of GaInN / GaN blue LEDs manufactured by Nichia Corporation (after Nakamura and Fasol, 1997).

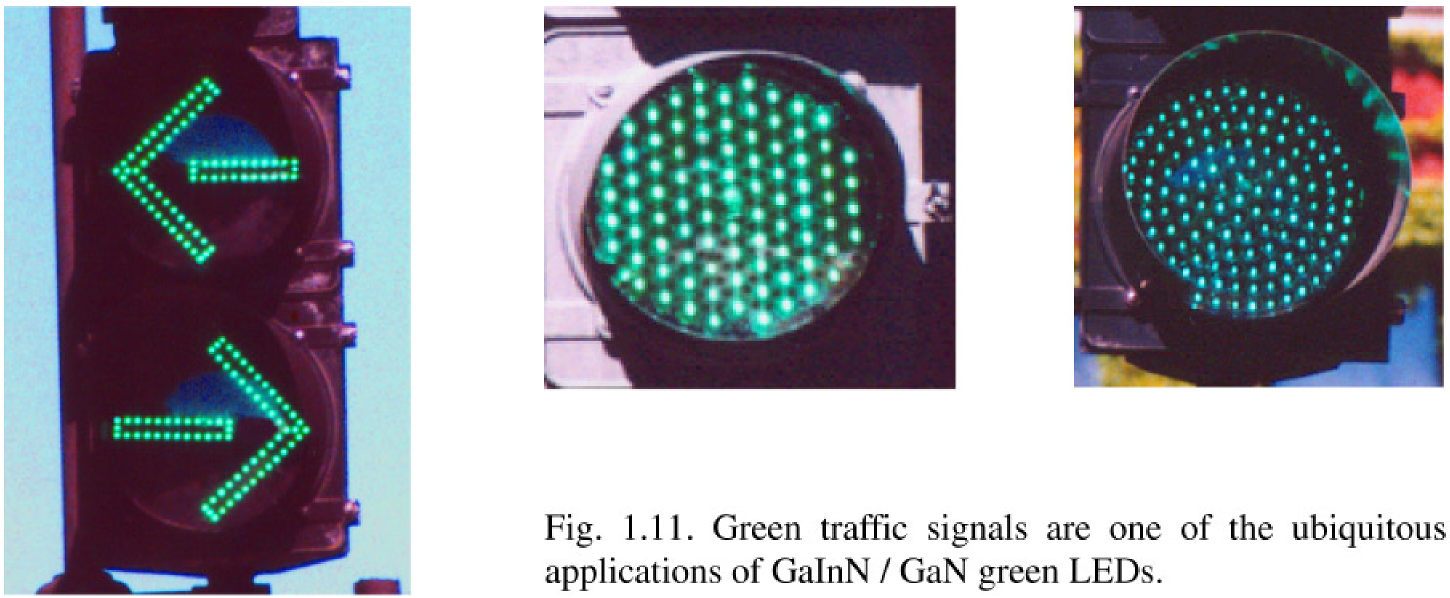

Fig. 1.11. Green traffic signals are one of the ubiquitous applications of GaInN / GaN green LEDs.

History of AlGaInP visible LEDs

Fig. 1.12. Example of red and amber AlGaInP / GaAs LEDs used in signage applications.

2

Radiative and nonradiative recombination

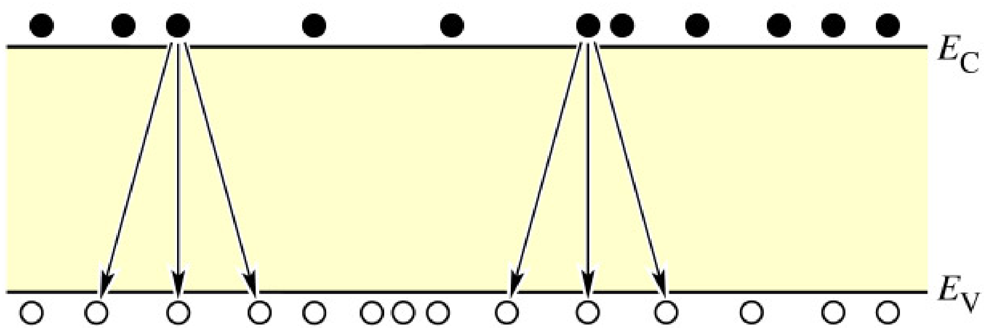

Fig. 2.1. Illustration of electron-hole recombination. The number of recombination events per unit time per unit volume is proportional to the product of electron and hole concentrations, *i. e.* $R \propto n\,p$.

Radiative electron-hole recombination

$$n = n_0 + \Delta n \qquad \text{and} \qquad p = p_0 + \Delta p$$

n	free electron concentration
n_0	equilibrium free electron concentration
Δn	excess electron concentration

$$R = -\frac{\mathrm{d}n}{\mathrm{d}t} = -\frac{\mathrm{d}p}{\mathrm{d}t} = B\,n\,p$$

R	recombination rate per cm^3 per s
B	bimolecular recombination coefficient

Carrier decay (low excitation)

$$\Delta n(t) = \Delta n_0 \, \mathrm{e}^{-B(n_0 + p_0)t}$$

$$\tau = \left[B \left(n_0 + p_0 \right) \right]^{-1}$$

τ	carrier lifetime
B	bimolecular recombination coefficient

Radiative recombination for low-level excitation

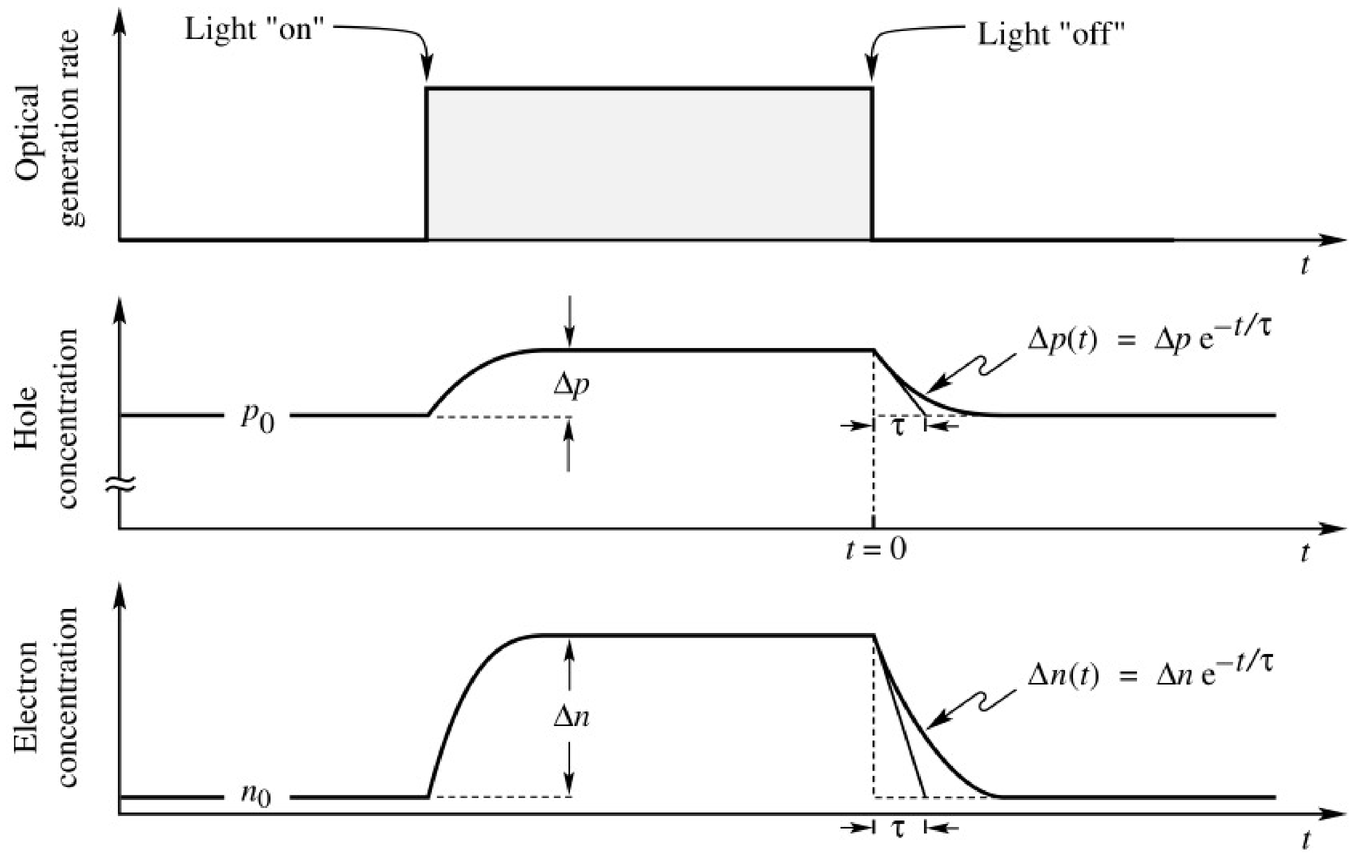

Fig. 2.2. Carrier concentration as a function of time before, during, and after an optical excitation pulse. The semiconductor is assumed to be p-type and thus it is $p_0 >> n_0$. Electrons and holes are generated in pairs, thus $\Delta p = \Delta n$. Under low-level excitation shown here, it is $\Delta n << p_0$. In most practical cases the equilibrium minority carrier concentration is extremely small so that $n_0 << \Delta n$.

Recombination lifetime: Theory versus experiment

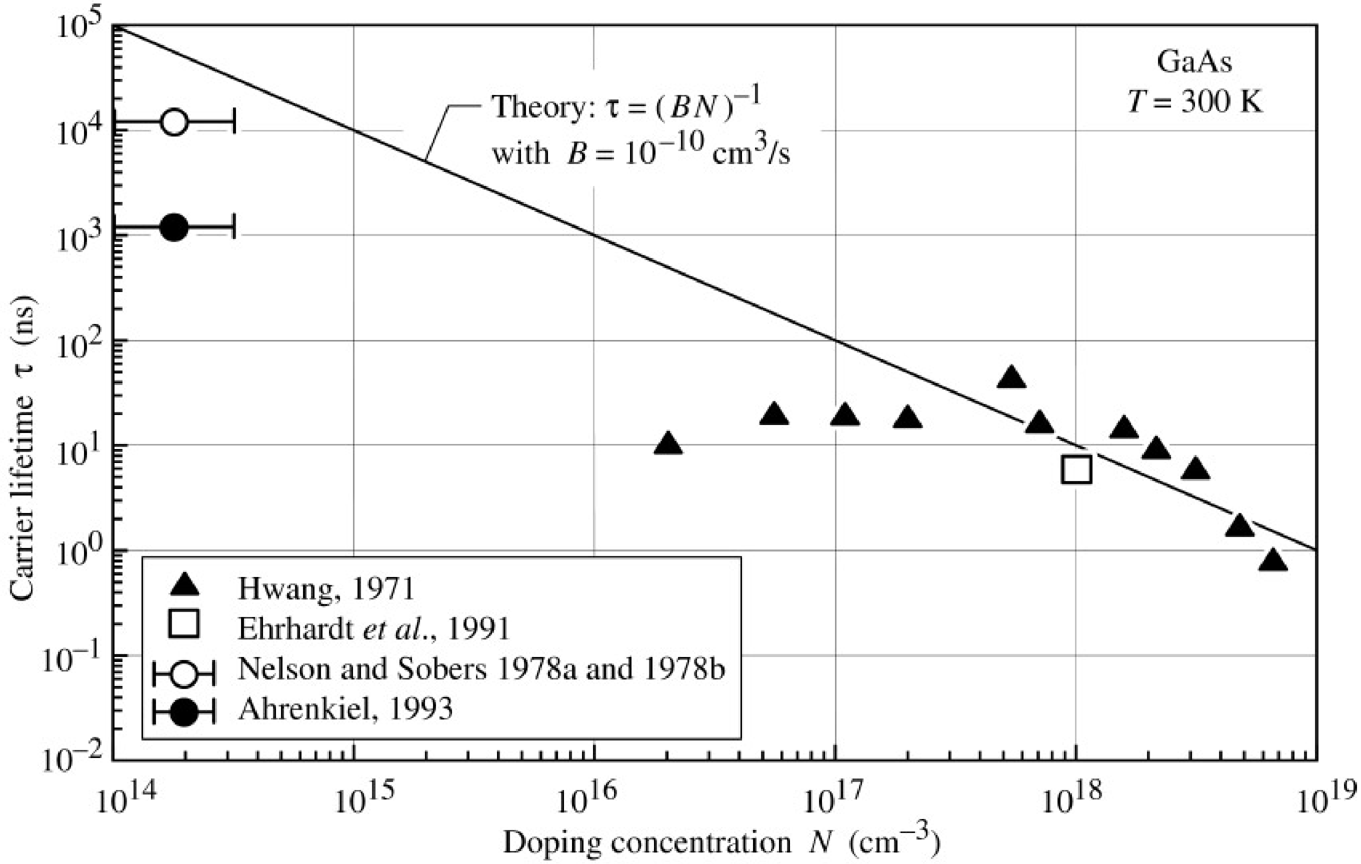

Fig. 2.3. Minority carrier lifetime as a function of doping concentration in GaAs at 300 K. The lifetime was inferred from luminescence decay mesurements. The data points of Nelson and Sobers (1978a and 1978b) and Ahrenkiel (1993) were measured on nominally undoped material with a doping concentration << 10^{15} cm^{-3}.

Nonradiative recombination in the bulk

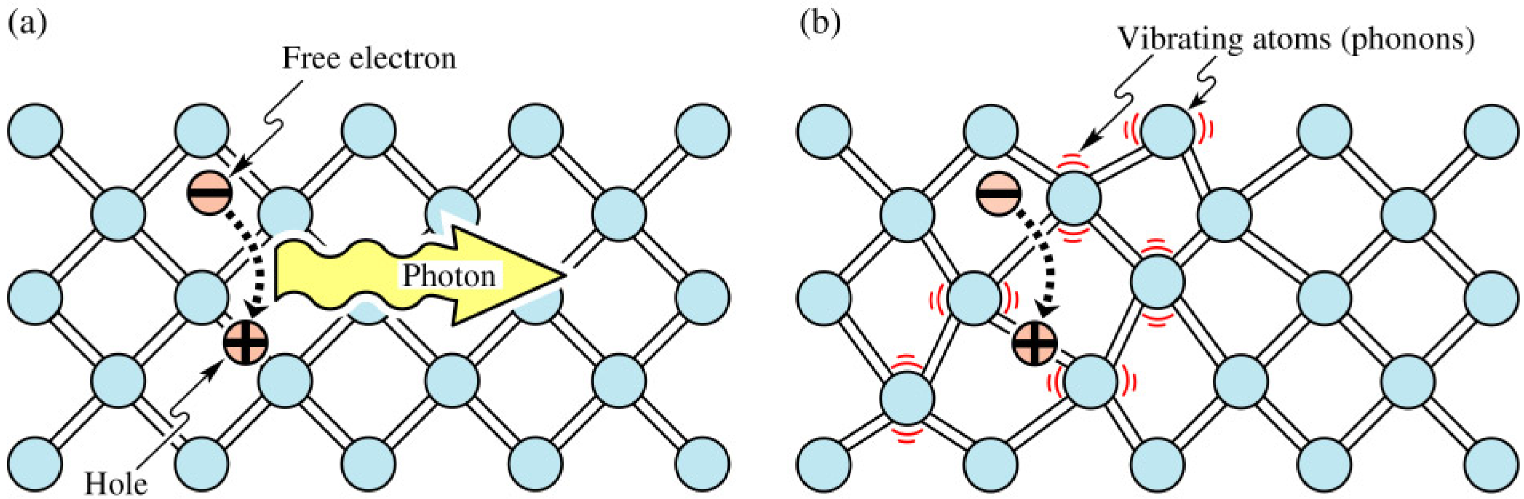

Fig. 2.5. (a) Radiative recombination of an electron-hole pair accompanied by the emission of a photon with energy $h\nu \approx E_g$. (b) In non-radiative recombination events, the energy released during the electron-hole recombination is converted to phonons (adopted from Shockley, 1950).

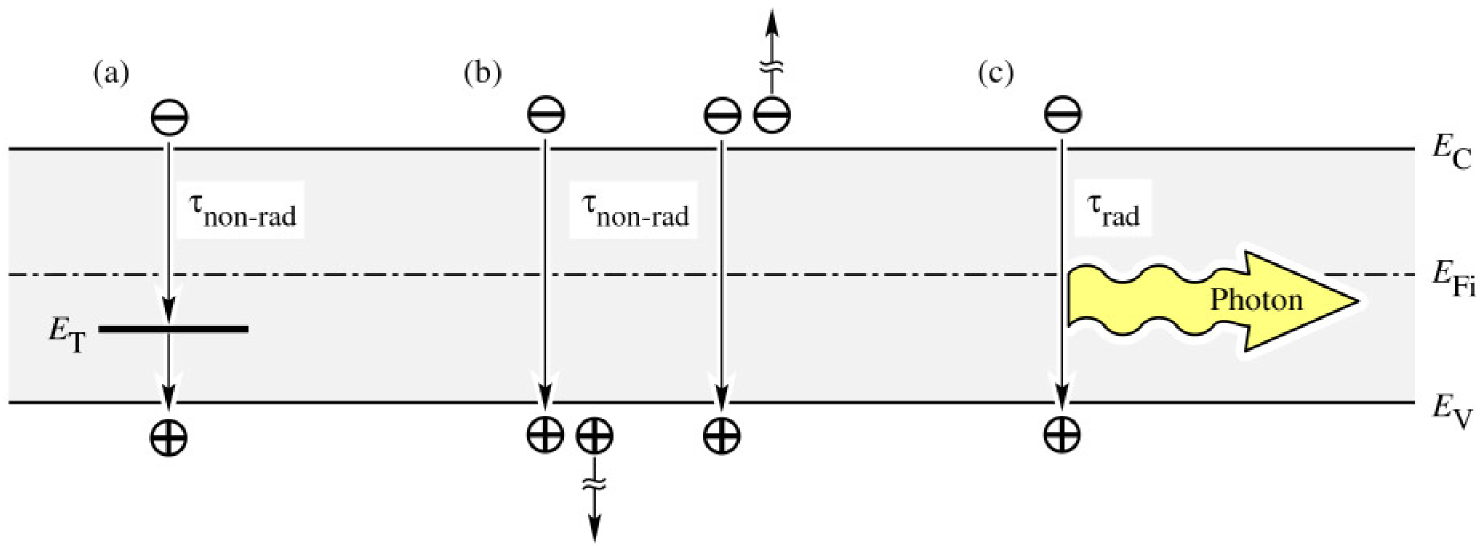

Fig. 2.6. Band diagram illustrating nonradiative recombination (a) via a deep level, (b) via an Auger process and (c) radiative recombination.

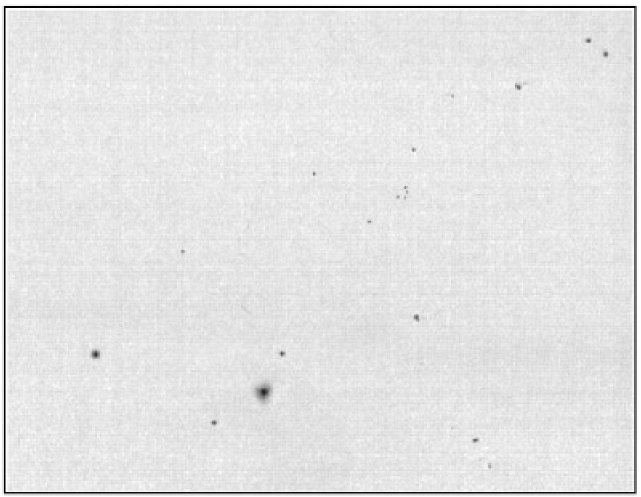

Fig. 2.7. Cathodoluminescence micrograph of a GaAs epitaxial layer. The dark spots are due to large clusters of non-radiative recombination centers (after Schubert, 1995).

… dark spots are clusters of defects

Shockley-Read recombination

$$R_{SR} = \frac{p_0\,\Delta n + n_0\,\Delta p + \Delta n \Delta p}{\left(N_t v_p \sigma_p\right)^{-1}\left(n_0 + n_1 + \Delta n\right) + \left(N_t v_n \sigma_n\right)^{-1}\left(p_0 + p_1 + \Delta p\right)}$$

$$\frac{1}{\tau} = \frac{p_0 + n_0 + \Delta n}{\left(N_t v_p \sigma_p\right)^{-1}\left(n_0 + n_1 + \Delta n\right) + \left(N_t v_n \sigma_n\right)^{-1}\left(p_0 + p_1 + \Delta p\right)}$$

$$\tau_i = \tau_{n_0}\left(1 + \frac{p_1 + n_1}{2n_i}\right) = \tau_{n_0}\left[1 + \cosh\left(\frac{E_T - E_{Fi}}{kT}\right)\right]$$

Mid-gap levels are effective non-radiative recombination centers

Nonradiative recombination at surfaces

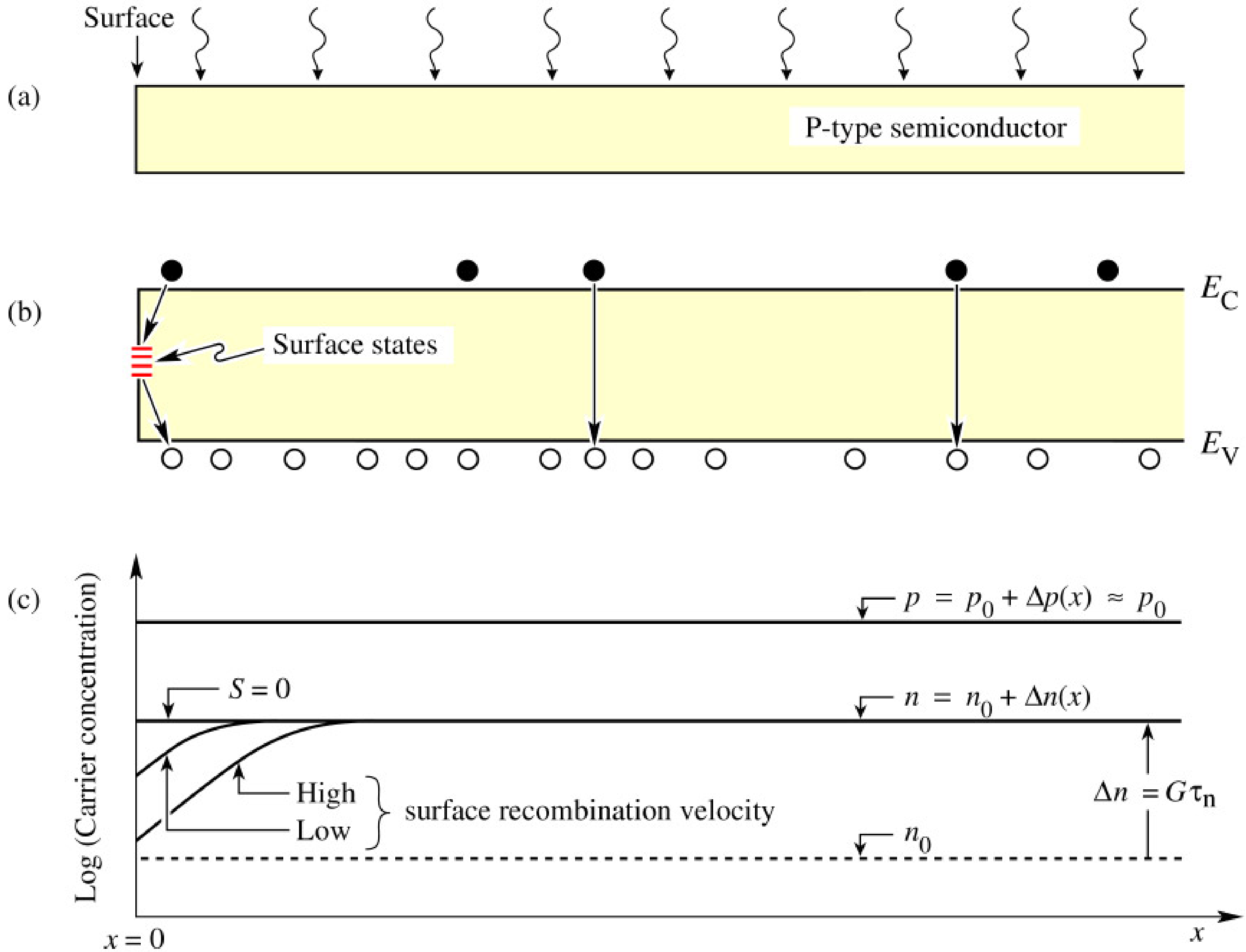

Fig. 2.9. (a) Illuminated p-type semiconductor, (b) band diagram, and (c) minority and majority carrier concentration near the surface assuming unifom carrier generation due to illumination. The excess carrier concentrations are Δn and Δp.

Surface recombination

$$n(x) \;=\; n_0 + \Delta n(x) \;=\; n_0 + \Delta n_\infty \left[1 - \frac{\tau_n S \;\exp(-x / L_n)}{L_n + \tau_n S} \right]$$

S	surface recombination velocity
x	distance from semiconductor surface
L_n	carrier diffusion length

Surface recombination velocities of some semiconductors

GaAs	$S = 10^6$ cm/s
GaP	$S = 10^6$ cm/s
InP	$S = 10^3$ cm/s
Si	$S = 10^1$ cm/s

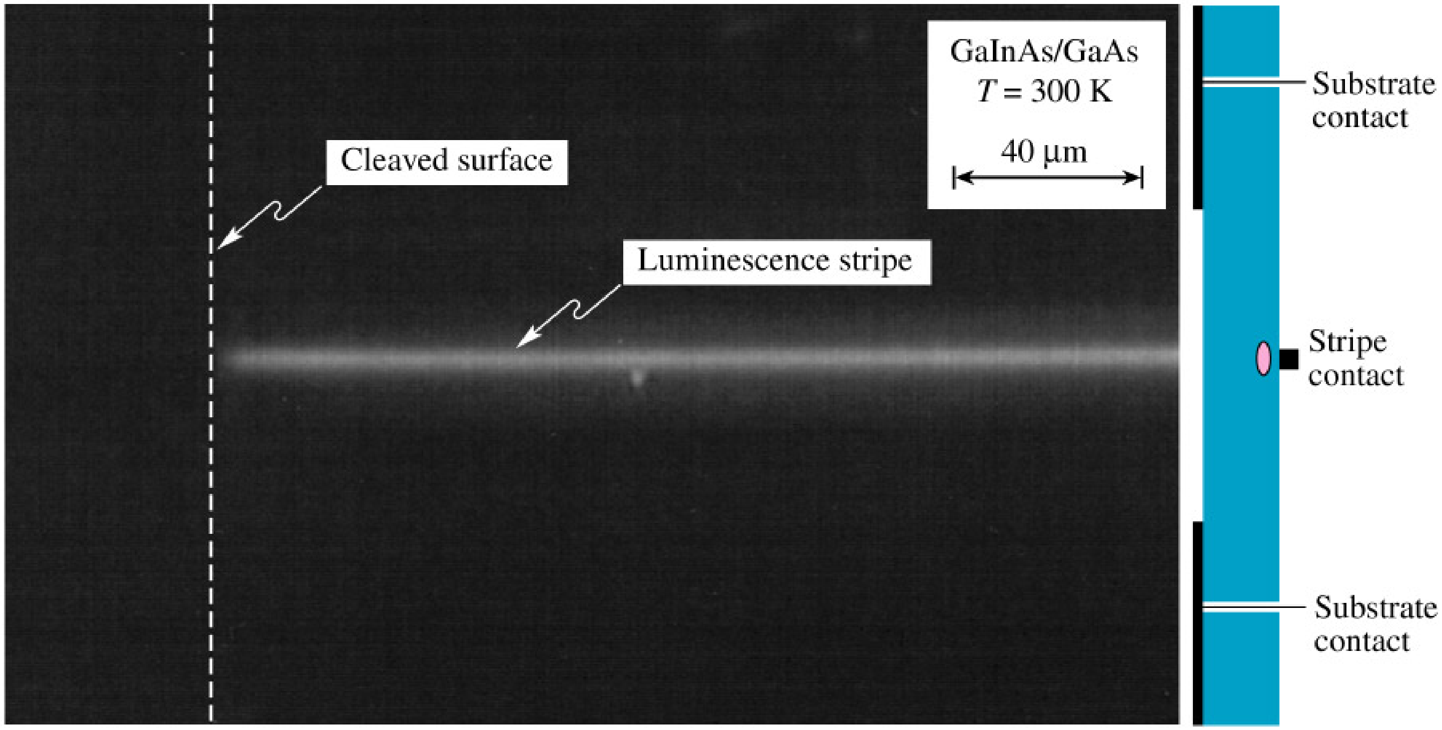

Fig. 2.10. Micrograph of a GaInAs/GaAs structure with a stripe-shaped contact on the top side and a contact widow at the substrate side of the device under current injection conditions. The luminescence emanating from the active region located below the stripe contact clearly decreases in the vicinity of the surface due to surface recombination.

… making surface recombination “visible”

Competition between radiative and nonradiative recombination

$$\tau^{-1} = \tau_r^{-1} + \tau_{nr}^{-1}$$

$$\eta_{int} = \frac{\tau_r^{-1}}{\tau_r^{-1} + \tau_{nr}^{-1}}$$

τ	carrier lifetime
τ_{nr}	nonradiative carrier lifetime
τ_r	radiative carrier lifetime
η_{int}	internal quantum efficiency

4

LED basics: Electrical properties

Shockley equation for p-n junction diodes

$$I = e A \left(\sqrt{\frac{D_\mathrm{p}}{\tau_\mathrm{p}}} \frac{n_\mathrm{i}^2}{N_\mathrm{D}} + \sqrt{\frac{D_\mathrm{n}}{\tau_\mathrm{n}}} \frac{n_\mathrm{i}^2}{N_\mathrm{A}} \right) \left(\mathrm{e}^{eV/kT} - 1 \right)$$

P-n junction band diagram

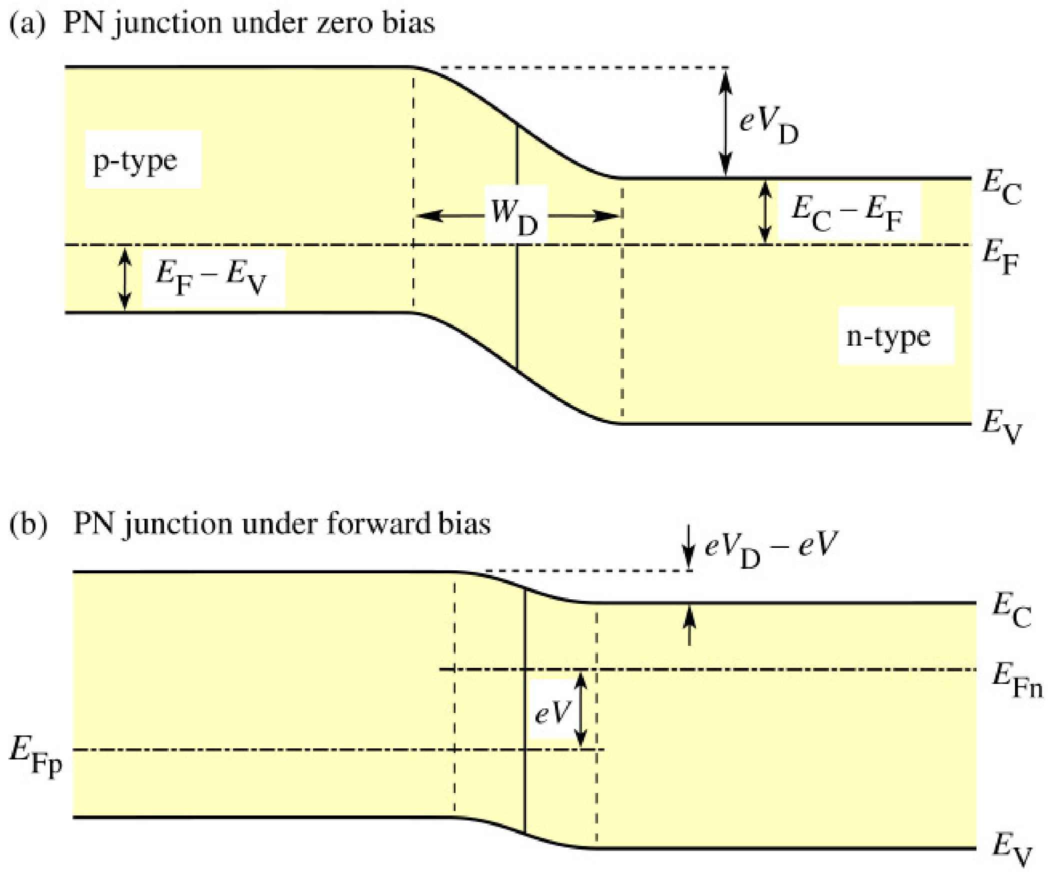

Fig. 4.1. P-N junction under (a) zero bias and (b) forward bias. Under forward bias conditions minority carriers diffuse into the neutral regions where they recombine.

Diode current-voltage characteristics

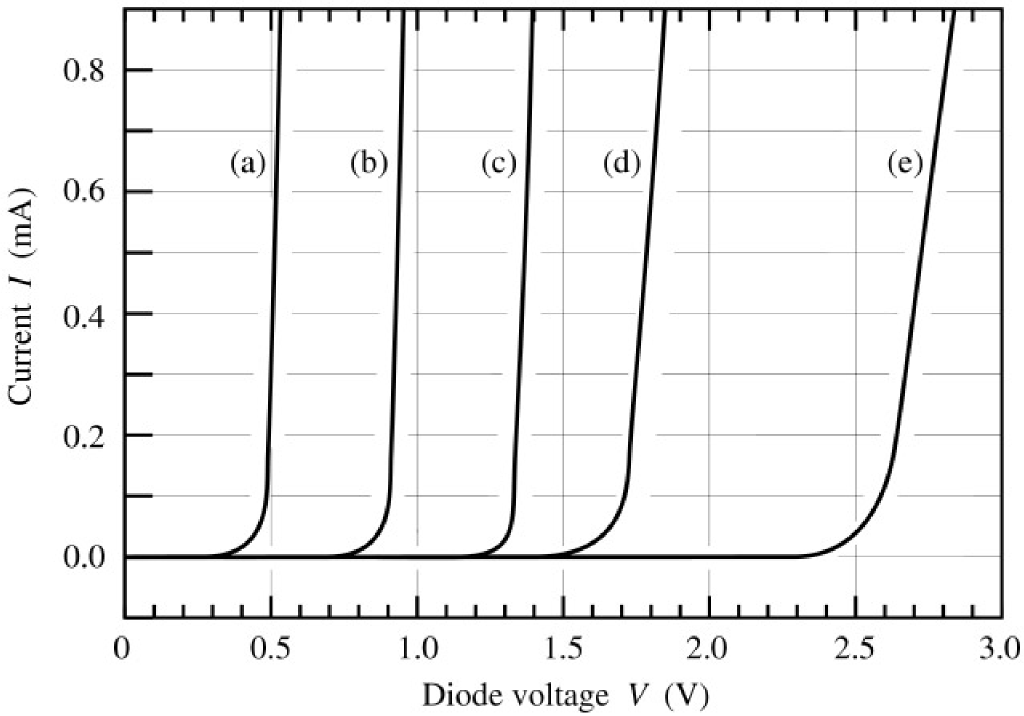

$T = 300$ K

(a)	Ge	$E_g \approx 0.7$ eV
(b)	Si	$E_g \approx 1.1$ eV
(c)	GaAs	$E_g \approx 1.4$ eV
(d)	GaAsP	$E_g \approx 2.0$ eV
(e)	GaInN	$E_g \approx 2.9$ eV

Fig. 4.2. Room temperature current - voltage characteristics of p-n junctions made of different semiconductors.

Forward voltage

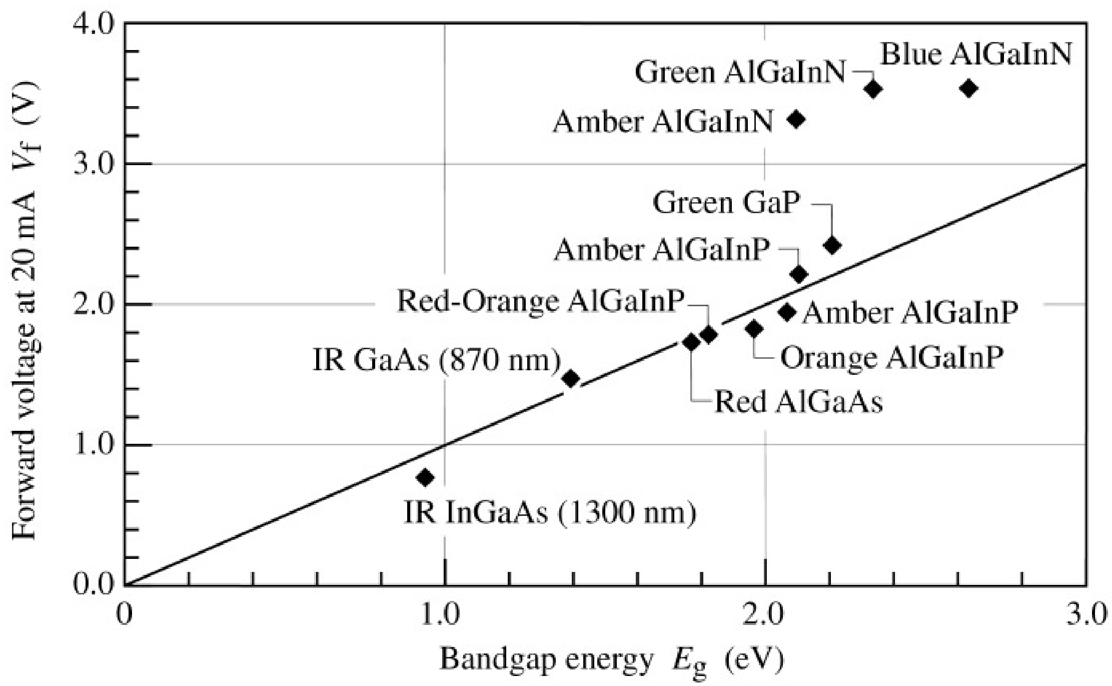

Fig. 4.3. Typical diode forward voltage versus bandgap energy for LEDs made from different materials (after Krames *et al.*, 2000).

Deviations from ideal I-V characteristic

$$I = I_s \; e^{eV/(n_{\text{ideal}} kT)}$$

$$I - \frac{(V - I R_s)}{R_p} = I_s \; e^{e(V - I R_s)/(n_{\text{ideal}} kT)}$$

n_{ideal}	ideality factor
R_s	parasitic series resistance
R_p	parasitic parallel resistance

Non-ideal I-V characteristics

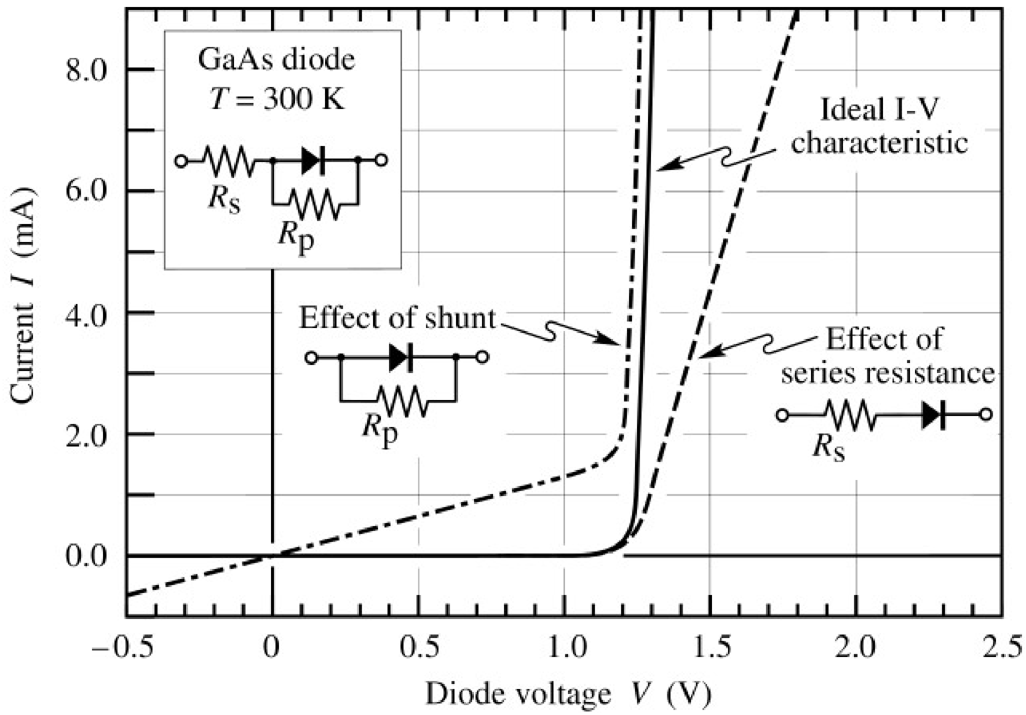

Fig. 4.4. Effect of series resistance and parallel resistance (shunt) on the I-V characteristic of a p-n-junction diode.

Method to determine series resistance

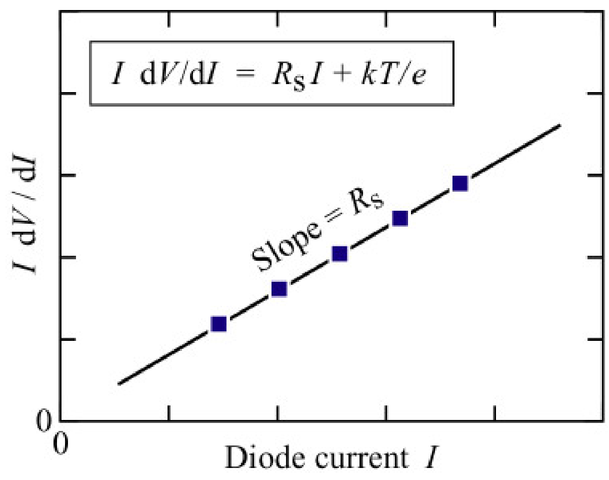

Fig. 4.5. Method for evaluating the diode series resistance. The equation shown as an inset is valid for forward bias ($V >> kT / e$)

Carrier distribution in pn homo- and heterojunctions

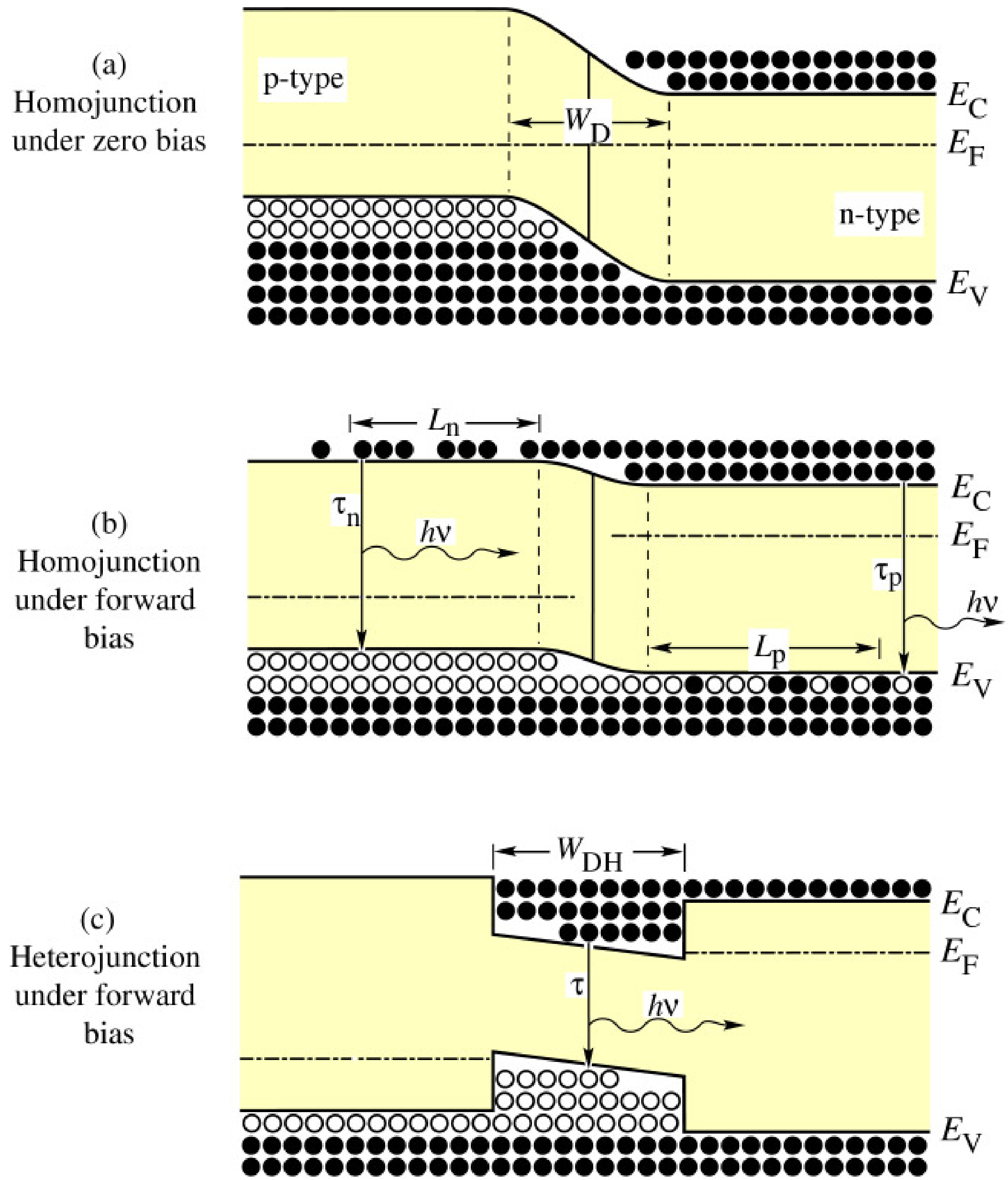

Fig. 4.6. P-N homojunction under (a) zero and (b) forward bias. P-N heterojunction (c) under forward bias. In homojunctions, carriers diffuse, on average, over the diffusion lengths L_n and L_p before recombining. In heterojunctions, carriers are confined by the heterojunction barriers.

Carrier overflow in double heterostructures

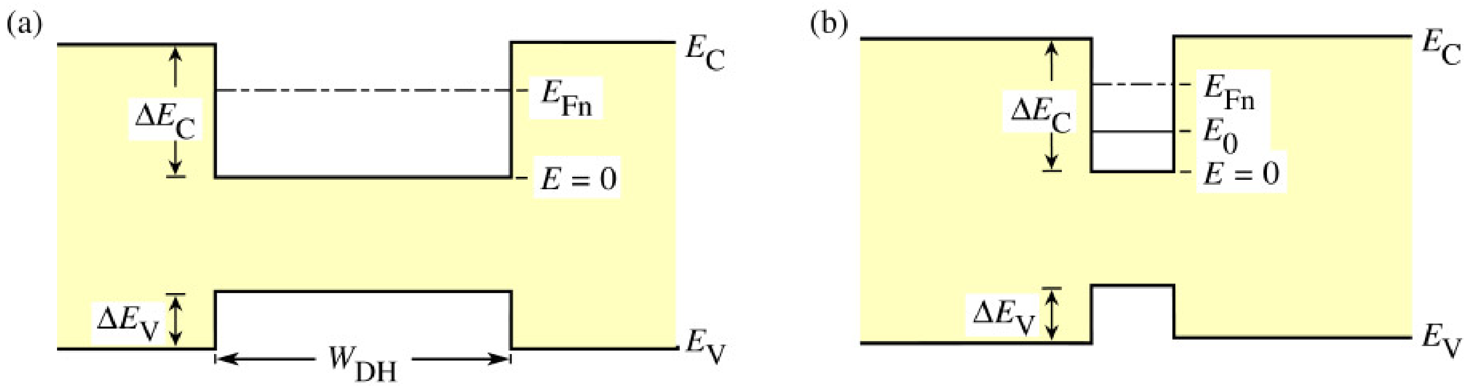

Fig. 4.10. Fermi level (E_{Fn}) and subband level (E_0) in (a) double hetero-structure and (b) a quantum well structure.

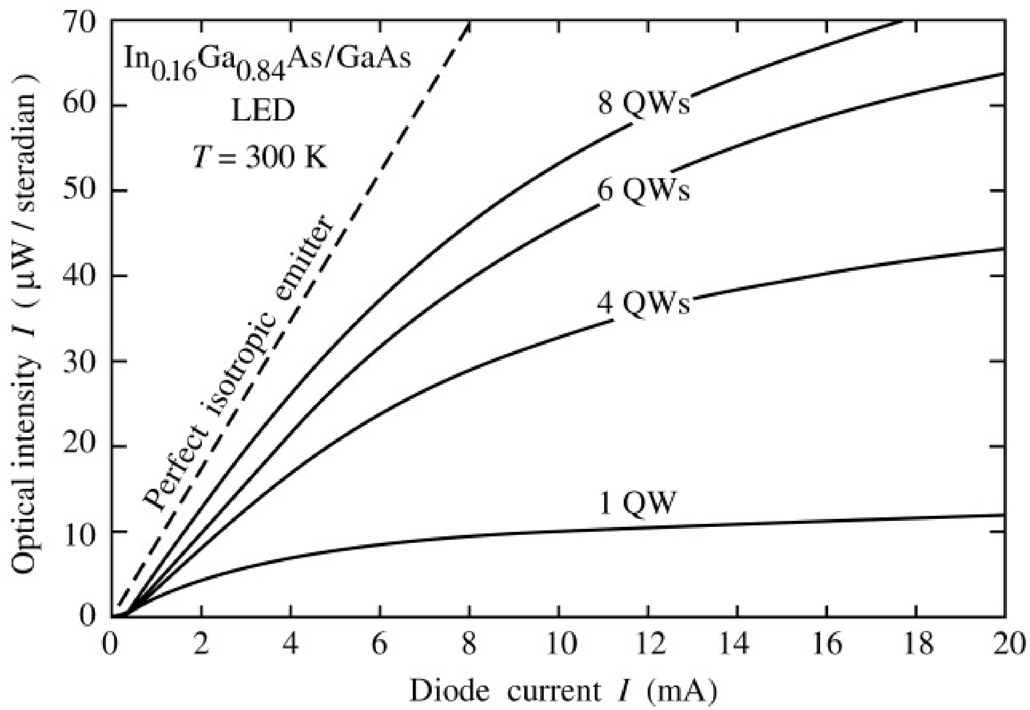

Fig. 4.11. Optical intensity emitted by $In_{0.16}Ga_{0.84}As$ / GaAs LEDs with active regions consisting of 1, 4, 6, and 8 quantum wells and theoretical intensity of a perfect isotropic emitter (dashed line) (after Hunt *et al*., 1992).

Electron blocking layers

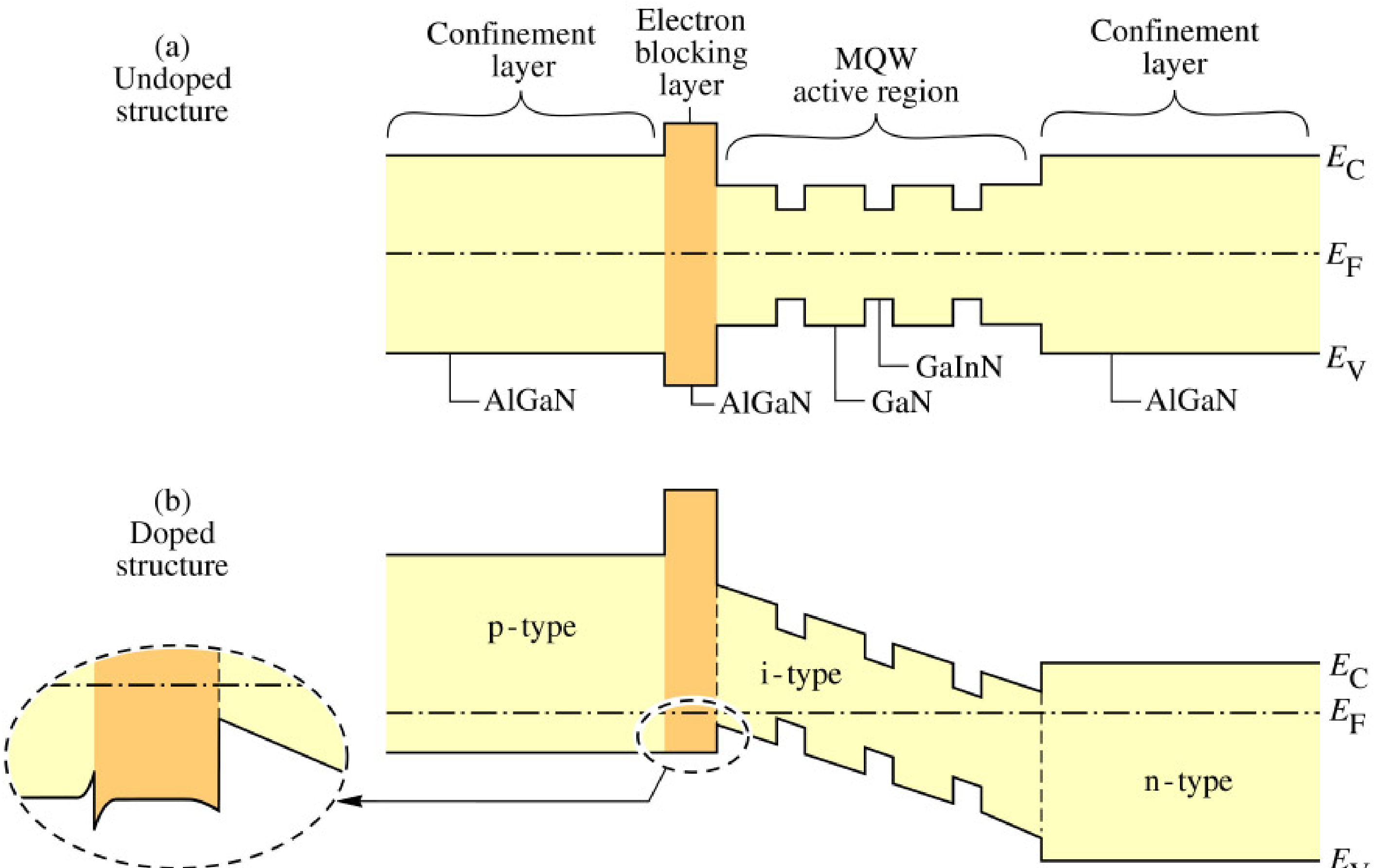

Fig. 4.12. Illustration of an AlGaN current blocking layer in an AlGaN / GaN / GaInN multi-quantum well (MQW) LED structure. (a) Band diagram without doping. (b) Band diagram with doping. The Al content in the electron blocking layer is higher than in the p-type confinement layer.

Diode voltage

$$V = h\nu / e \approx E_g / e$$

$$V = \frac{E_g}{e} + I R_s + \frac{\Delta E_C - E_0}{e} + \frac{\Delta E_V - E_0}{e}$$

$I R_s$ resistive loss

$\Delta E_C - E_0$ electron energy loss upon injection into quantum well

$\Delta E_V - E_0$ hole energy loss upon injection into quantum well

Temperature dependence of diode voltage

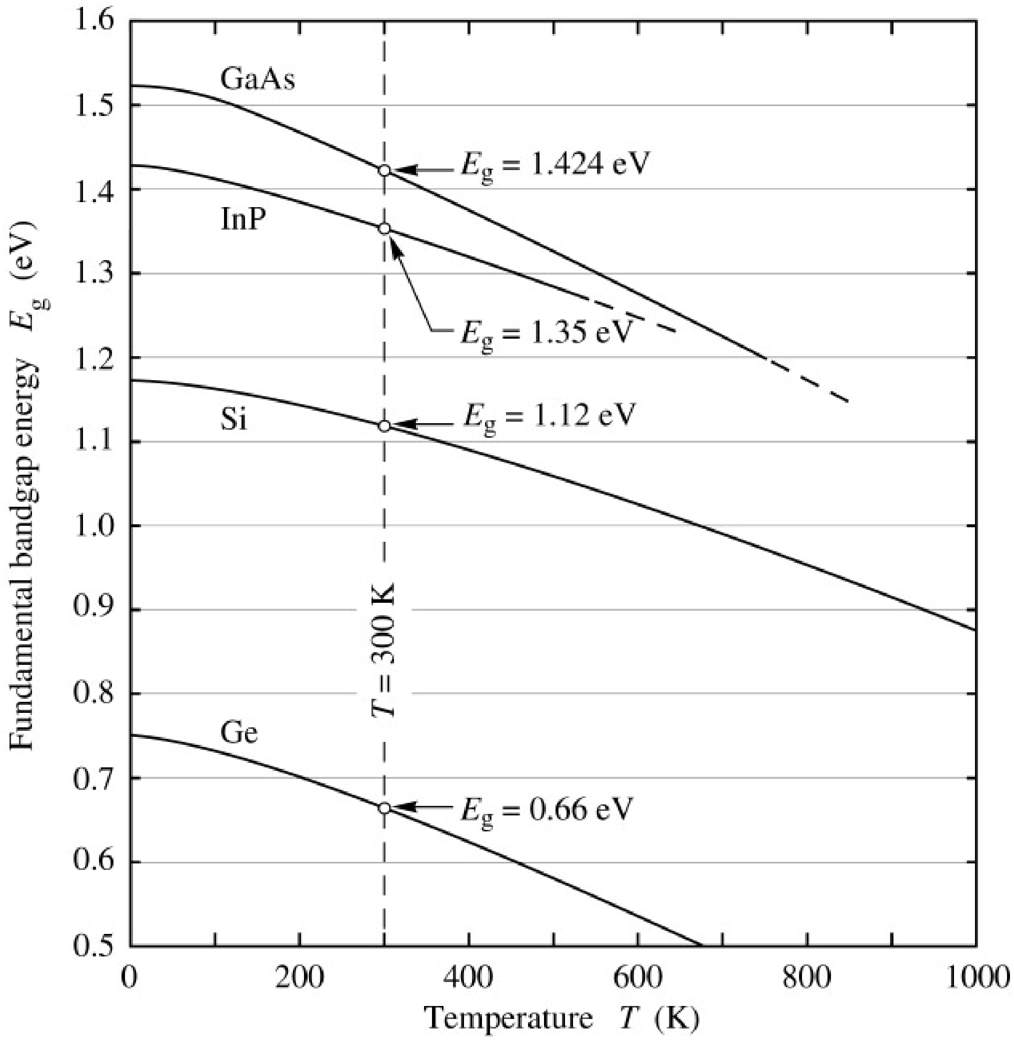

$$E_g = E_g(0\text{K}) - \frac{\alpha T^2}{T + \beta}$$

	E_g(0K)	α (10^{-4} $\frac{\text{eV}}{\text{K}}$)	β (K)
GaAs	1.519	5.41	204
InP	1.425	4.50	327
Si	1.170	4.73	636
Ge	0.744	4.77	235

Fig. 4.14. Fundamental bandgap energy of GaAs, InP, Si, and Ge as a function of temperature. The bandgap energy is approximated by a parabolic equation with the fitting parameters α and β.

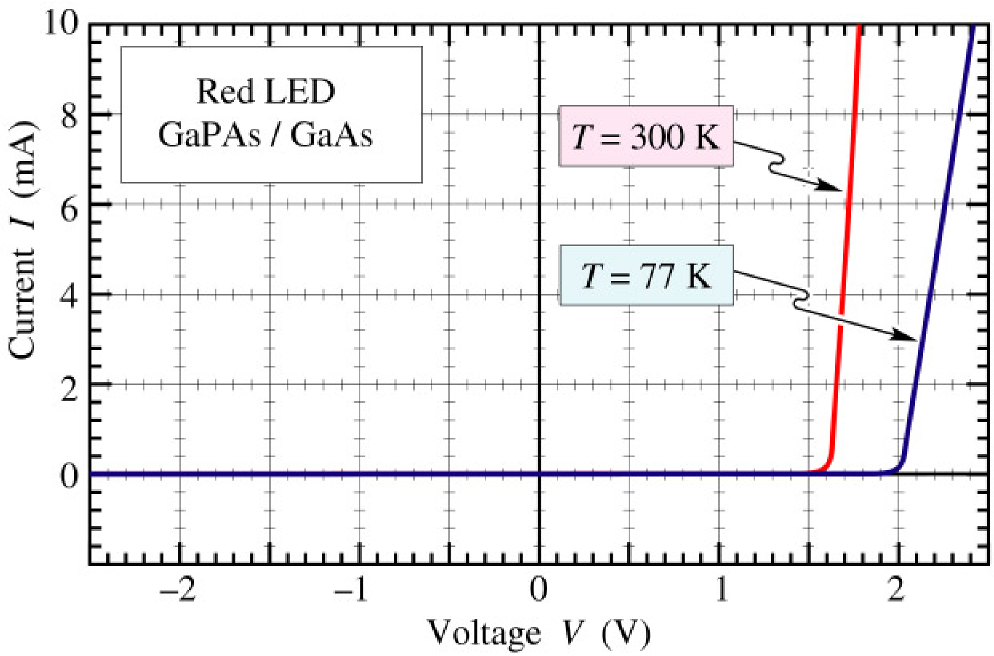

Fig. 4.15. Current-voltage characteristic of a GaAsP / GaAs LED emitting in the red part of the visible spectrum, measured at 77 K and 300 K. The threshold voltages are 2.0 V and 1.6 V, at 77 K and 300 K respectively.

Constant current and constant voltage DC drive circuits

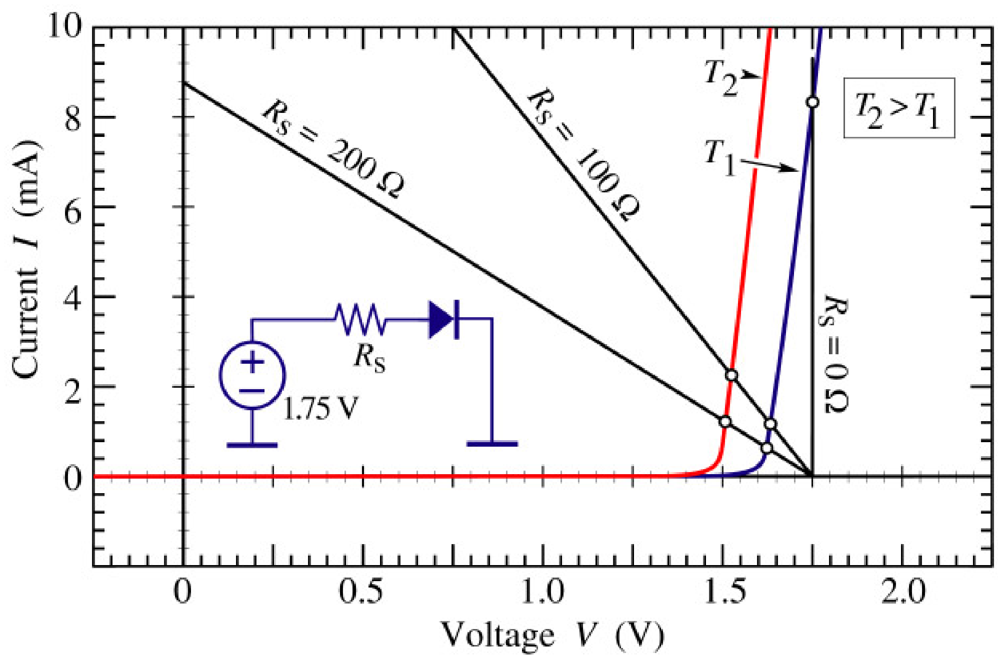

Fig. 4.16. LED drive circuit with series resistance R_S. The intersection between the diode I-Vs and the load lines are the points of operation. Small series resistances result in an increased diode current at high temperatures, thus allowing for compensation of a lower LED radiative efficiency.

5

LED basics: Optical properties

Internal, extraction, external, and power efficiency

$$\eta_{\text{int}} = \frac{\text{\# of photons emitted from active region per second}}{\text{\# of electrons injected into LED per second}} = \frac{P_{\text{int}} / (h\nu)}{I / e}$$

$$\eta_{\text{extraction}} = \frac{\text{\# of photons emitted into free space per second}}{\text{\# of photons emitted from active region per second}}$$

$$\eta_{\text{ext}} = \frac{\text{\# of photons emitted into free space per sec.}}{\text{\# of electrons injected into LED per sec.}} = \frac{P / (h\nu)}{I / e} = \eta_{\text{int}}\, \eta_{\text{extraction}}$$

$$\eta_{\text{power}} = \frac{P}{IV}$$

Emission spectrum

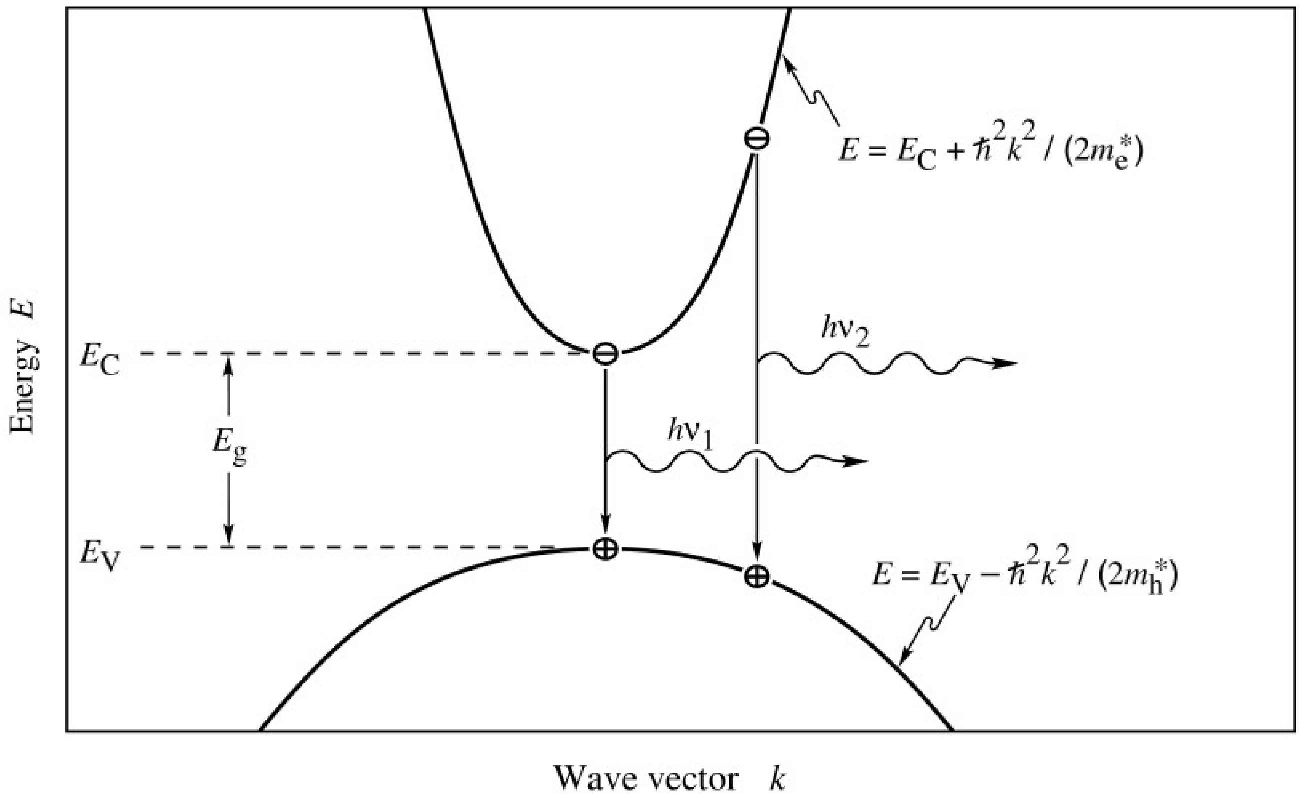

Fig. 5.1. Parabolic electron and hole dispersion relations showing "vertical" electron-hole recombination and photon emission.

$$I(E) \quad \propto \quad \sqrt{E - E_{\mathrm{g}}} \quad \mathrm{e}^{-E/(kT)}$$

$I(E)$ emission spectrum

Maximum emission intensity

$$E \quad = \quad E_{\mathrm{g}} \; + \; \frac{1}{2}\, k\, T$$

$$\Delta E \quad = \quad 1.8 \;\; k\, T$$

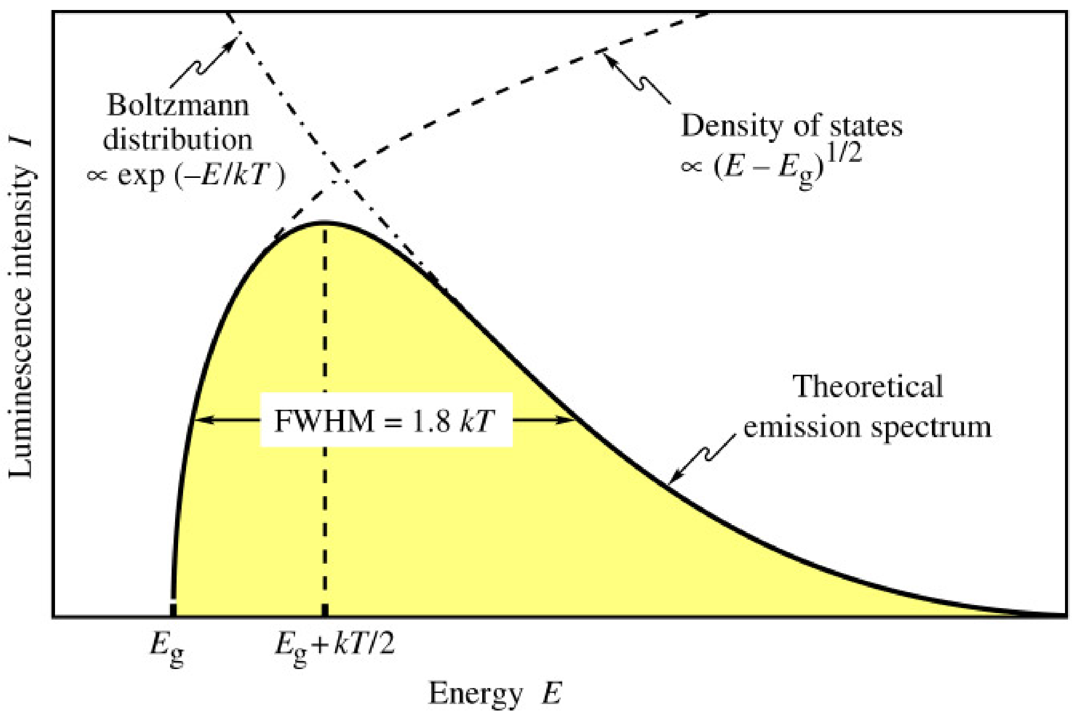

Fig. 5.2. Theoretical emission spectrum of an LED. The full width at half maximum (FWHM) of the emission line is 1.8 kT.

The light escape cone

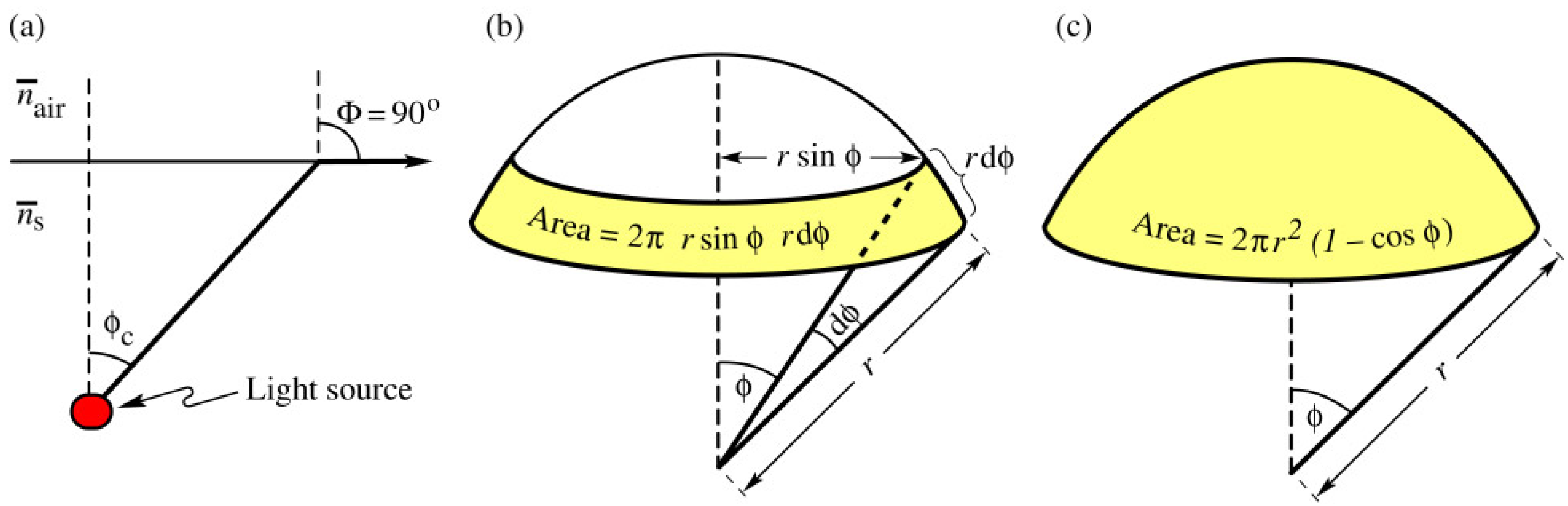

Fig. 5.3. (a) Definition of the escape cone by the critical angle ϕ_c. (b) Area element dA. (c) Area of calotte defined by radius r and angle ϕ_c.

Light escape in planar LEDs

$$\frac{P_{\text{escape}}}{P_{\text{source}}} \approx \frac{1}{2}\left[1 - \left(1 - \frac{\phi_c{}^2}{2}\right)\right] = \frac{1}{4}\,\phi_c{}^2$$

ϕ_c critical angle of total internal reflection

Problem: Only small fraction of light can escape from semiconductor

$$\frac{P_{\text{escape}}}{P_{\text{source}}} = \frac{1}{4}\,\frac{\bar{n}_{\text{air}}{}^2}{\bar{n}_{\text{s}}{}^2}$$

The lambertian emission pattern

$$I_{\text{air}} = \frac{P_{\text{source}}}{4\pi r^2} \frac{\bar{n}_{\text{air}}^2}{\bar{n}_{\text{s}}^2} \cos\Phi$$

I_{air}	emission intensity in air
Φ	angle with respect to surface normal

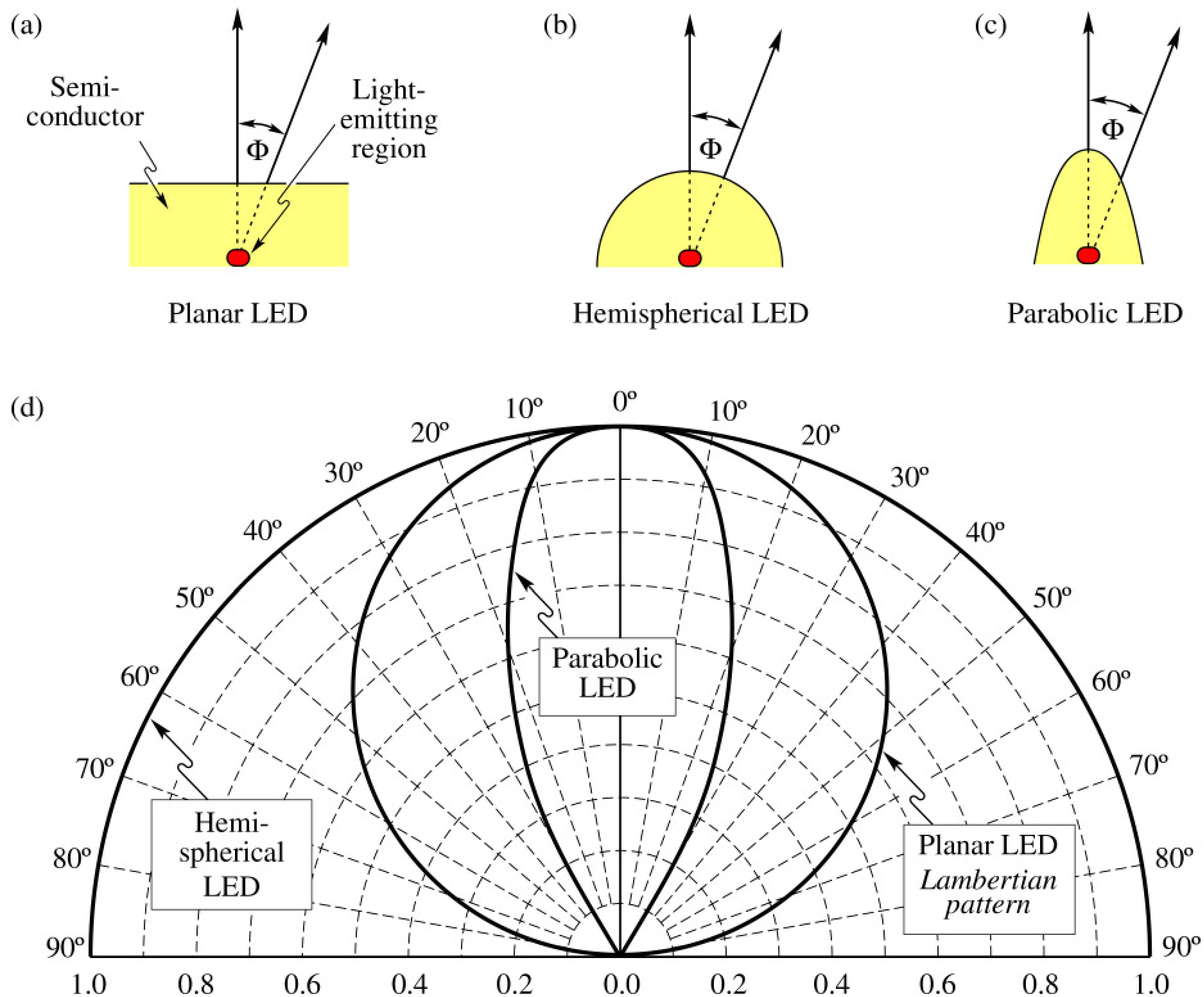

Fig. 5.5. Light-emitting diodes with (a) planar, (b) hemispherical, and (c) parabolic surfaces. (d) Far-field patterns of the different types of LEDs. At an angle of $\Phi = 60$ º, the Lambertian emission pattern decreases to 50 % of its maximum value occuring at $\Phi = 0$ º. The three emission patterns are normalized to unity intensity at $\Phi = 0$ º.

The effect of epoxy

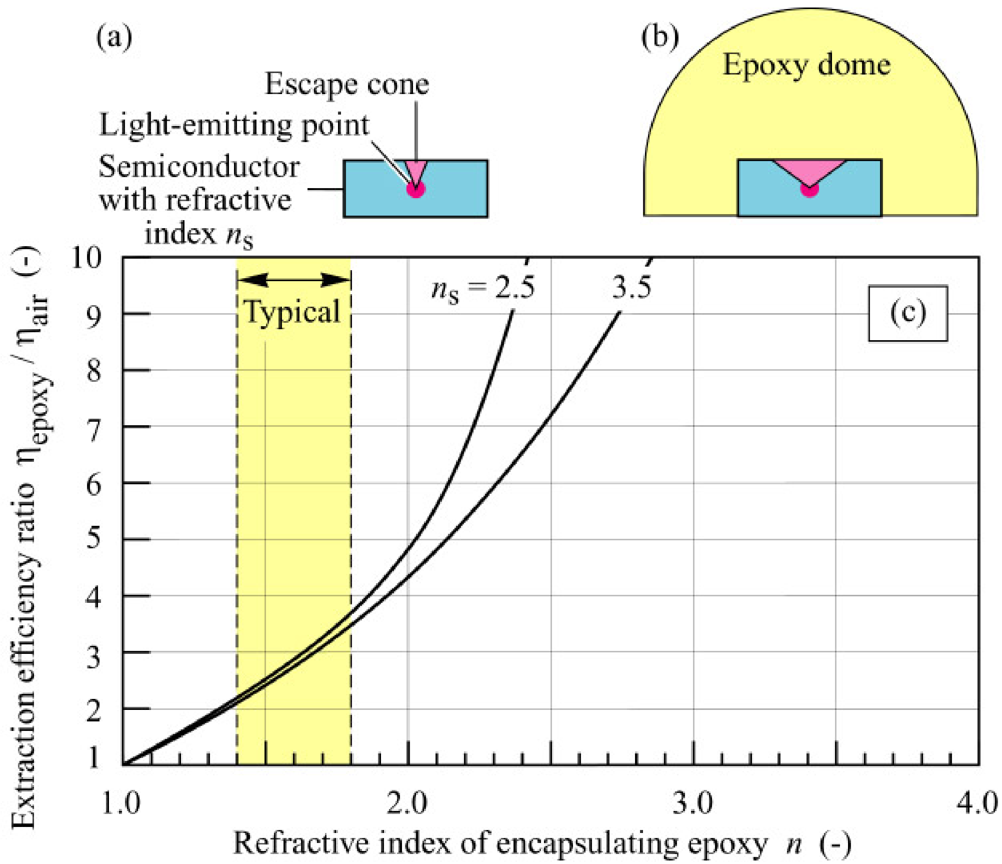

Fig. 5.6. (a) LED without and (b) with dome-shaped epoxy encapsulant. A larger escape angle is obtained for the LED with an epoxy dome. (c) Calculated ratio of light extraction efficiency emitted through the top surface of a planar LED with and without an epoxy dome. The refractive indices of typical epoxies range between 1.4 and 1.8 (adopted from Nuese *et al.*, 1969).

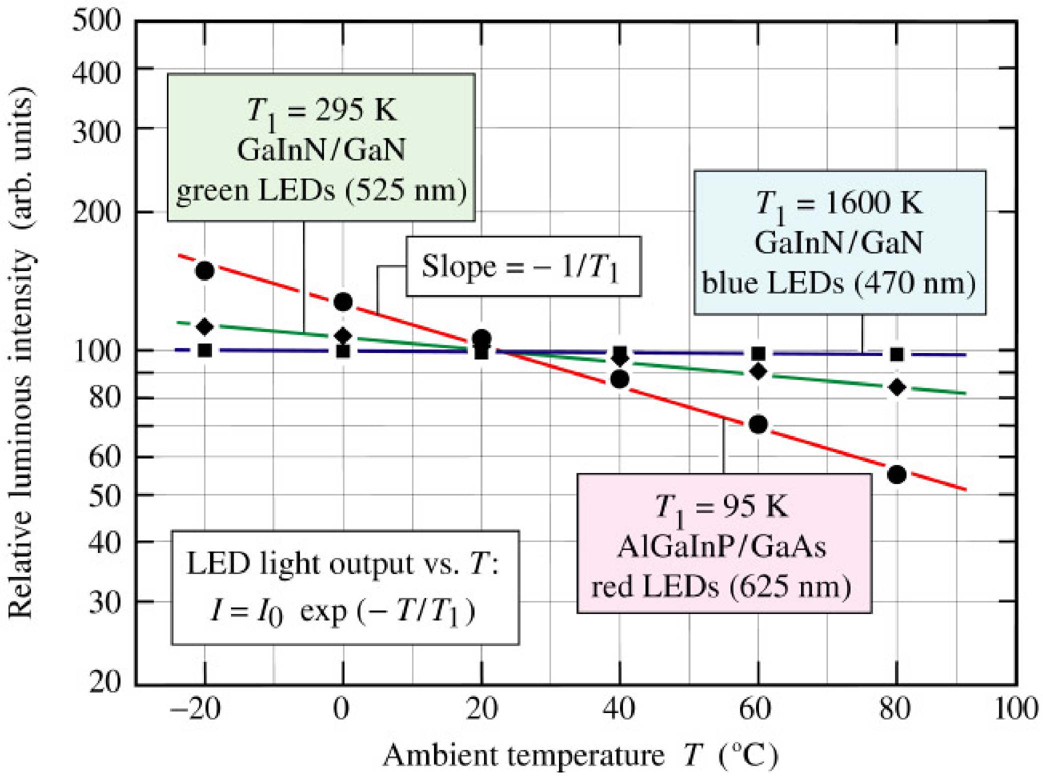

Fig. 5.7. Characteristic temperature T_1 of GaInN / GaN blue, GaInN / GaN green, and AlGaInP / GaAs red LEDs near room temperature (after data of Toyoda Gosei Corp., 2000).

6

High internal efficiency LED designs

Double heterostructures

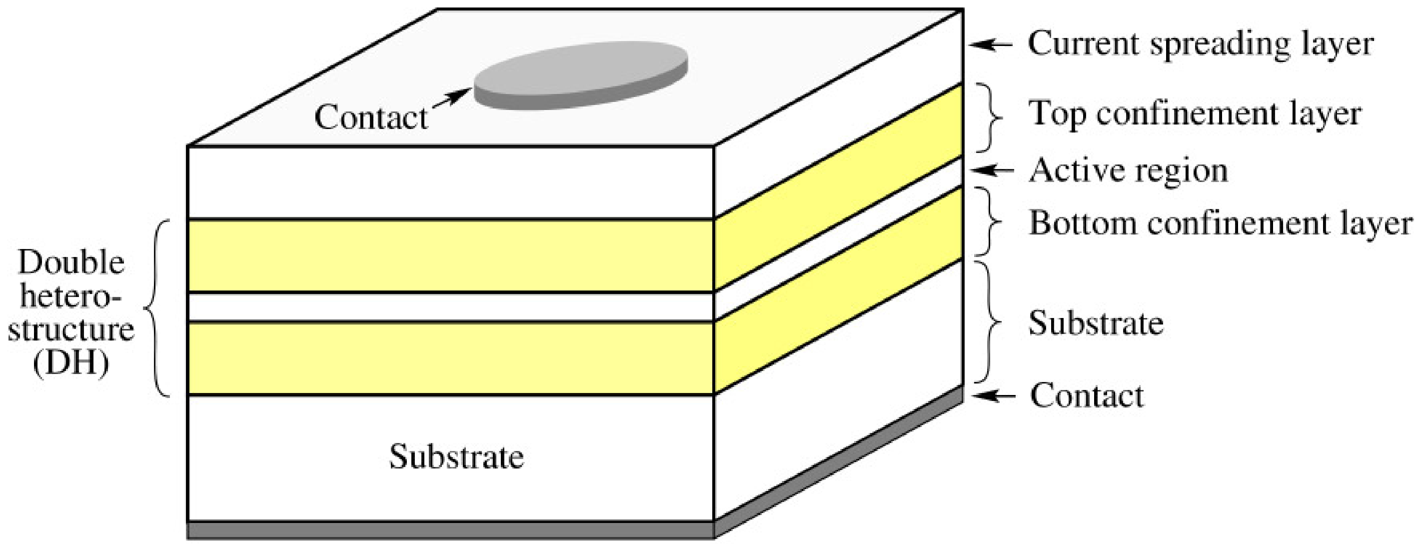

Fig. 6.1. Illustration of a double heterostructure consisting of a bulk or quantum well active region and two confinement layers. The *confinement* layers are frequently called *cladding* layers.

Homostructures versus double heterostructures

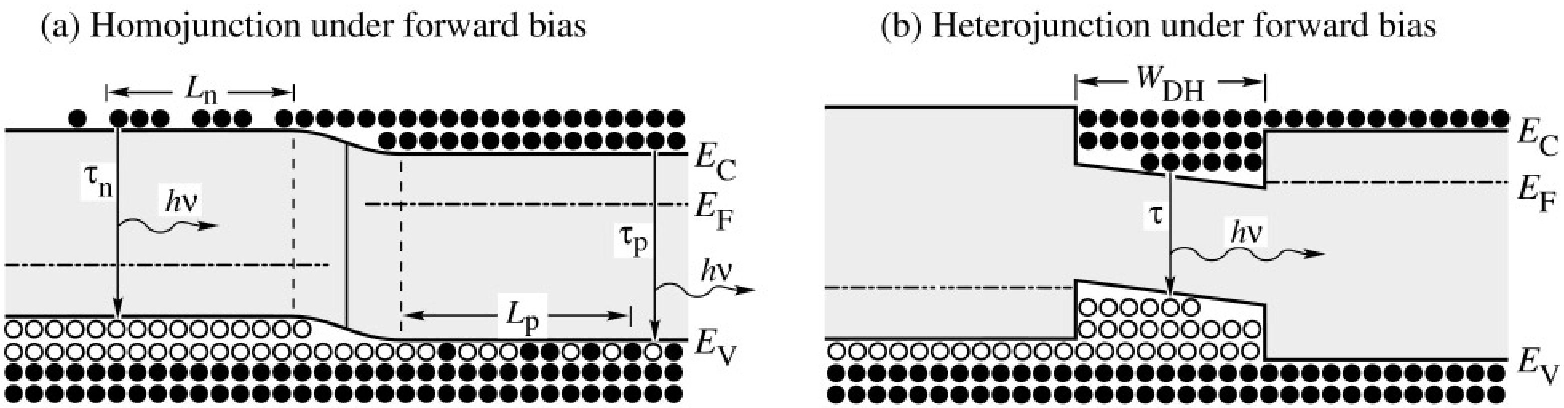

Fig. 6.2. Illustration of the free carrier distribution in a (a) homojunction and (b) heterojunction under forward bias conditions. In homojunctions, carriers are distributed over the diffusion length. In heterojunctions, carriers are confined to the well region.

Efficiency versus active layer thickness

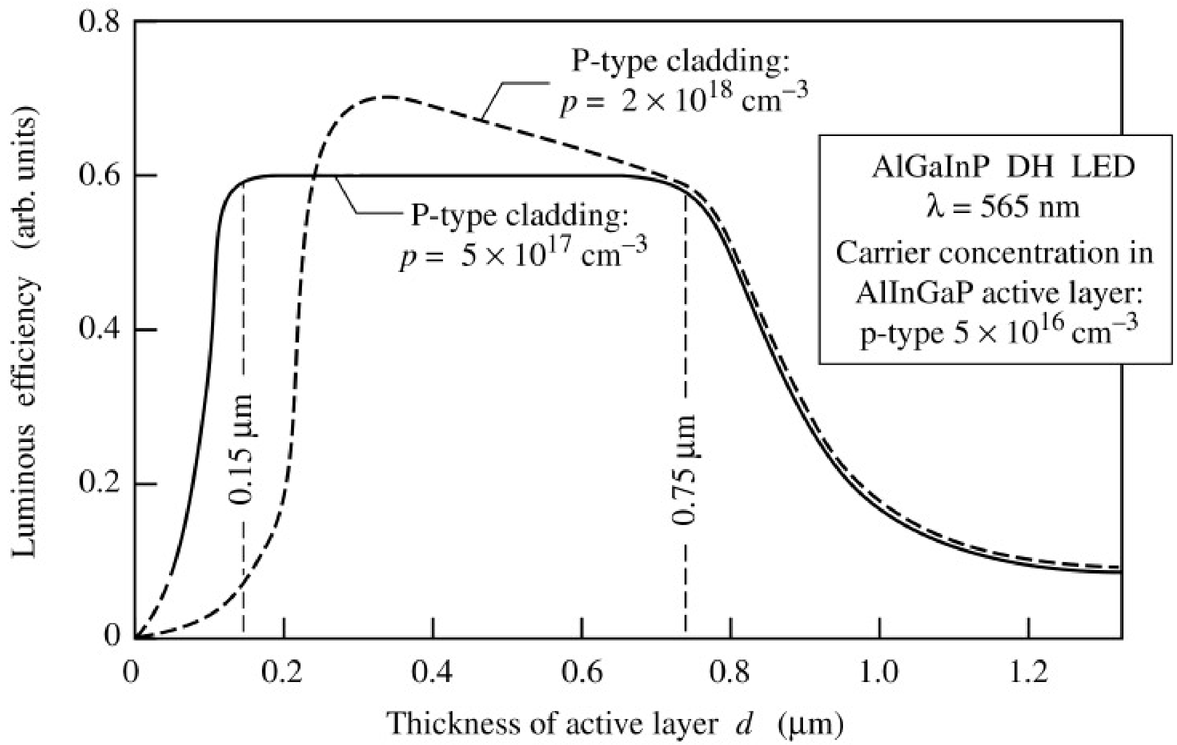

Fig. 6.3. Dependence of the luminous efficiency of an AlGaInP double heterostructure LED emitting at 565 nm on the active layer thickness. The figure reveals an optimum active region thickness of 0.15 – 0.75 µm (after Sugawara *et al*., 1992).

Doping of active region

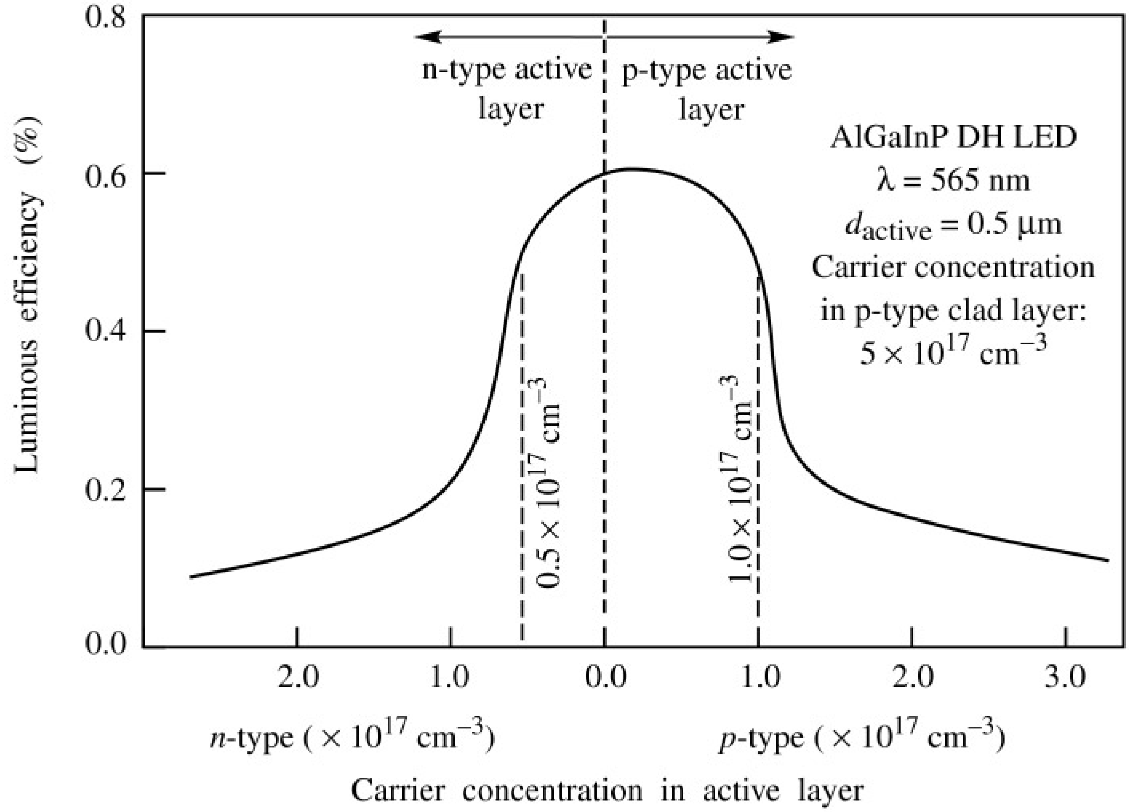

Fig. 6.4. Dependence of the luminous efficiency of an AlGaInP double heterostructure LED emitting at 565 nm on the active layer doping concentration (after Sugawara *et al*., 1992).

Non-radiative recombination and lifetime

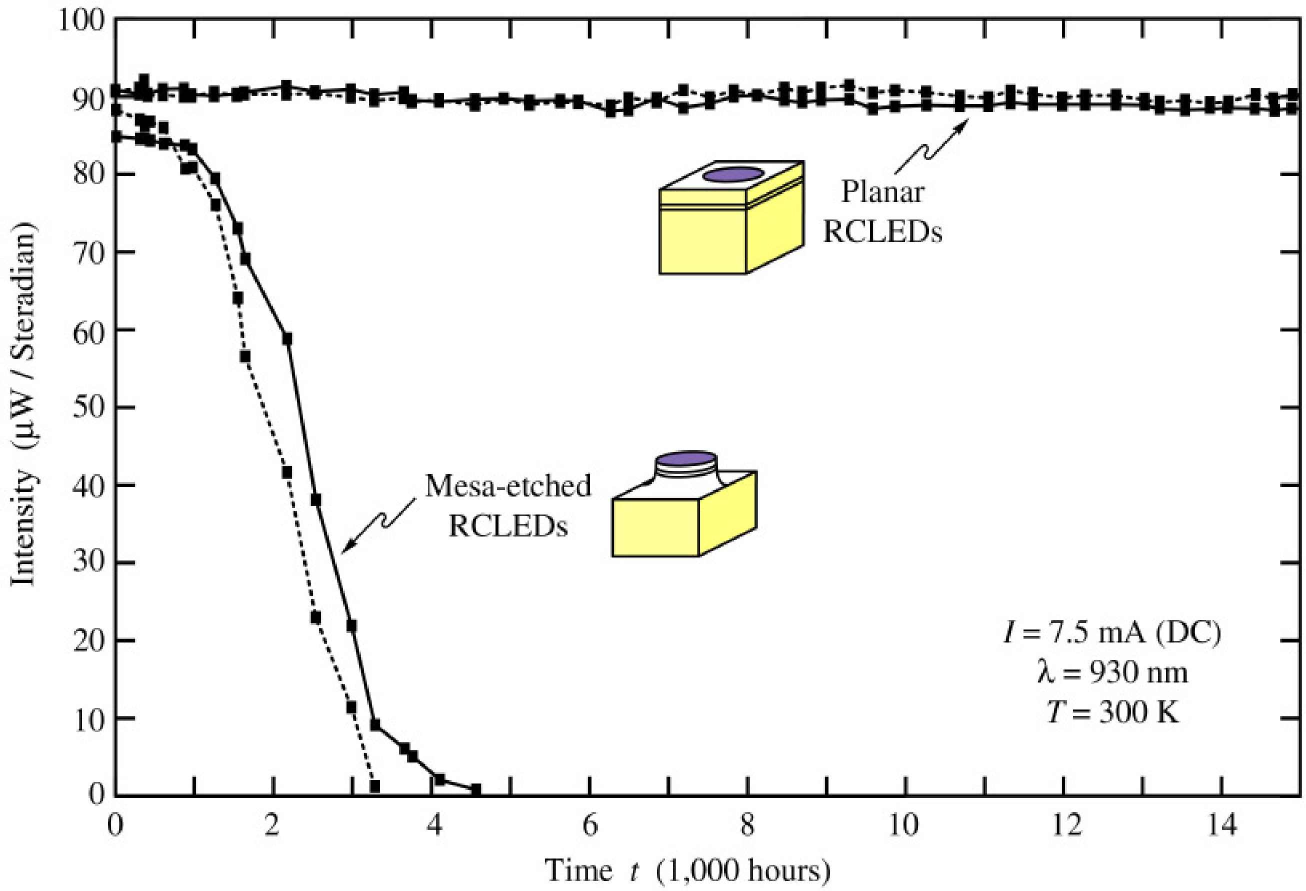

Fig. 6.11. Emission intensity of two mesa-etched LEDs and two planar LEDs versus time (after Schubert and Hunt, 1998)

Lattice matching

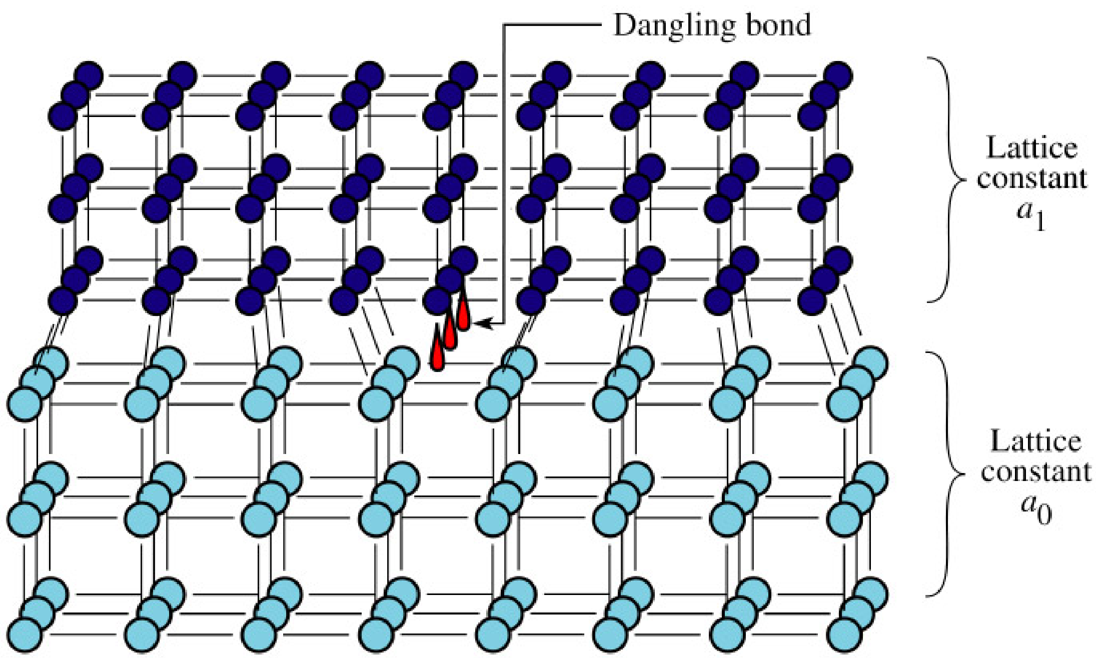

Fig. 6.12. Illustration of two crystals with mismatched lattice constant resulting in dislocations at or near the interface between the two semiconductors.

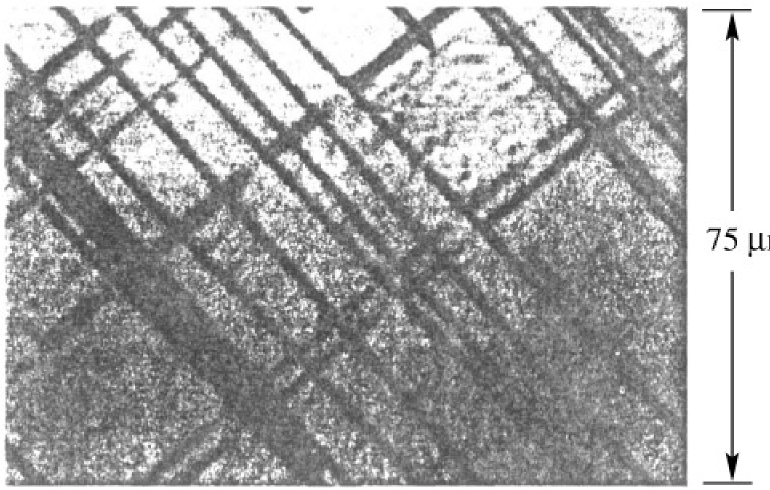

Fig. 6.13. Cathodoluminescence image of a 0.35 µm thick $Ga_{0.95}In_{0.05}As$ layer grown on a GaAs substrate. The dark lines forming a cross-hatch pattern are due to misfit dislocations (after Fitzgerald *et al*., 1989).

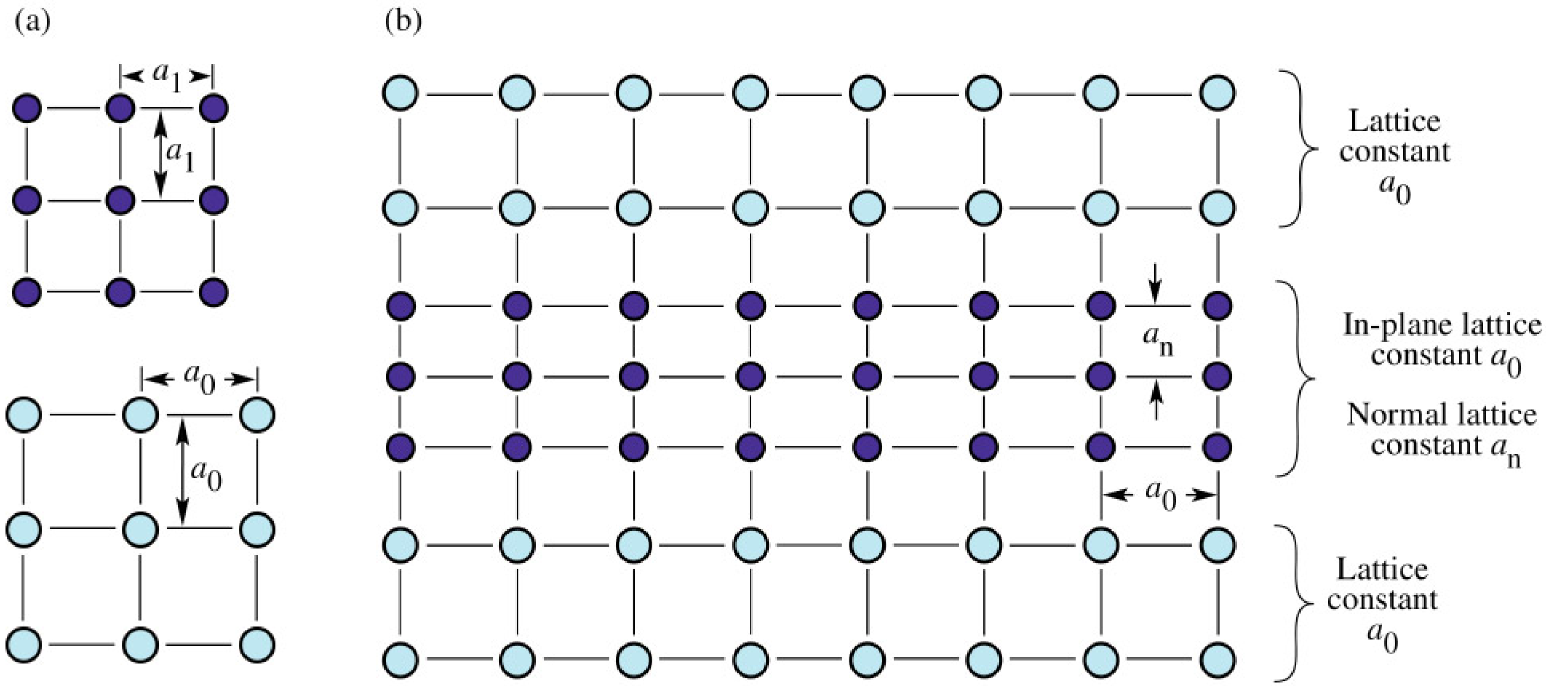

Fig. 6.14. (a) Illustration of two cubic-symmetry crystals with equilibrium lattice constant a_1 and a_0. (b) Illustration of a thin, coherently strained crystal layer with equilibrium lattice constant a_1 sandwiched between two semiconductors with a equilibrium lattice constant a_0. The coherently strained layer assumes an in-plane lattice constant a_0 and a normal lattice constant a_n.

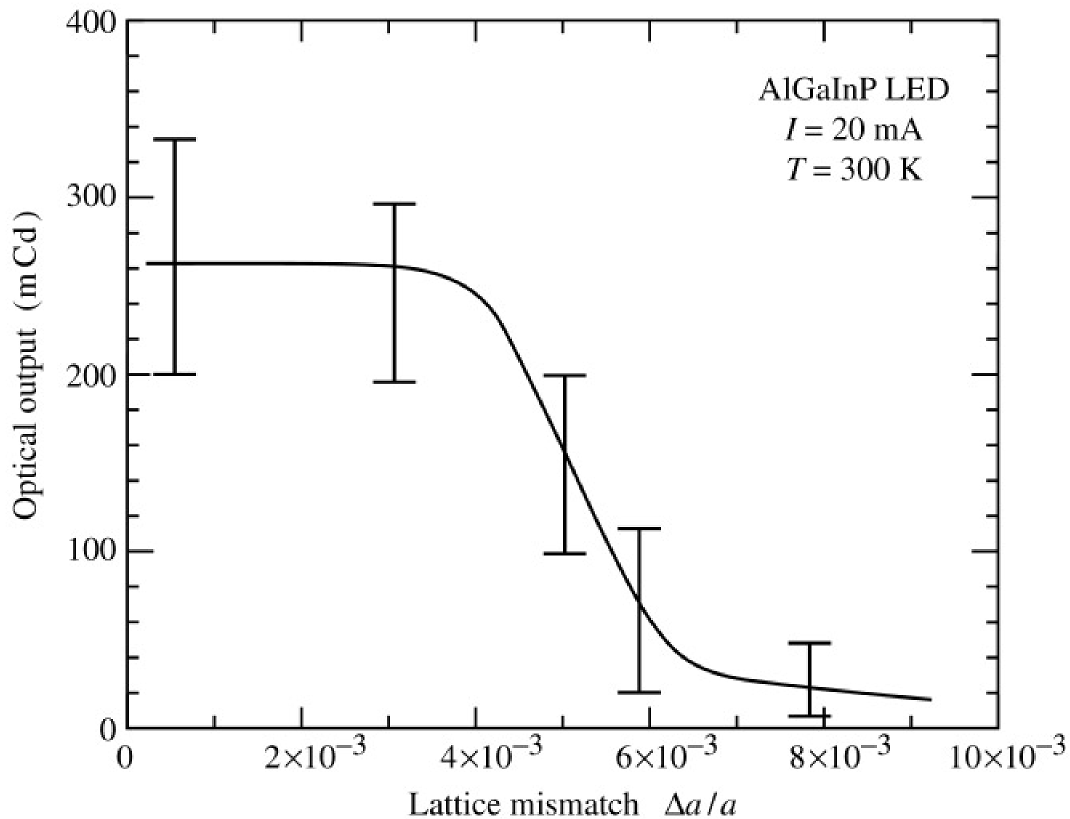

Fig. 6.15. Optical output intensity of an AlGaInP LED driven with an injection current of 20 mA versus lattice mismatch between the AlInGaP active region and the GaAs substrate (after Watanabe and Usui, 1987).

7

High extraction efficiency structures

Absorption of below-bandgap light in semiconductors

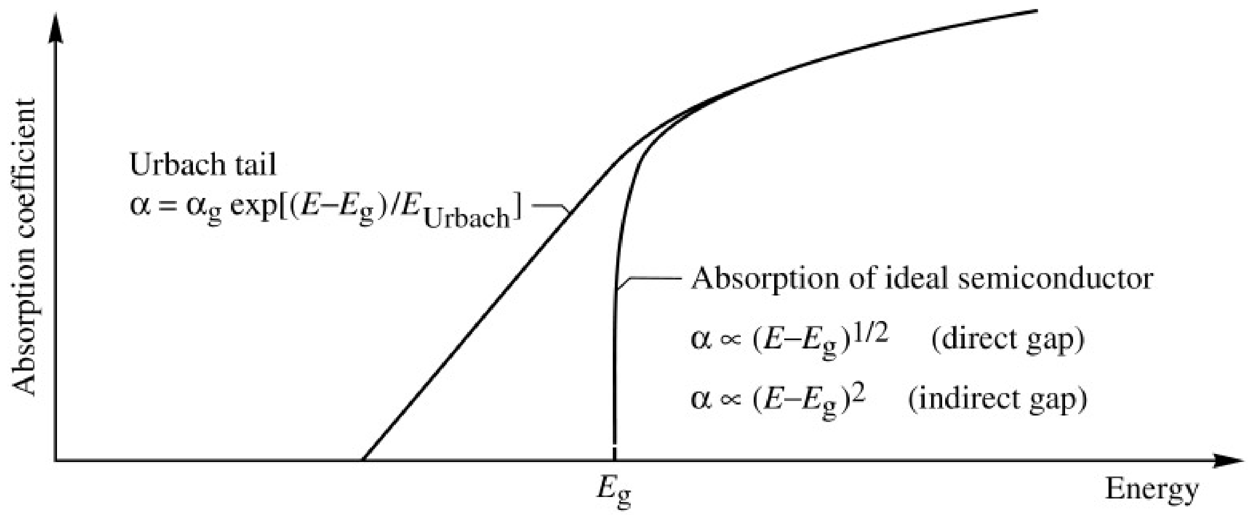

Fig. 7.1. Absorption coefficient of a semiconductor. No light is absorbed in an idealized semiconductor for photon energies below the bandgap. The below-bandgap absorption in a real semiconductor can be described by the "Urbach tail".

Double heterostructures are optically transparent

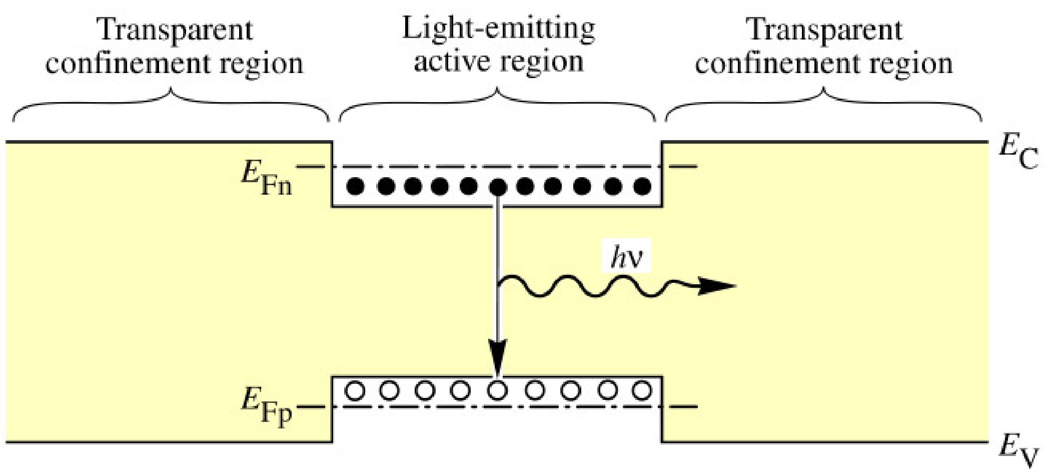

Fig. 7.2. Double heterostructure (DH) with optically transparent confinement regions. Reabsorption in the active region is unlikely due to the high carrier concentration in the active region and the resultiung Burstein-Moss shift of the absorption edge.

Shaping of LED dies

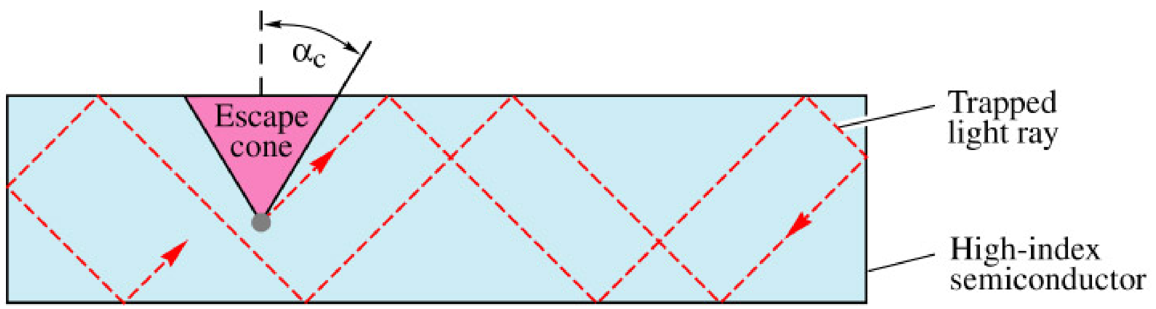

Fig. 7.3. Illustration of "trapped light" that cannot escape from a cube-shaped semiconductor for emission angles larger than α_c due to total internal reflection.

LED die structures with high extraction efficiency

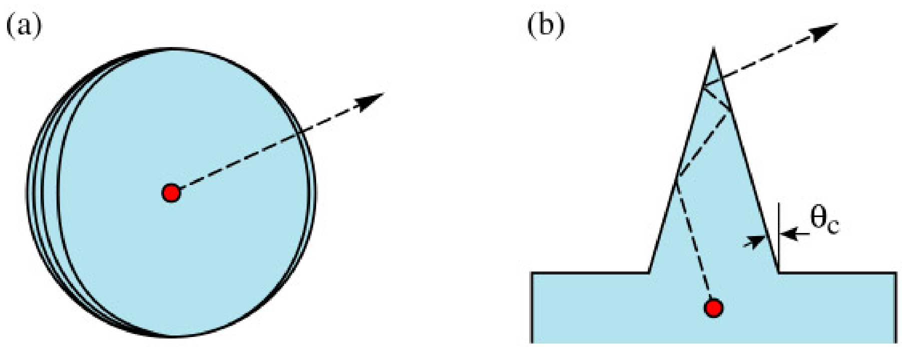

Fig. 7.4. Schematic illustration of different geometric shapes for LEDs with perfect extraction efficiency. (a) Spherical LED with point-like light-emitting region in the center of the sphere. (b) Cone-shaped LED.

Rectangular parallelepiped versus cylinder

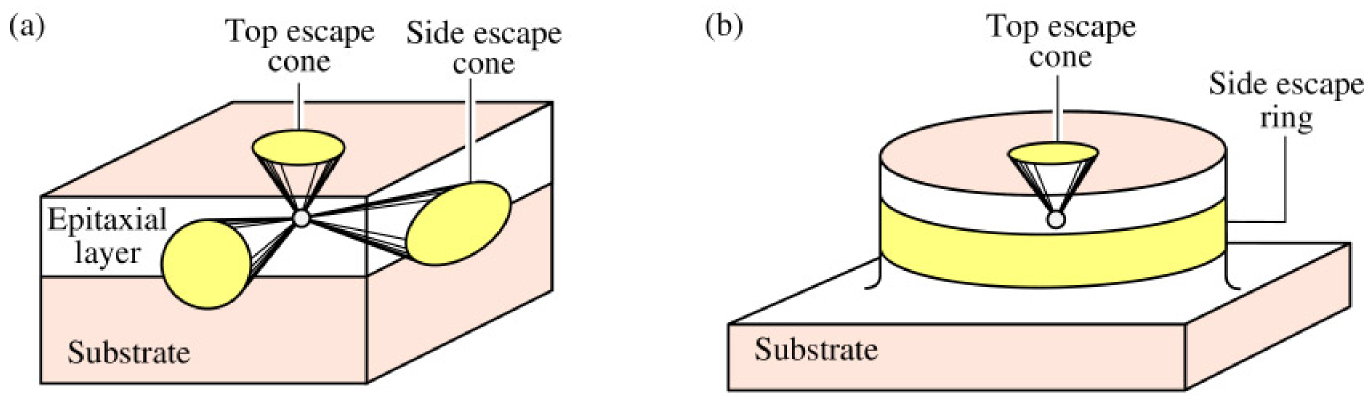

Fig. 7.5. Illustration of different geometric shapes of LEDs. (a) Rectangular parallelepipedal LED dice with a total of six escape cones. (b) Cylindrical LED with top escape cone and side escape ring.

Truncated inverted pyramid (TIP) LED

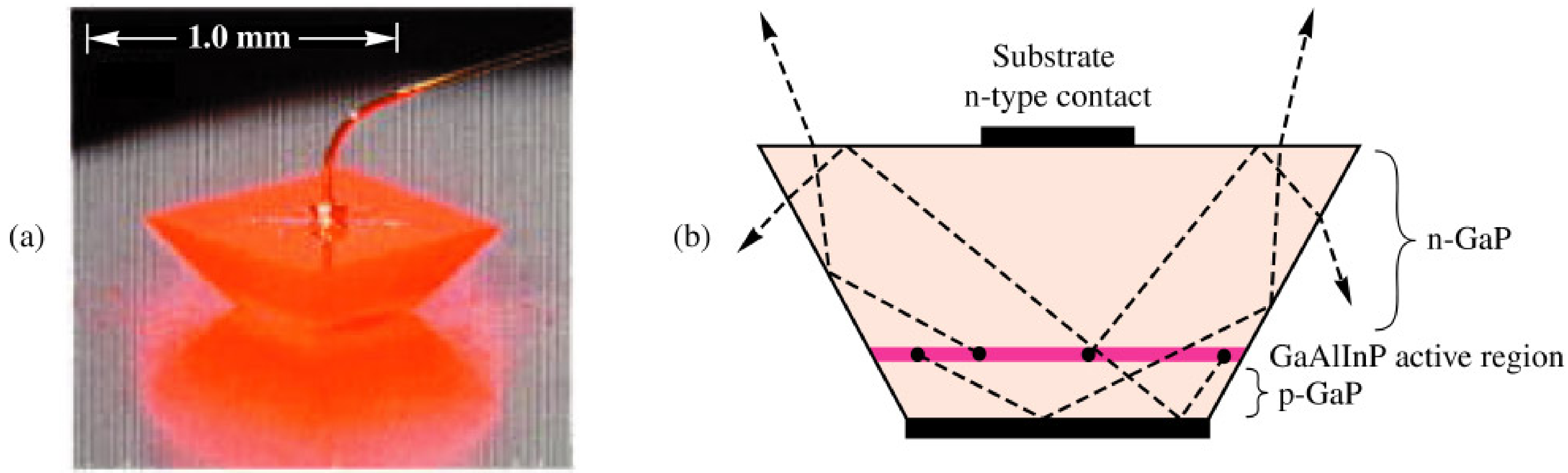

Fig. 7.6. Truncated inverted pyramid (TIP) AlInGaP/GaP LED. (a) LED driven by an electrical injection current. (b) Schematic diagram of the LED illustrating the enhanced light extraction efficiency (after Krames *et al*., 1999).

Effect of current spreading layer

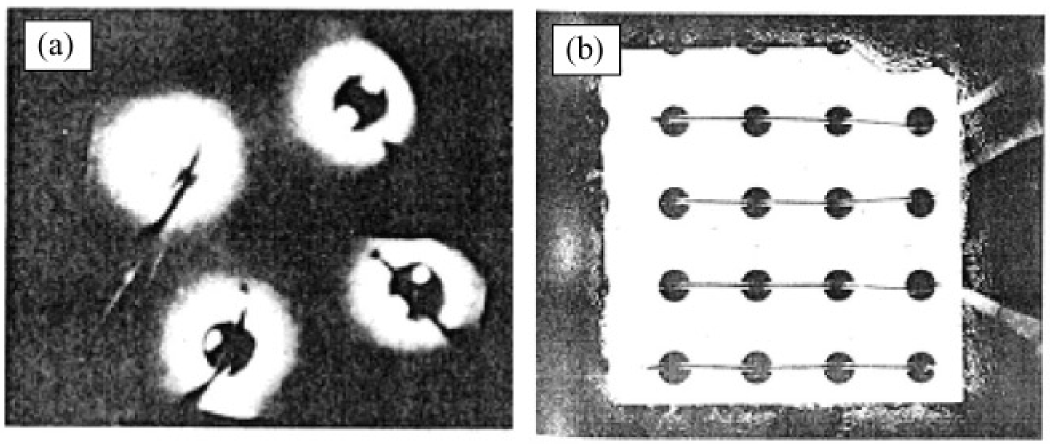

Fig. 7.8. Effect of current spreading layer on LED light output. (a) Top view of LED without current spreading layer. Light emission occurs only near the perimeter of the contact. (b) Top view of LED with current spreading layer (after Nuese *et al*., 1969).

Current spreading layer

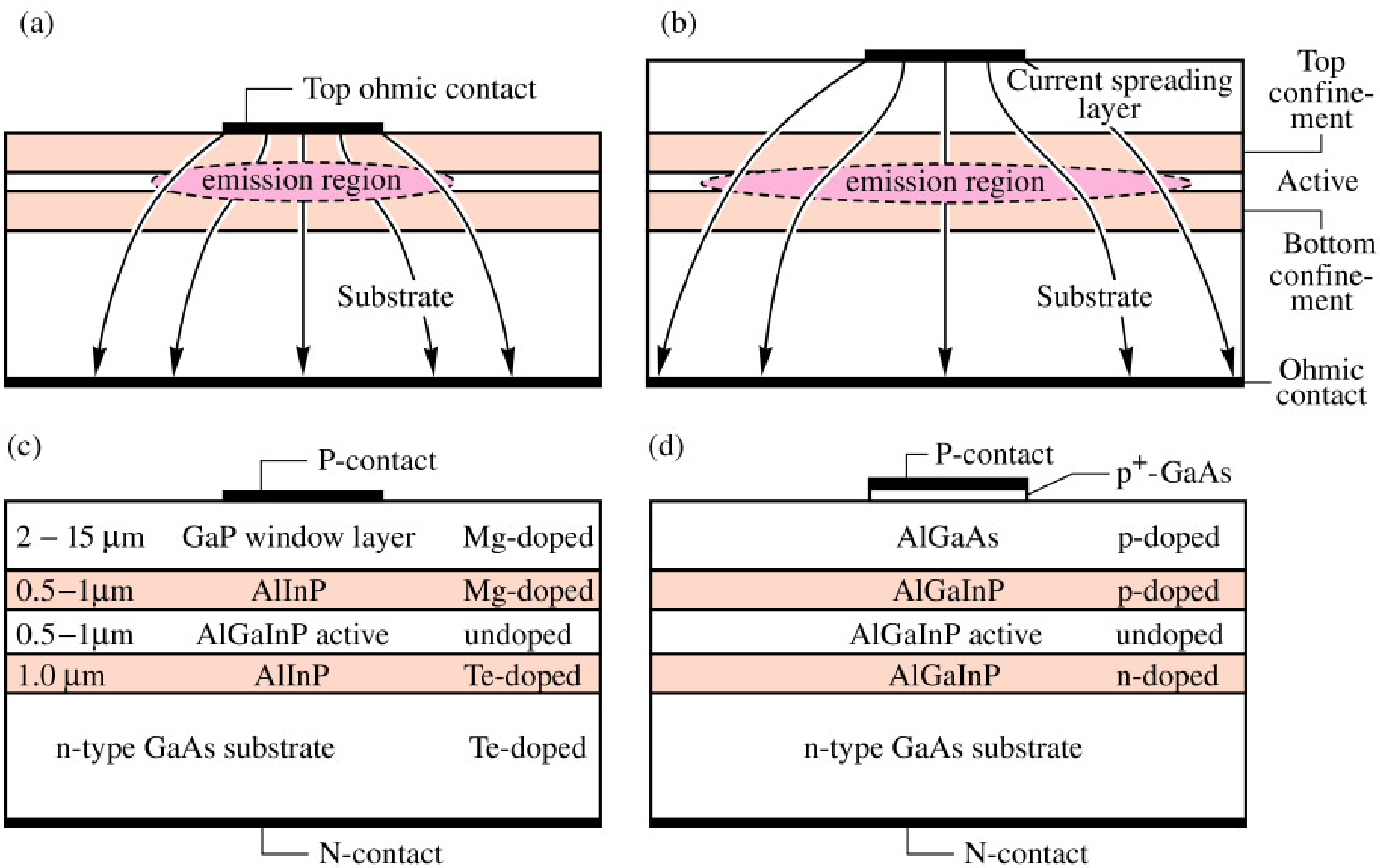

Fig. 7.9. Current spreading structures in high-brightness AlGaInP LEDs. Illustration of the effect of a current spreading layer for LEDs (a) without and (b) with a spreading layer on the light extraction efficiency. (c) GaP current spreading structure (Fletcher *et al.*, 1991). (d) AlGaAs currect spreading structure (Sugawara *et al.*,1992).

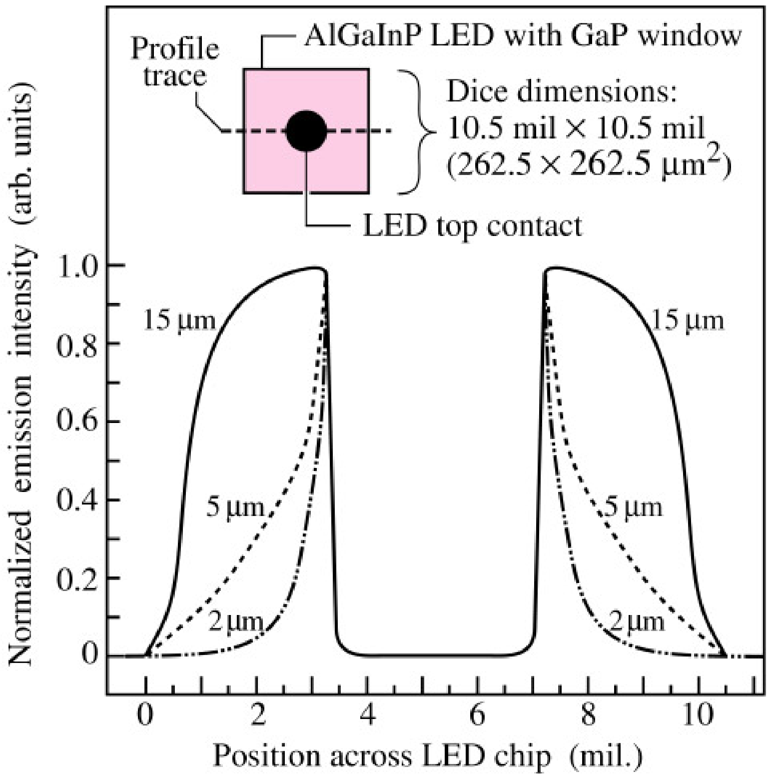

Fig. 7.10. The effect of GaP window thickness on current spreading is illustrated by surface light emission intensity profiles for three different AlGaInP LED chips with window layer thicknesses of 2, 5, and 15 μm. The profile is indicated by the dashed line in the inset. The dip in the middle of the profiles is due to the opaque ohmic contact pad. A microscope fitted with a video camara was used in the measurements (after Fletcher *et al.*, 1991a).

Theory of current spreading

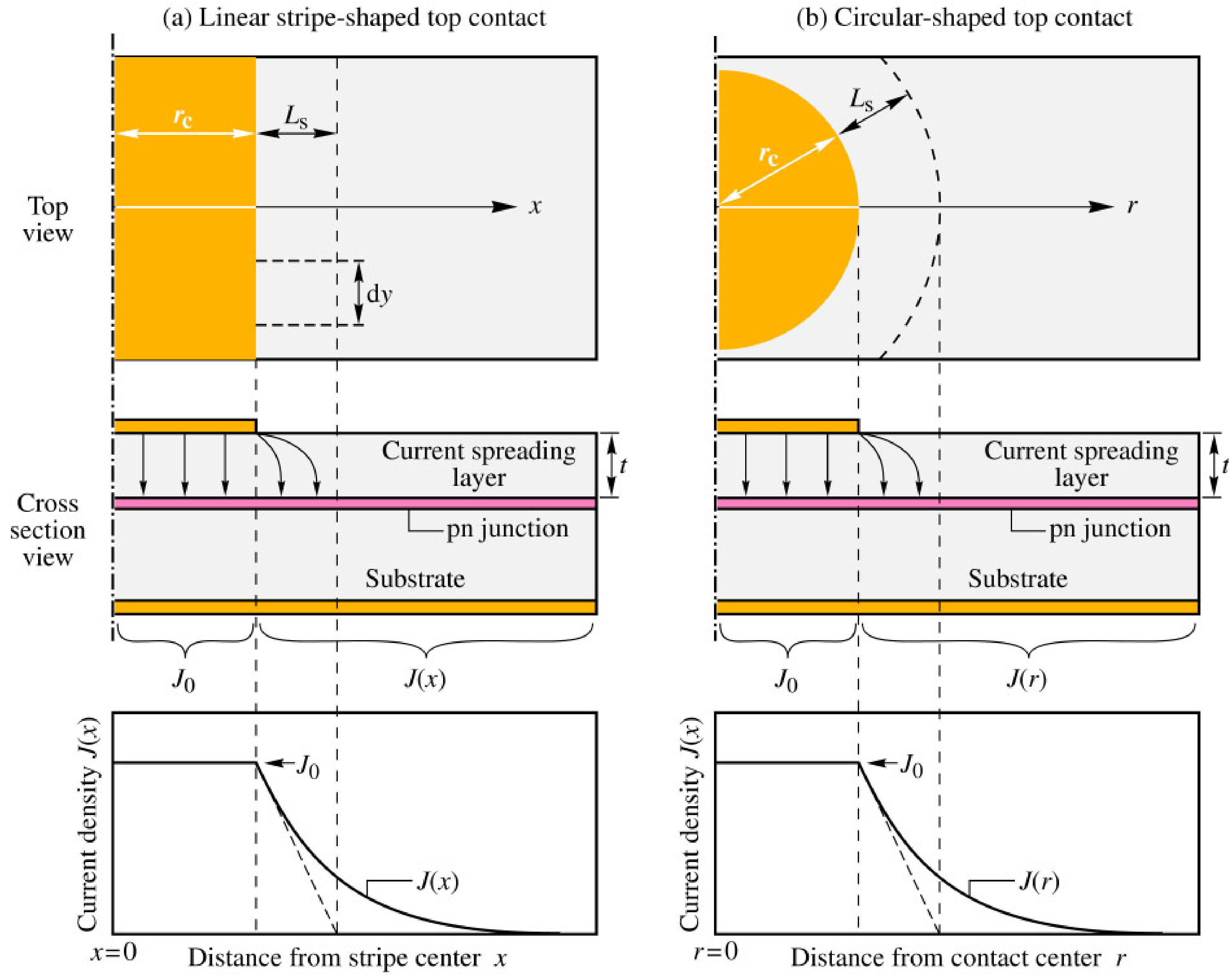

Fig. 7.13. Schematic illustration of current spreading in structures with different top contact geometries. (a) Linear stripe contact geometry. (b) Circular contact geometry.

Theory of current spreading

Current spreading length

$$L_s = \sqrt{\frac{t\, n_{\text{ideal}}\, kT}{\rho\, J_0\, e}}$$

$$t = \rho\, L_s^{\,2}\, J_0 \frac{e}{n_{\text{ideal}}\, kT}$$

t = thickness of current spreading layer

Current crowding in LEDs on insulating substrates

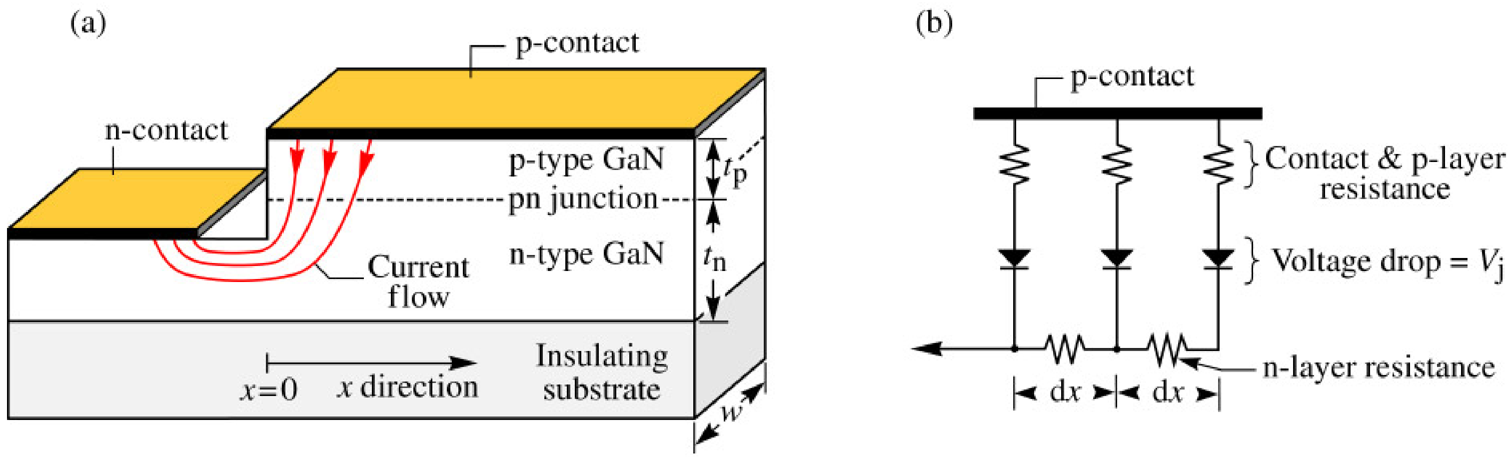

Fig. 7.14. (a) Illustration of current spreading in a mesa-structure GaN-based LED grown on an insulating or semi-insulating substrate. (b) Equivalent circuit consisting of n-type and p-type layer resistances, p-type contact resistance, and ideal diodes representing the pn junction.

Theory of current crowding in LEDs on insulating substrates

s

$$J(x) \quad = \quad J(0)\exp\left(-x/L_{\mathrm{s}}\right)$$

$$L_{\mathrm{s}} \quad = \quad \sqrt{(\rho_{\mathrm{c}} + \rho_{\mathrm{p}} t_{\mathrm{p}})\; t_{\mathrm{n}} \;/\; \rho_{\mathrm{n}}}$$

L_{s} current spreading
length

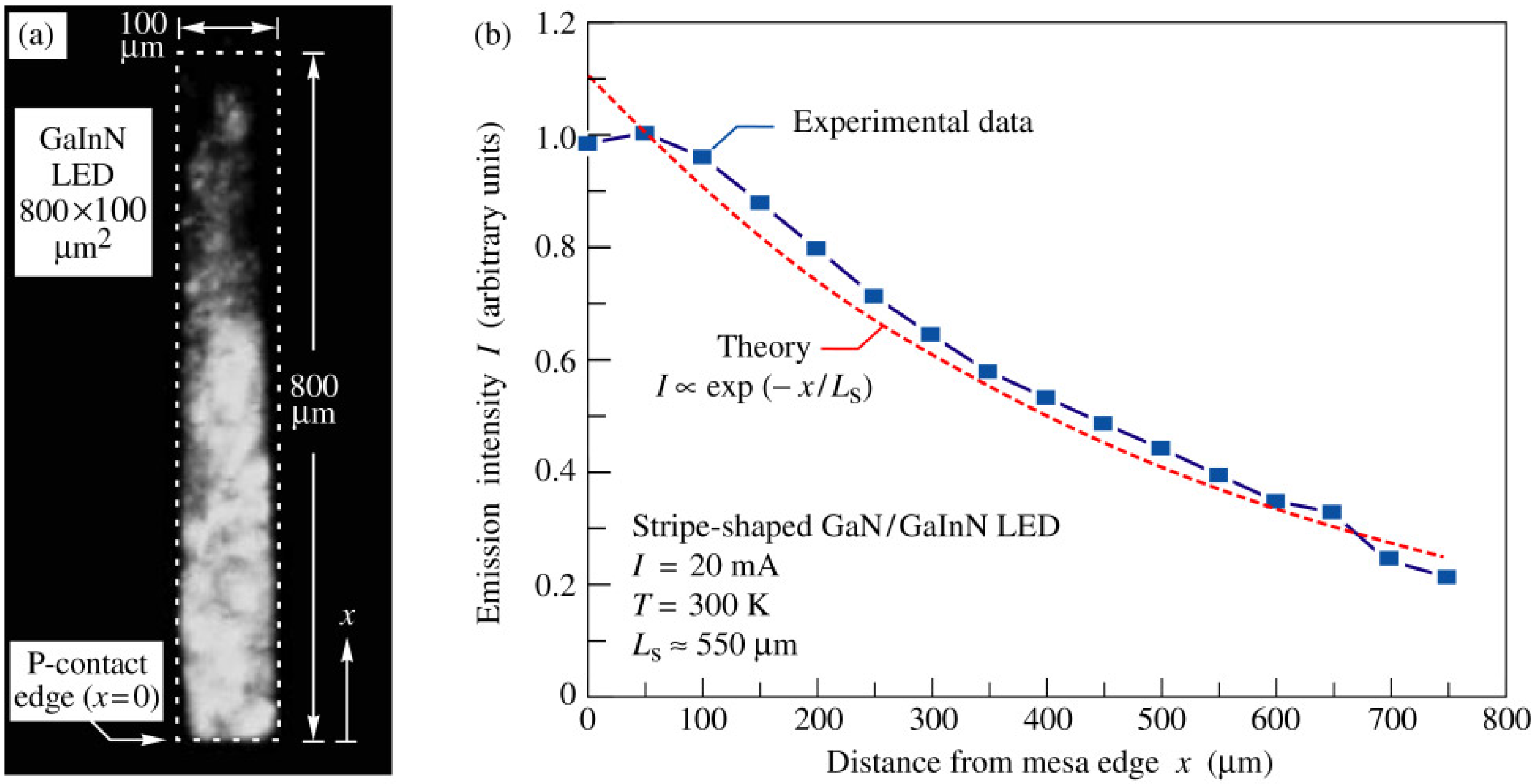

Fig. 7.15. (a) Micrograph of optical emission from mesa-structure GaInN / GaN LED grown on an insulating sapphire substrate. The LED has a stripe-shaped 800 µm × 100 µm p-type contact. (b) Theoretical and experimental emission intensity versus distance from the mesa edge (after Guo and Schubert, 2001).

Cross-shaped contacts and other contact geometries

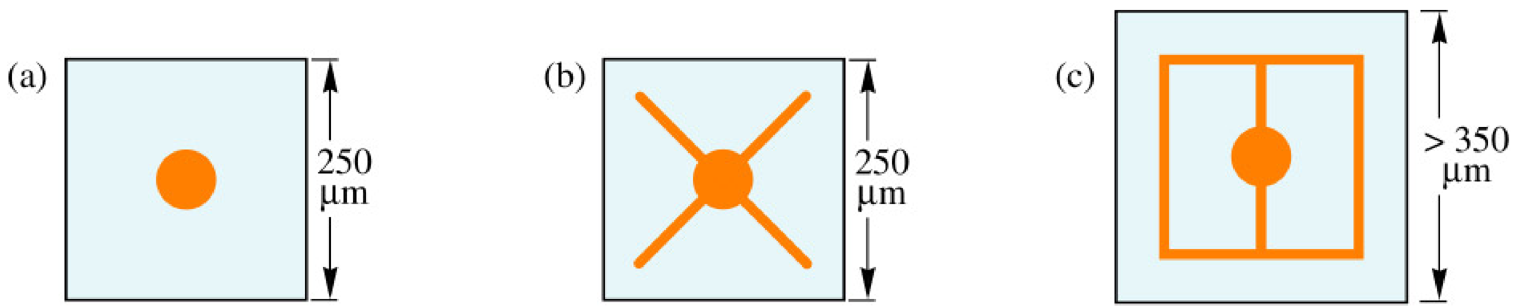

Fig. 7.16. Top view on LED dice with (a) a circular contact also serving as bond pad and (b) a cross-shaped contact with circular bond pad. (c) Typical contact geometry used for larger LED dies.

Transparent substrate technology

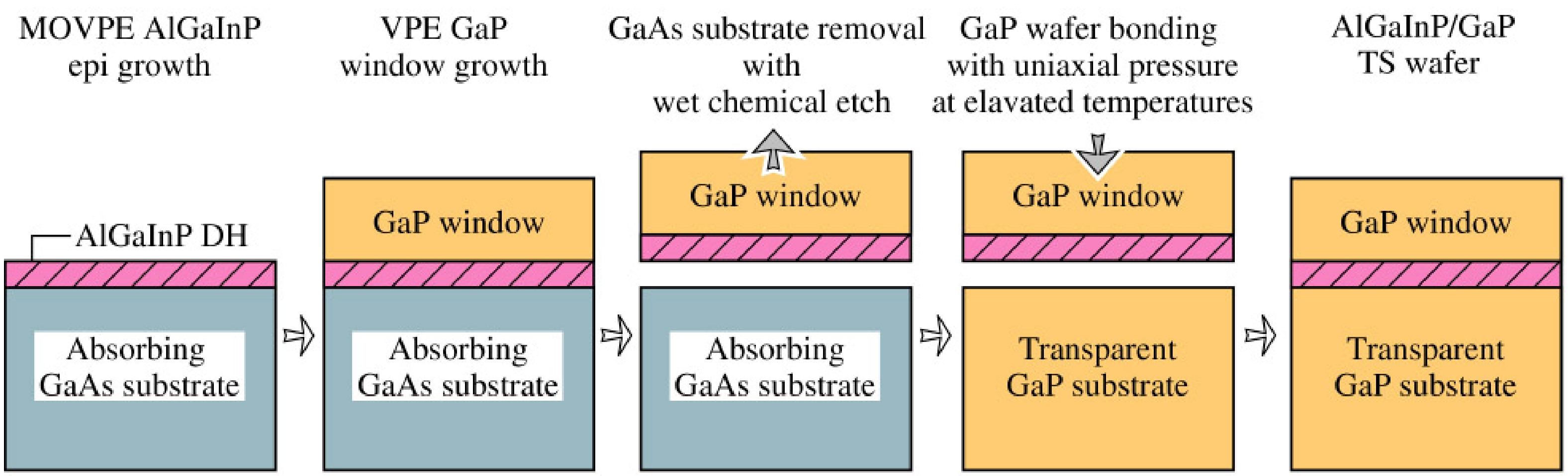

Fig. 7.17. Schematic fabrication process for wafer-bonded tarnsparent substrate (TS) AlGaInP / GaP LEDs. After the selective removal of the original GaAs substrate, elevated temperature and uniaxial pressure are applied, resulting in the formation of a single TS LED wafer (adopted from Kish *et al*., 1994).

Small forward-voltage penalty for TS technology

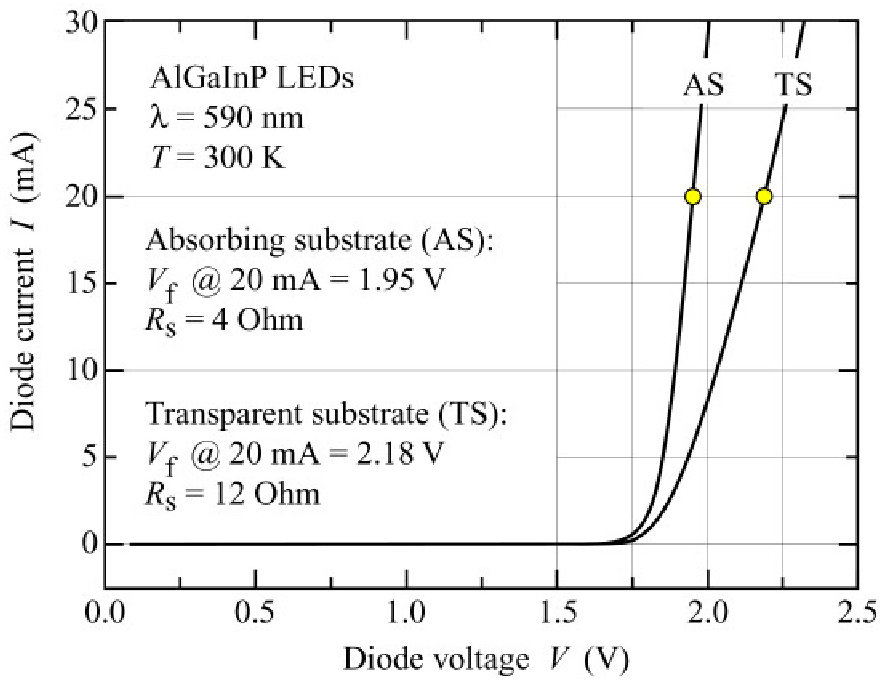

Fig. 7.18. Current-voltage characteristic, forward voltage, and series resistance of absorbing-substrate (GaAs) and transparent-substrate (GaP) LEDs with AlGaInP active regions.

AS versus TS technology

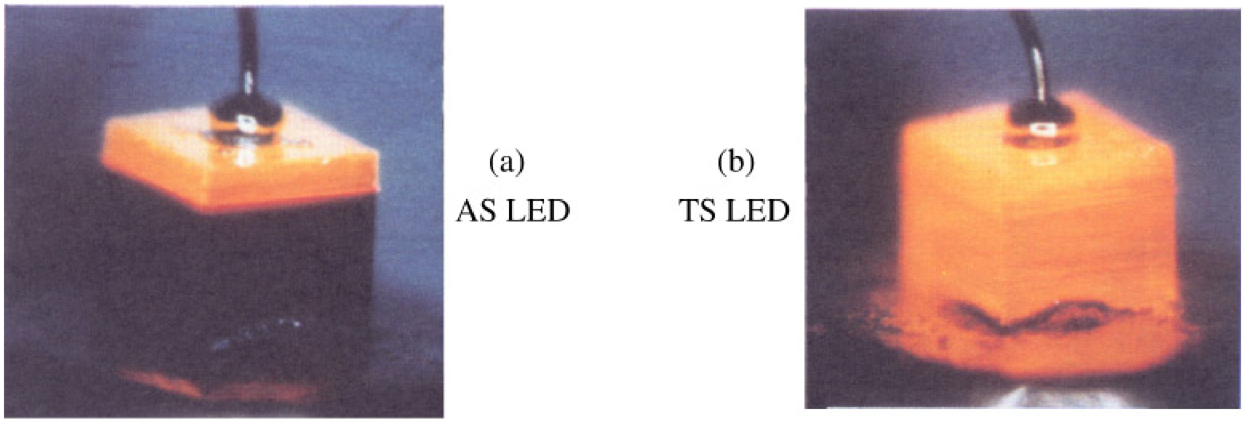

Fig. 7.19. (a) Amber GaP/AlGaInP/GaAs LED with GaP window layer and absorbing GaAs substrate (AS). (b) Amber GaP/AlGaInP/GaP LED with GaP window layer and transparent GaP substarte (TS) fabricated by a wafer bonding. Conductive Ag-loaded die-attach epoxy can be seen at the bottom of the TS LED (after Kish and Fletcher, 1997).

$$R = \frac{(\bar{n}_{\mathrm{s}} - \bar{n}_{\mathrm{air}})^2}{(\bar{n}_{\mathrm{s}} + \bar{n}_{\mathrm{air}})^2}$$

Dielectric material	***Refractive index***	***Transparency range***
SiO_2 (Silica)	1.45	> 0.15 μm
Al_2O_3 (Alumina)	1.76	> 0.15 μm
TiO_2 (Titania)	2.50	> 0.35 μm
Si_3N_4 (Silicon nitride)	2.00	> 0.25 μm
ZnS (Zinc sulfide)	2.29	> 0.34 μm
CaF_2 (Calcium fluoride)	1.43	> 0.12 μm

Table 7.1. Refractive index and transparency range of common dielectrics suitable as anti-reflection (AR) coatings (after Palik, 1998)

Epoxy dome

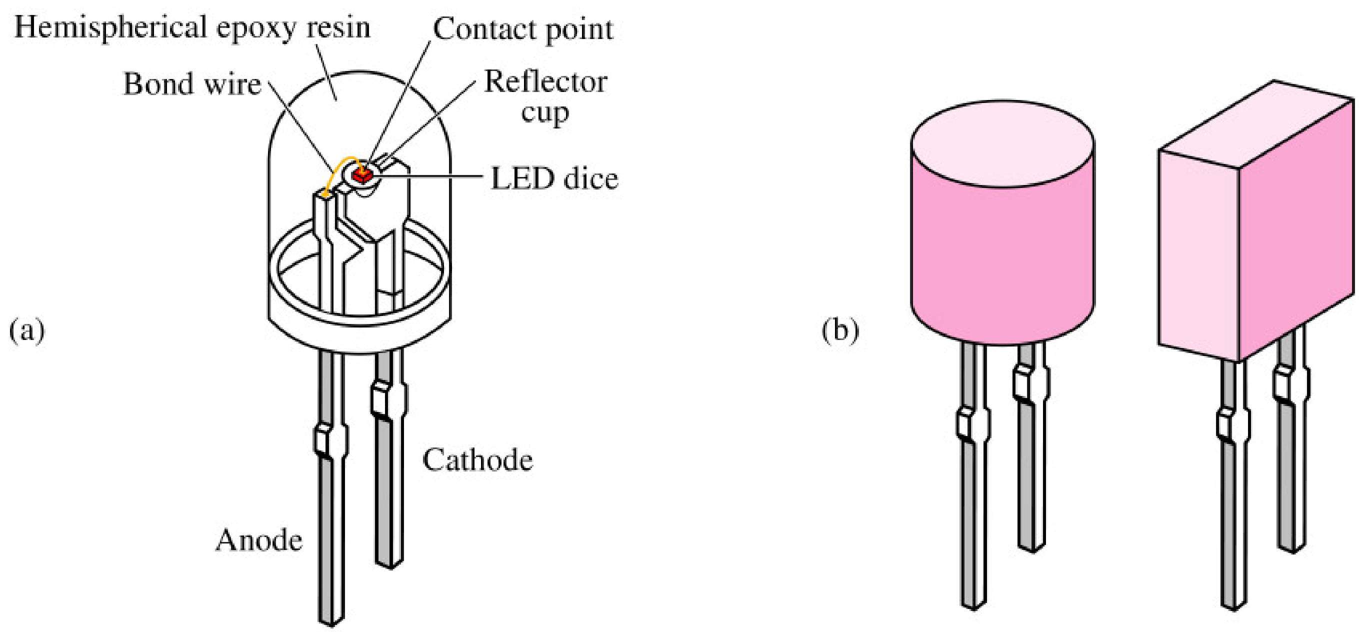

Fig. 7.21. Typical packages of LEDs. (a) LED with hemispherical epoxy dome. (b) LEDs with cylindrical and rectangular epoxy packages.

Distributed Bragg reflectors

$$t_{l,h} \;=\; \lambda_{l,h} / 4 \;=\; \lambda_0 / (4\, \bar{n}_{l,h})$$

… valid for normal incidence

$$t_{l,h} \;=\; \lambda_{l,h} / (\, 4 \cos\Theta_{l,h}\,) \;=\; \lambda_0 / (\, 4\, \bar{n}_{l,h} \cos\Theta_{l,h}\,)$$

… valid for oblique incidence

LED with DBR

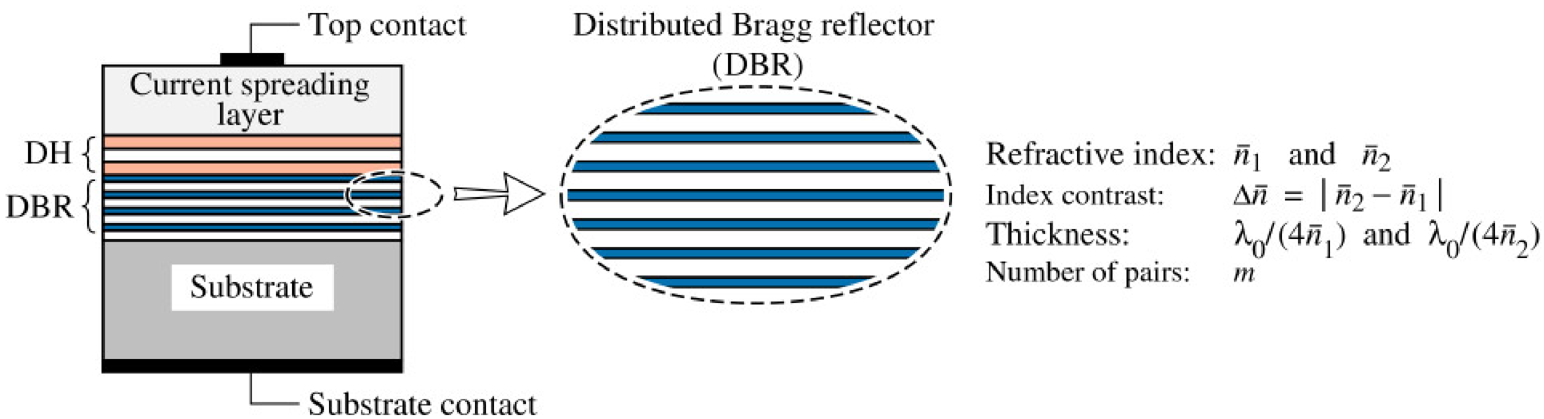

Fig. 7.22. LED with distributed Bragg reflector (DBR) located between substrate and lower confinement layer.

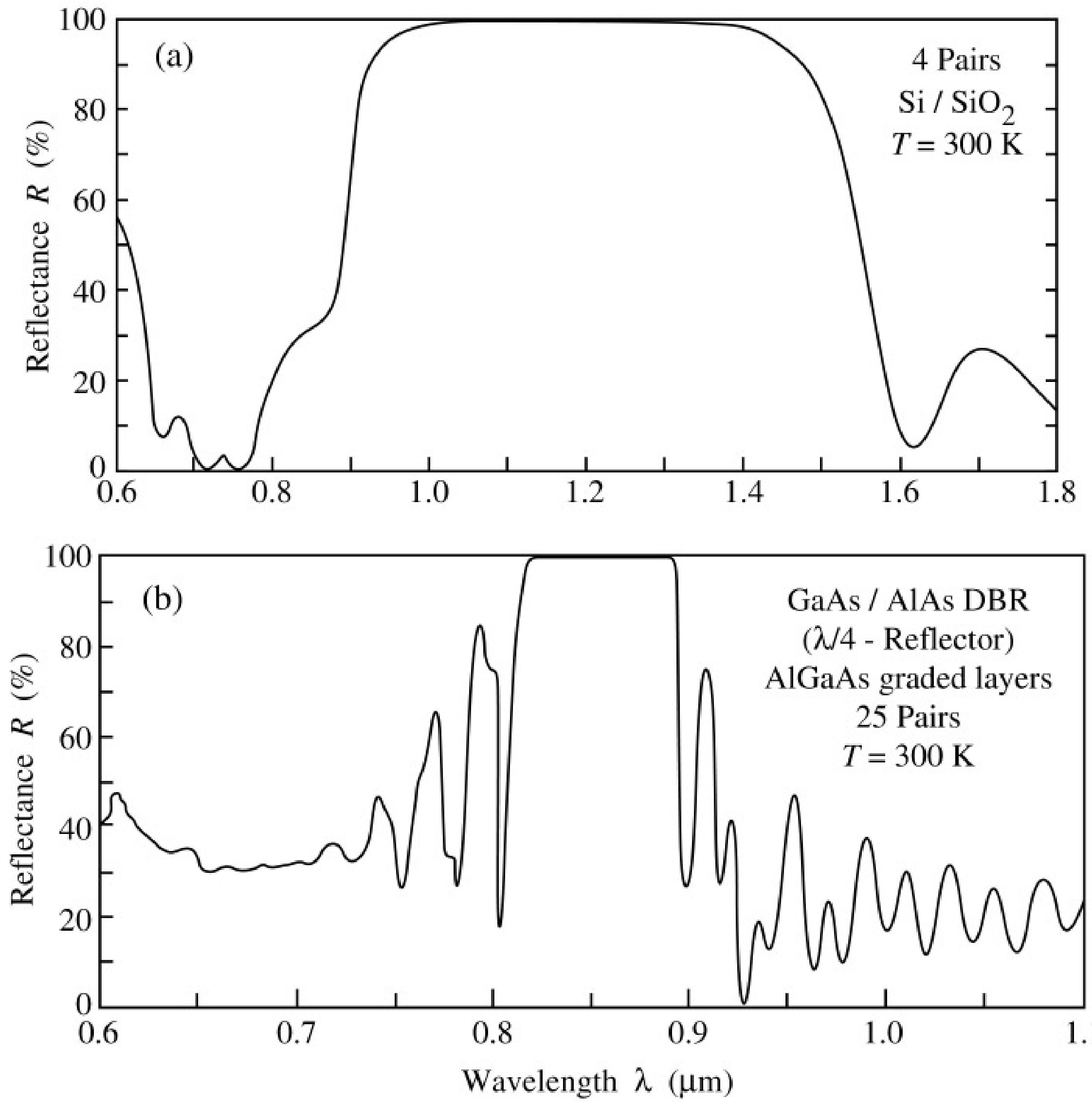

Fig. 7.23. Reflectance of two distributed Bragg reflectors (DBRs) versus wavelength. (a) 4 pair Si-SiO_2 reflector with high index contrast. (b) 25 pair AlAs-GaAs reflector. The high-index-contrast DBR only needs 4 pairs to attain high reflectivity. Note that the stop band of the high-index-contrast DBR is wider as compared to the low-contrast DBR.

Material system	***Bragg wavelength***	$\overline{n}_{\mathrm{l}}$	$\overline{n}_{\mathrm{h}}$	$\Delta\overline{n}$	***Transparency range***
$Al_{0.5}In_{0.5}P$ / GaAs	590 nm	3.13	3.90	0.87	> 870 nm (lossy)
$Al_{0.5}In_{0.5}P$ / $Ga_{0.5}In_{0.5}P$	590 nm	3.13	3.74	0.87	> 649 nm (lossy)
$Al_{0.5}In_{0.5}P$ / $(Al_{0.3}Ga_{0.7})_{0.5}In_{0.5}P$	615 nm	3.08	3.45	0.37	> 592 nm
$Al_{0.5}In_{0.5}P$ / $(Al_{0.4}Ga_{0.6})_{0.5}In_{0.5}P$	590 nm	3.13	3.47	0.34	> 576 nm
$Al_{0.5}In_{0.5}P$ / $(Al_{0.5}Ga_{0.5})_{0.5}In_{0.5}P$	570 nm	3.15	3.46	0.31	> 560 nm
AlAs / GaAs	900 nm	2.97	3.54	0.57	> 870 nm
SiO_2 / Si	1300 nm	1.46	3.51	2.05	> 1106 nm

Table 7.2. Properties of distributed Bragg reflector (DBR) materials used for visible and infrared LED applications. The DBRs marked as ‘lossy’ are absorbing at the Bragg wavelength (data after Adachi, 1990; Adachi *et al*., 1994; Kish and Fletcher, 1997; Babic *et al*., 1999; Palik, 1998).

8

Visible-spectrum LEDs

The GaAsP, GaP, GaAsP:N and GaP:N material system

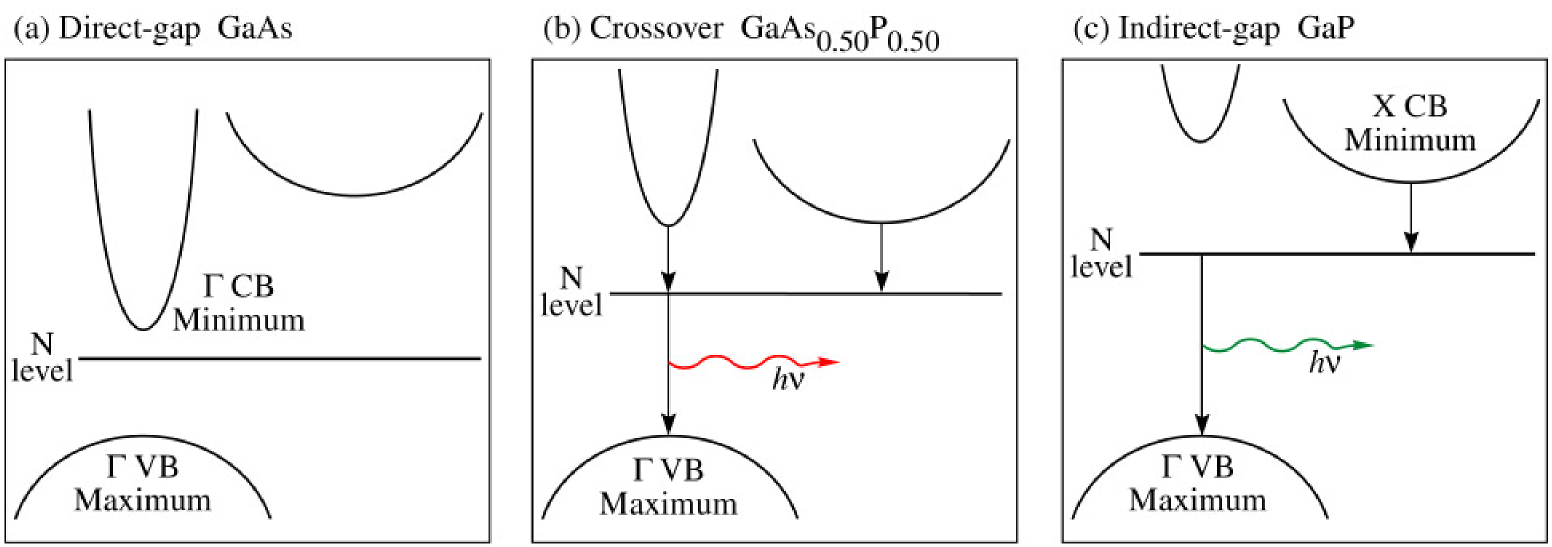

Fig. 8.1. Schematic band structure of GaAs, GaAsP, and GaP. Also shown is the nitrogen level. At a P mole fraction of about 45 - 50 %, the direct-indirect crossover occurs.

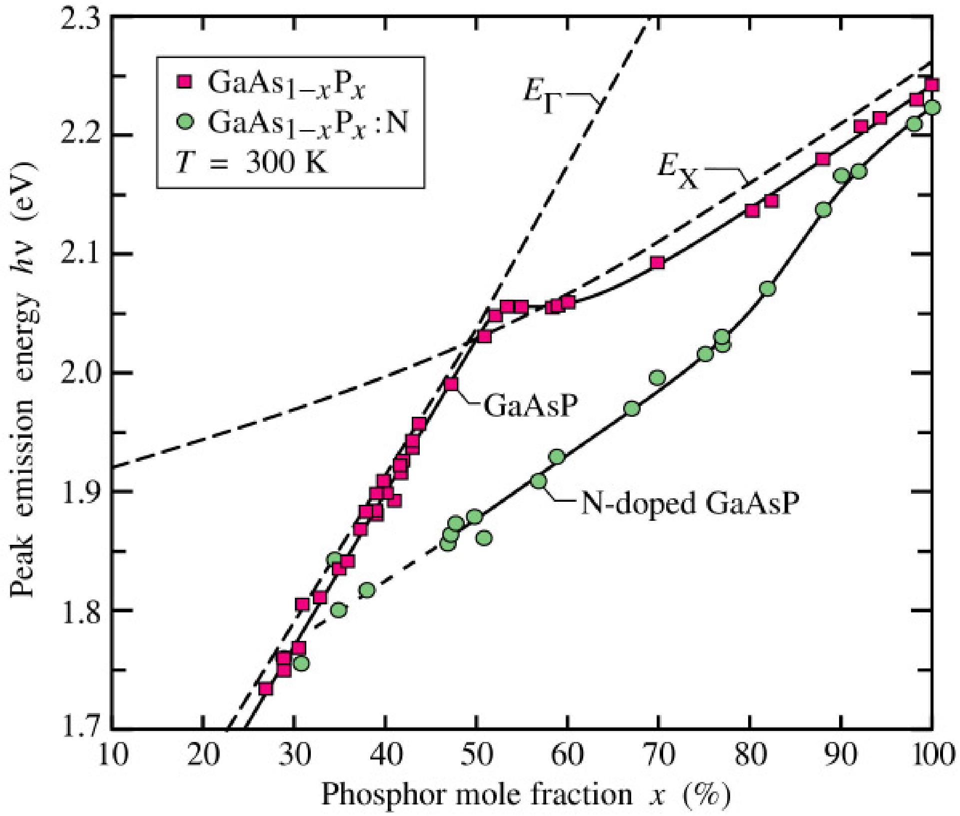

Fig. 8.2. Room temperature peak emission energy versus alloy composition for undoped and nitrogen - doped GaAsP light - emitting diodes injected with a current density of 5 A / cm^2. Also shown is the energy gap of the direct - to - indirect (E_Γ - to - E_X) transition. The direct-indirect crossover occurs at $x \approx 50$ % (after Craford *et al*. 1972).

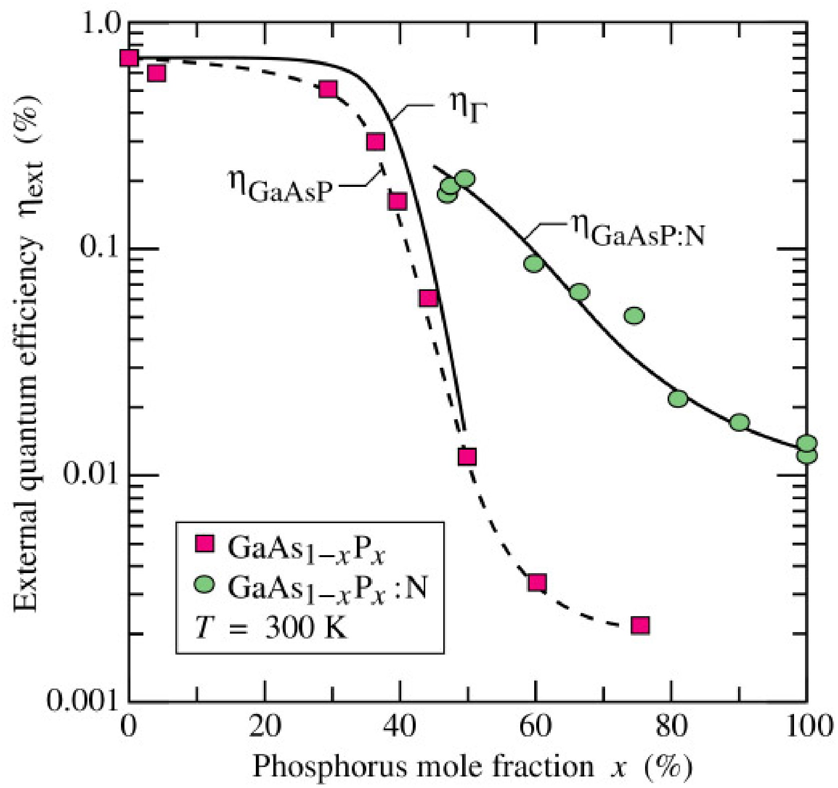

Fig. 8.3. Experimental external quantum efficiency of undoped and N-doped GaAsP versus P mole fraction. Also shown is the calculated direct-gap (Γ) transition efficiency, η_Γ, and the calculated nitrogen (N) related transition efficiency, η_N (solid lines). Note that the nitrogen-related efficiency is higher than the direct-gap efficiency in the indirect bandgap (x > 50 %) regime (after Campbell *et al.*, 1974).

Summary: The GaAsP, GaP, GaAsP:N and GaP:N material system has the fundamental problem of lattice mismatch and is not suitable for high-power LEDs

The AlGaAs / GaAs material system

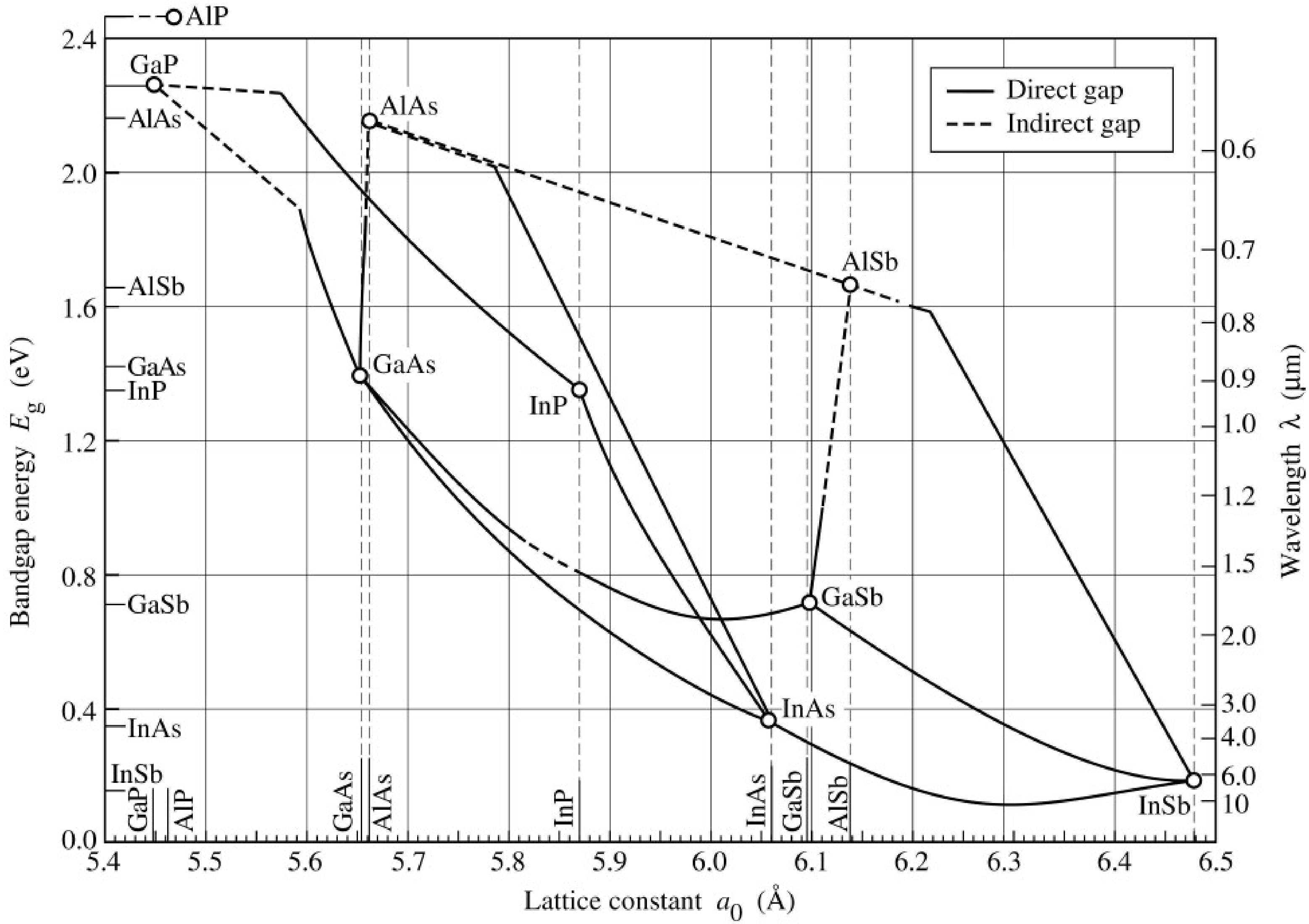

Fig. 8.6. Bandgap energy and lattice constant of various III-V semiconductors at room temperature (adopted from Tien, 1988).

The AlGaInP / GaAs material system

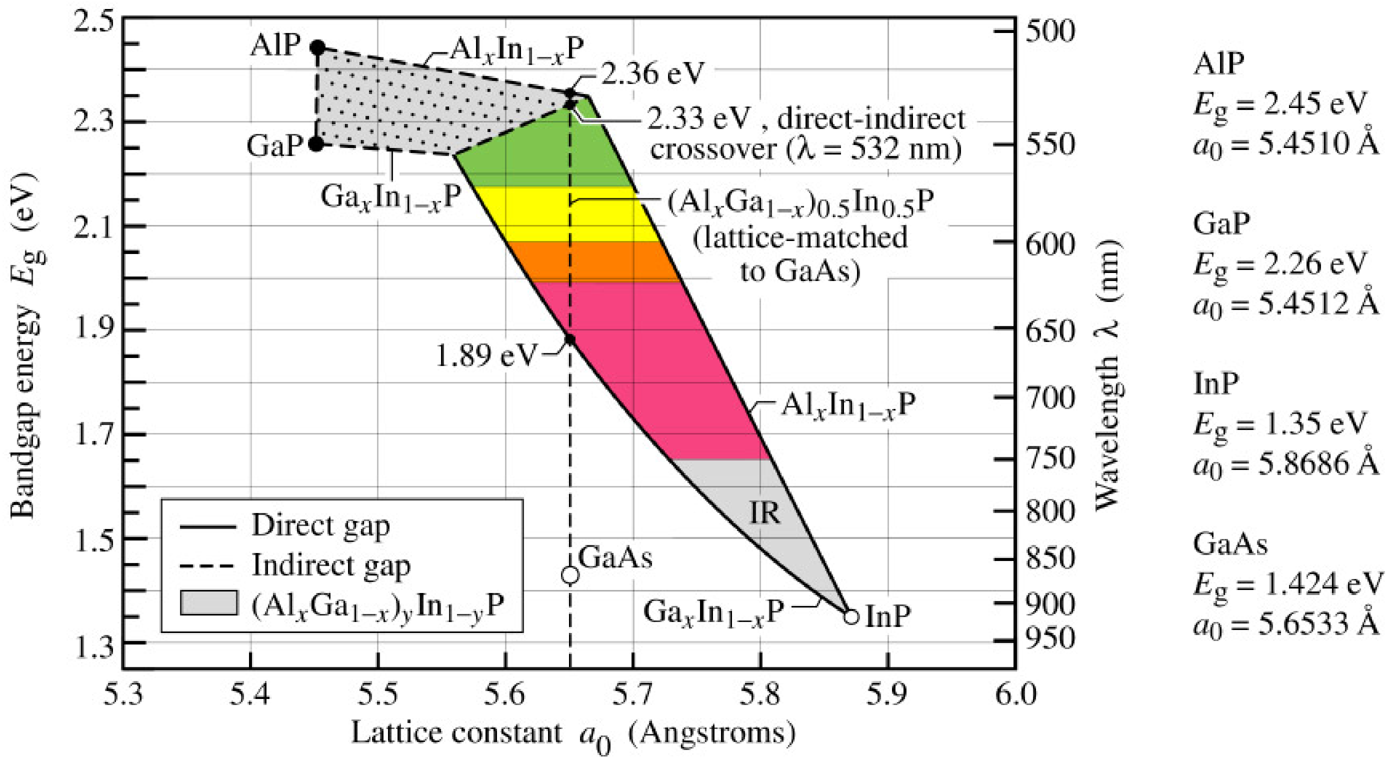

Fig. 8.9. Bandgap energy and corresponding wavelength versus lattice constant of $(Al_xGa_{1-x})_yIn_{1-y}P$ at 300 K. The dashed vertical line shows $(Al_xGa_{1-x})_{0.5}In_{0.5}P$ lattice matched to GaAs (adopted from Chen *et al.*, 1997).

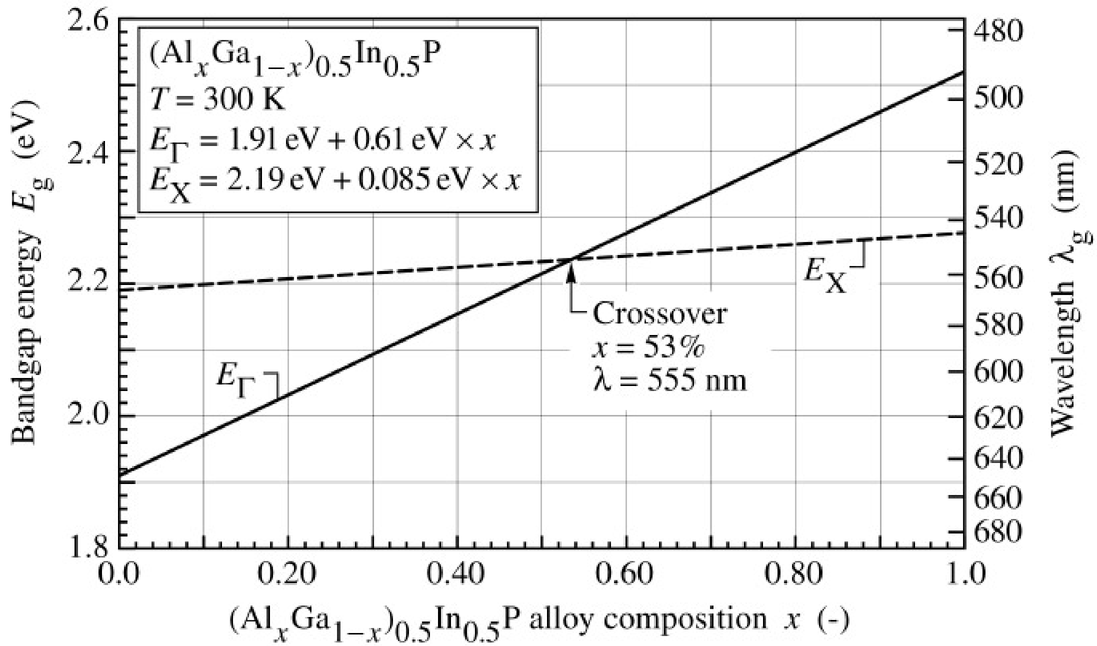

Fig. 8.10. Bandgap energy and emission wavelength of the unordered AlGaInP quaternary semiconductor lattice-matched to GaAs at room temperature. E_Γ denotes the direct gap at the Γ point and E_X denotes the indirect gap at the X point of the Brillouin zone (adopted from Prins *et al*., 1995 and Kish and Fletcher, 1997).

The GaInN material system a

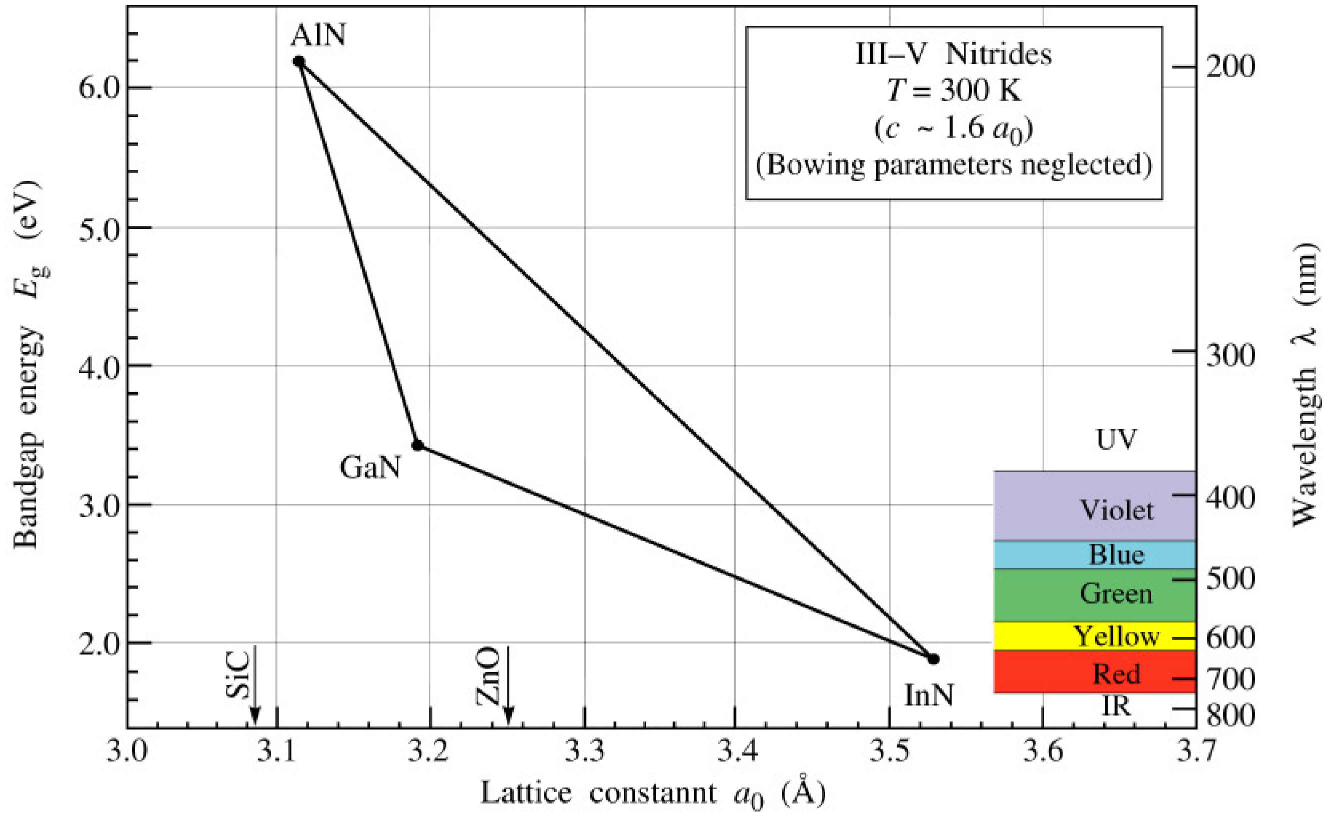

Fig. 8.12. Bandgap energy versus lattice constant of III-V nitride semiconductors at room temperature.

Summary: The GaInN material system is suited for UV, violet, blue, cyan and green high-power LEDs. Efficiency decreases in the green spectral range.

General characteristics of high-brightness LEDs

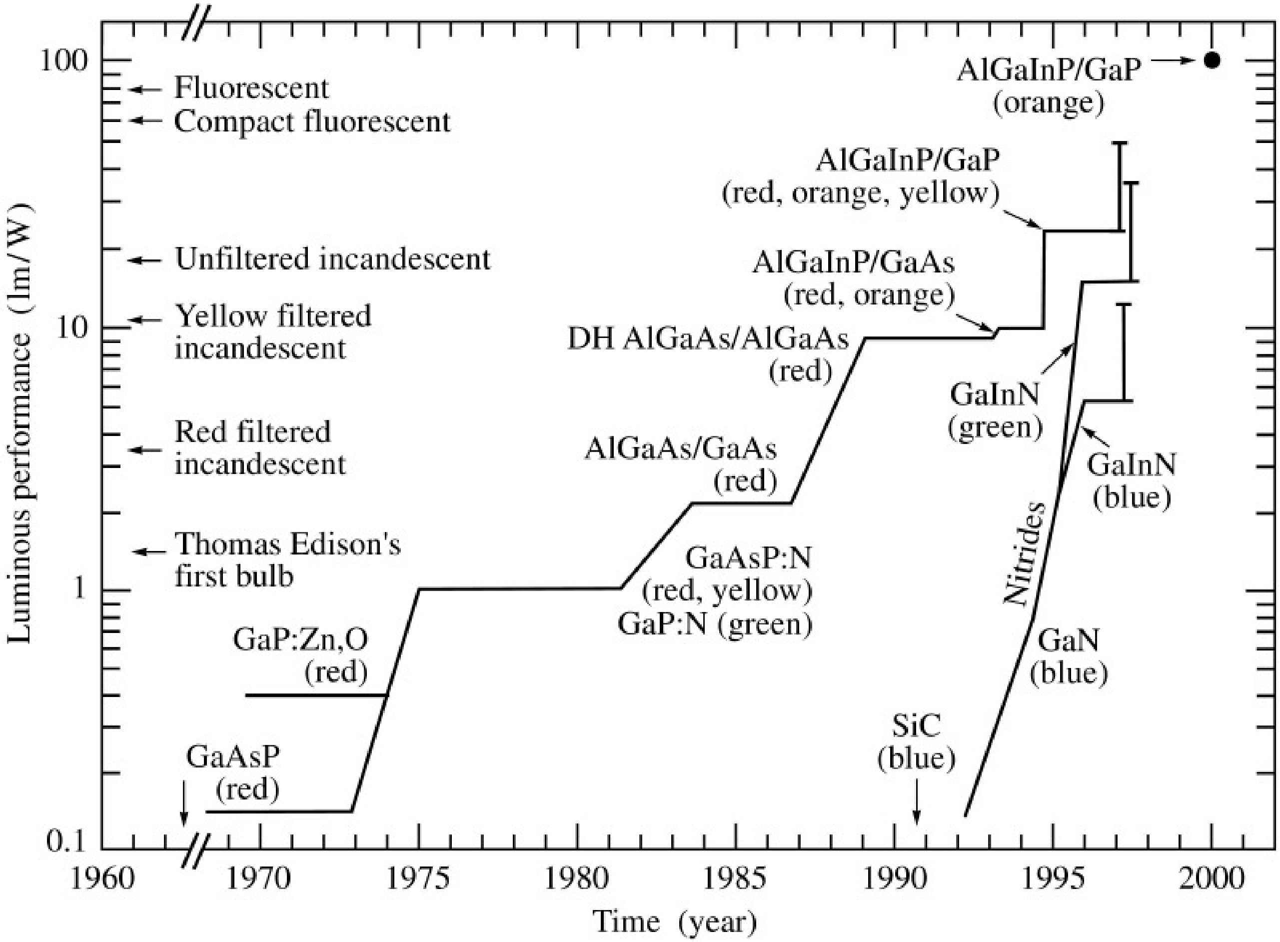

Fig. 8.13. Luminous performance of visible LEDs versus time. Also shown is the luminous performance to other light sources (adopted from Craford, 1997, 1999, updated 2000).

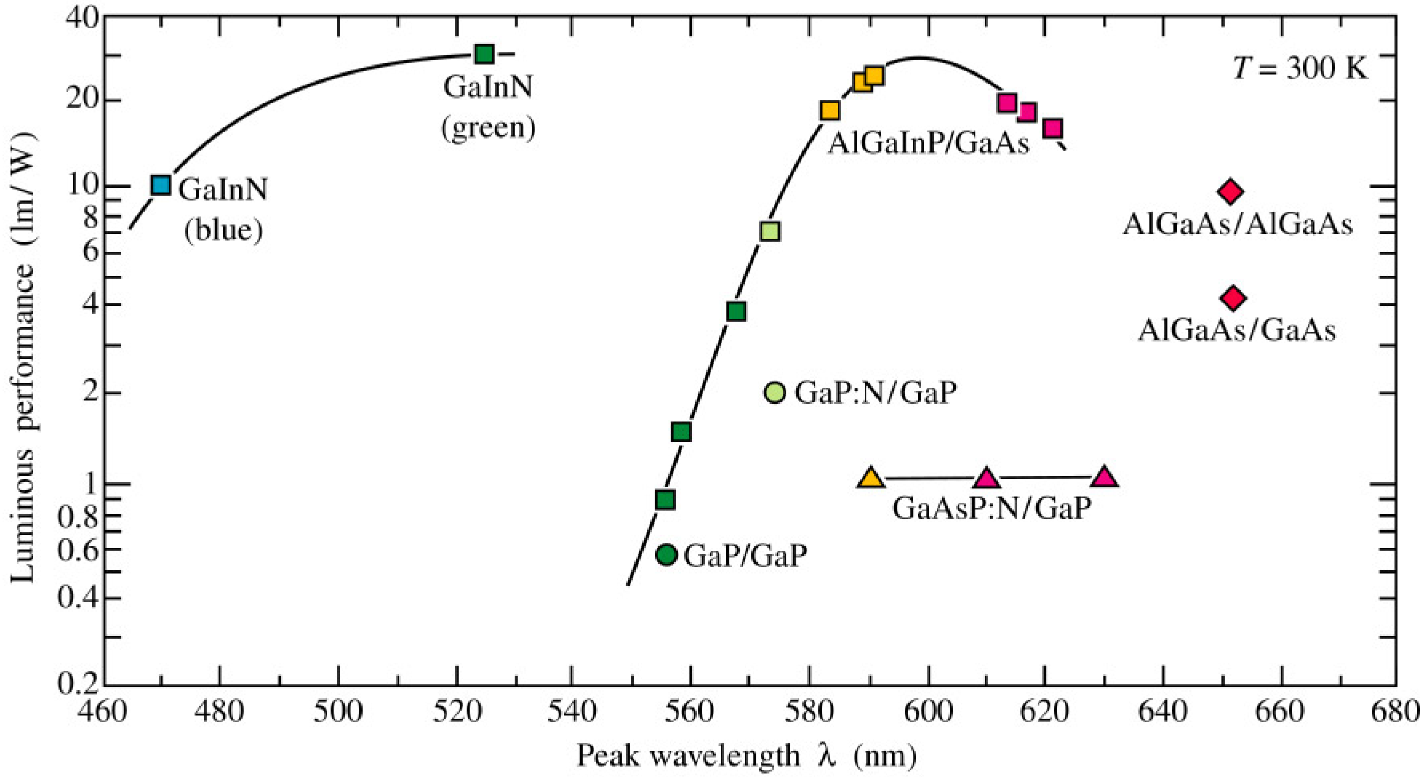

Fig. 8.14. Overview of luminous performance of visible LEDs made from the phosphide, arsenide, and nitride material system (adopted from United Epitaxy Corporation, 1999; updated 2000).

Note: The lack of high-power LEDs at 550 nm is sometimes referred to as the "green gap".

Comparison: Light bulb versus LED

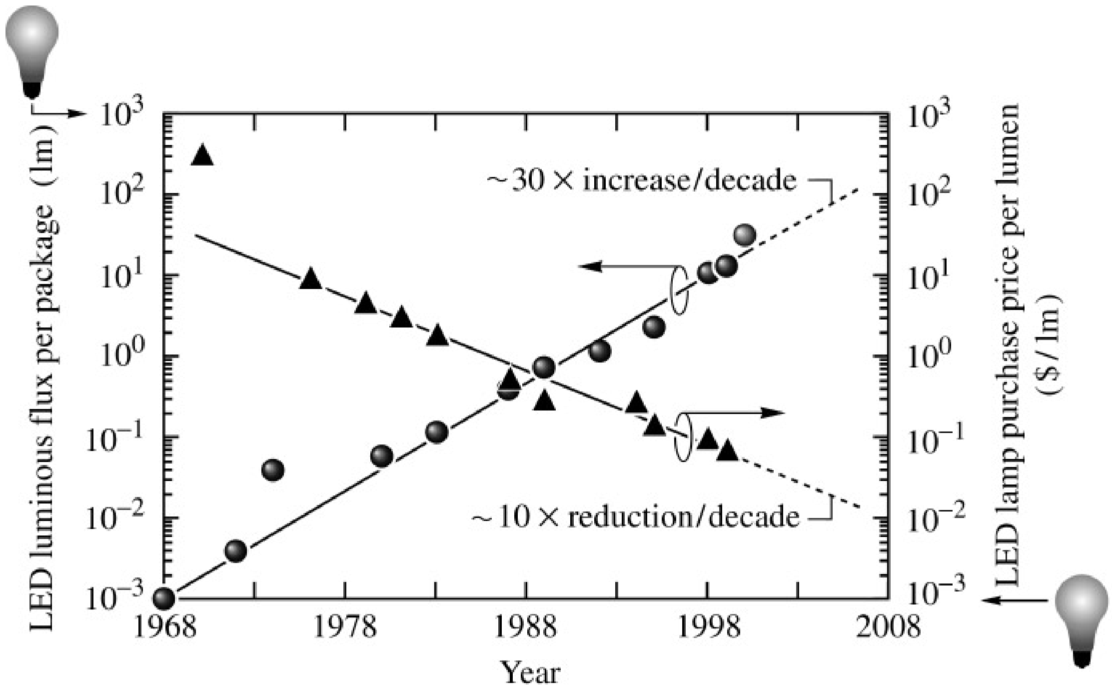

Fig. 8.15. LED luminous flux per package and LED lamp purchase price per lumen versus year. Also shown are the values for a 60 W incandescent tungsten-filament light bulb with a luminous performance of about 17 lm/W and a luminous flux of 1000 lm with an approximate price of US $ 1.00 (after Krames *et al.*, 2000).

… 10 to 20 more years are needed to compete with light bulbs

Optical characteristics of high-brightness LEDs

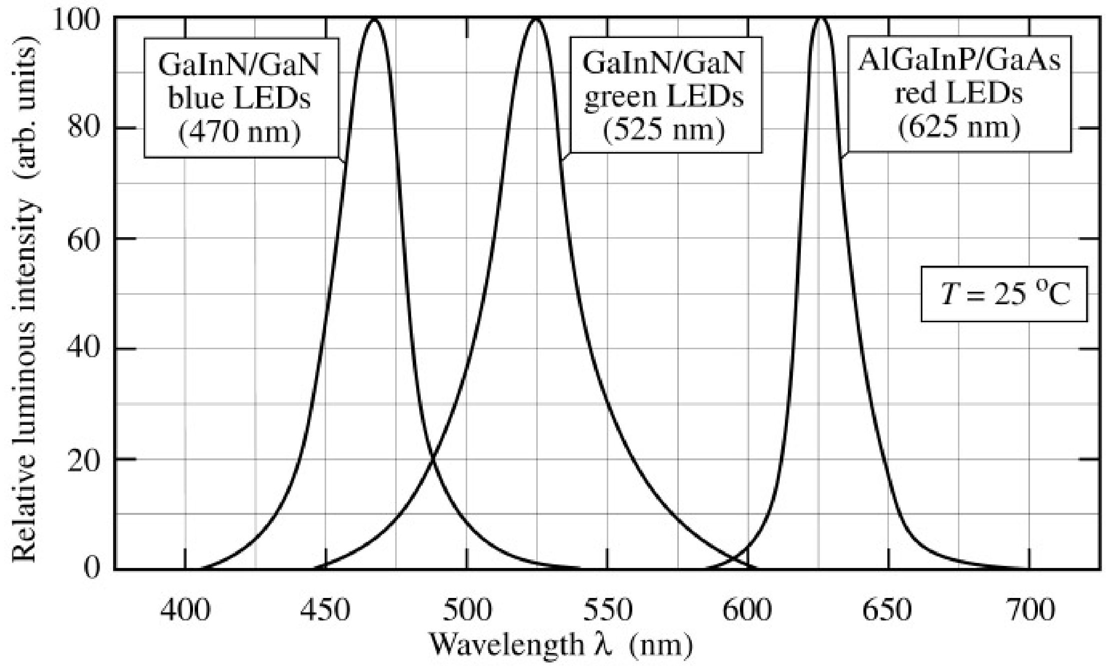

Fig. 8.16. Typical emission spectrum of GaInN/GaN blue, GaInN/GaN green, and AlGaInP/GaAs red LEDs at room temperature (after Toyoda Gosei Corp., 2000).

Light output power (LOP) versus current

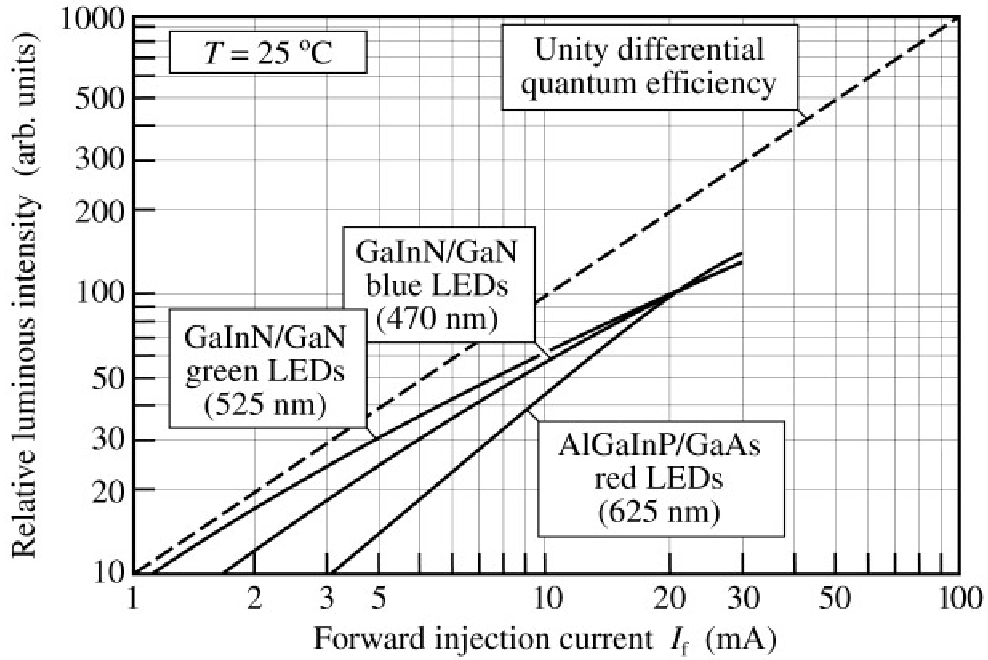

Fig. 8.17. Typical light output power versus injection current of GaInN / GaN blue, GaInN / GaN green, and AlGaInP / GaAs red LEDs at room temperature (adopted from Toyoda Gosei Corp., 2000).

… AlGaInP is more mature than GaInN

Electrical characteristics of high-brightness LEDs

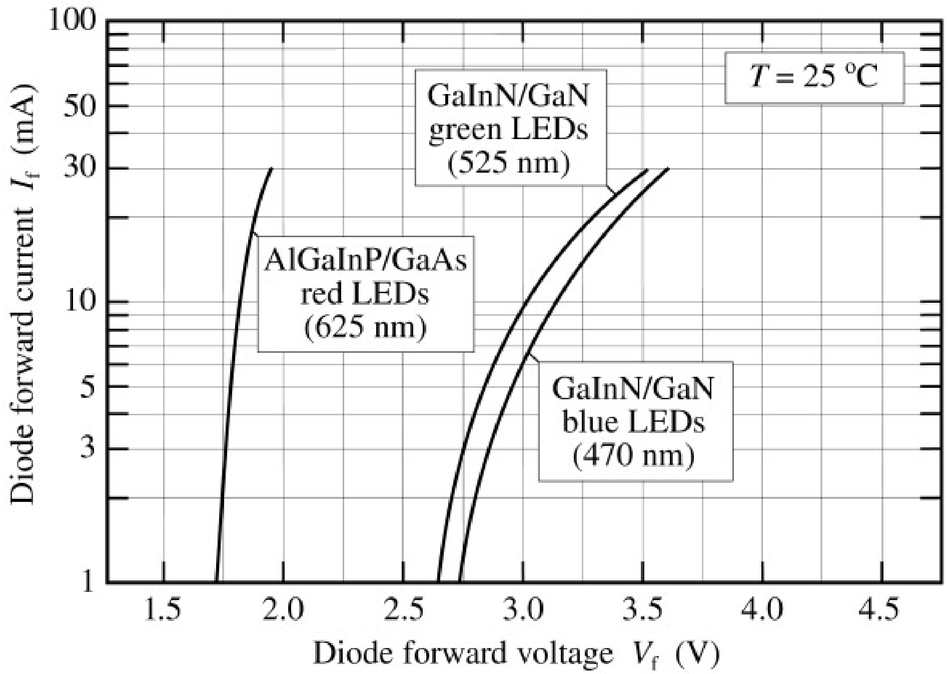

Fig. 8.19. Typical forward current - voltage (I-V) characteristic of GaInN / GaN blue, GaInN / GaN green, and AlGaInP / GaAs red LEDs at room temperature (after Toyoda Gosei Corporation, 2000).

… AlGaInP is more mature than GaInN

10

Resonant-cavity light-emitting diodes

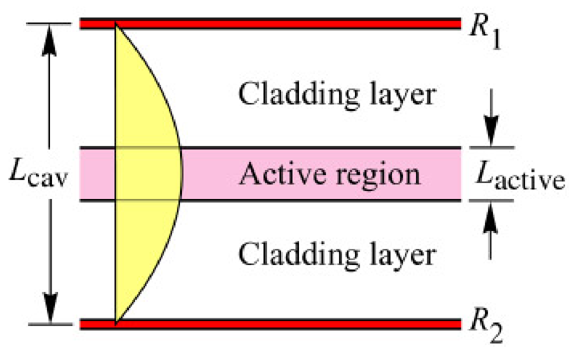

Fig. 10.1. Schematic illustration of resonant cavity consisting of two metal mirrors with reflectivity R_1 and R_2. The active region has a thickness L_{active} and an absorption coefficient α. Also shown is the standing optical wave. The cavity length is L_{cav} is equal to λ / 2.

RCLED design rules

First design rule

$$R_1 \quad << \quad R_2$$

(Light-exit mirror should have lower reflectivity than back mirror)

Second design rule

Use shortest possible cavity length L_{cav}. Typically $L_{cav} = \lambda / 2$

Third design rule

$$2\,\xi\,\alpha\,L_{active} \quad < \quad \left(1 \;-\; R_1\right)$$

(Absorption loss in active region should be smaller than the mirror loss of the light-exit mirror)

Cavity modes

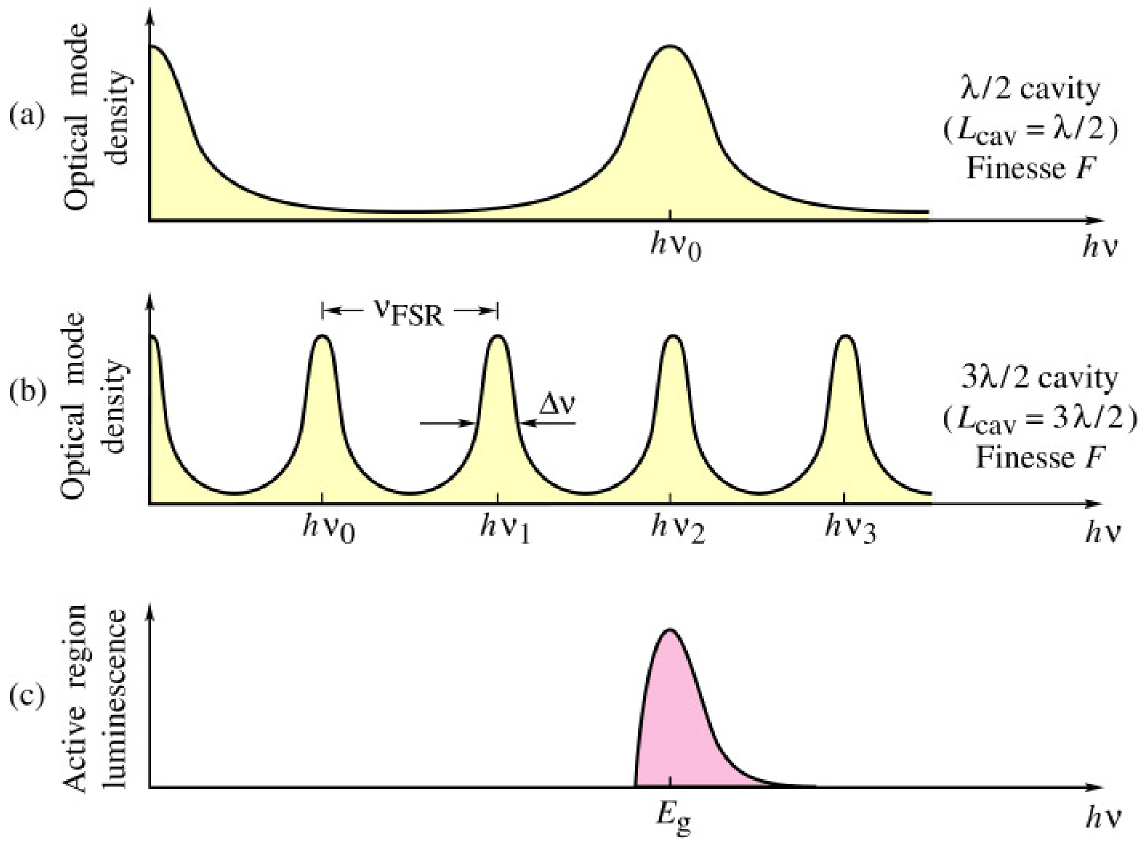

Fig. 10.2. Optical mode density for a (a) short and (b) long cavity with the same finesse F. (c) Spontaneous free space emission spectrum of an LED active region. The spontaneous emission spectrum has a better overlap with the short-cavity mode-spectrum as compared to the long-cavity mode-spectrum.

VCSEL versus RCLED

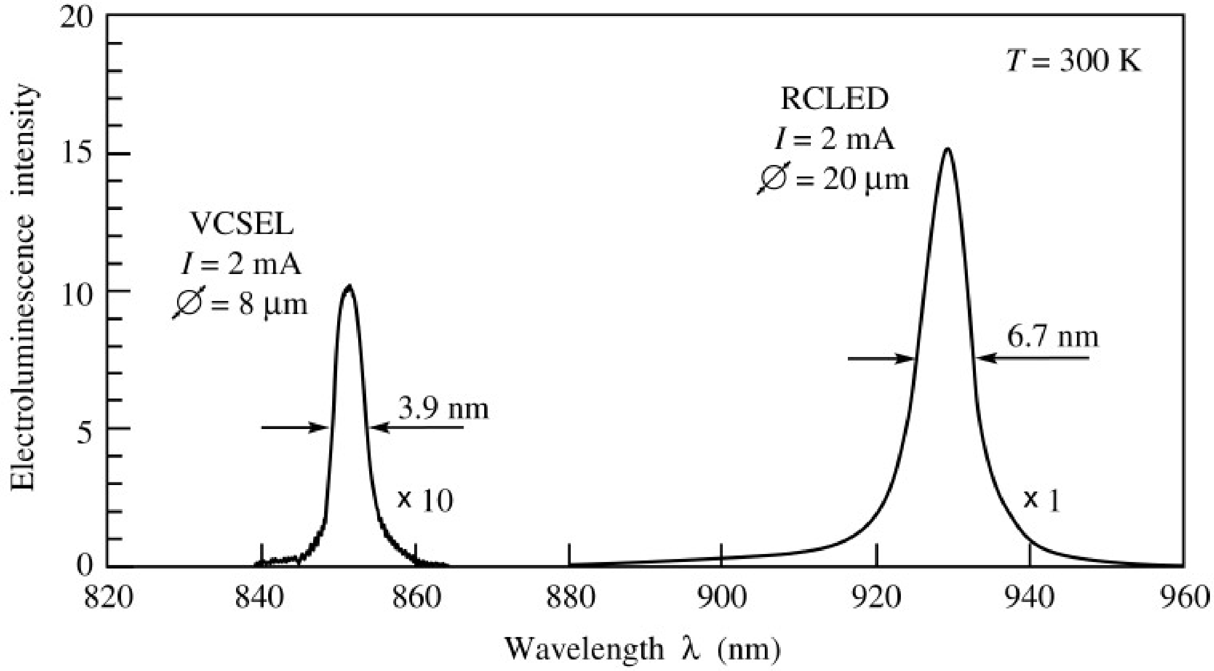

Fig. 10.3. Spontaneous electroluminescence spectrum of a vertical-cavity surface-emitting laser (VCSEL) emitting at 850 nm and of a resonant-cavity light-emitting diode (RCLED) emitting at 930 nm. The drive current for both devices is 2 mA. The VCSEL spectrum is multiplied by a factor of ten. The threshold current of the VCSEL is 7 mA (after Schubert *et al.*, 1996).

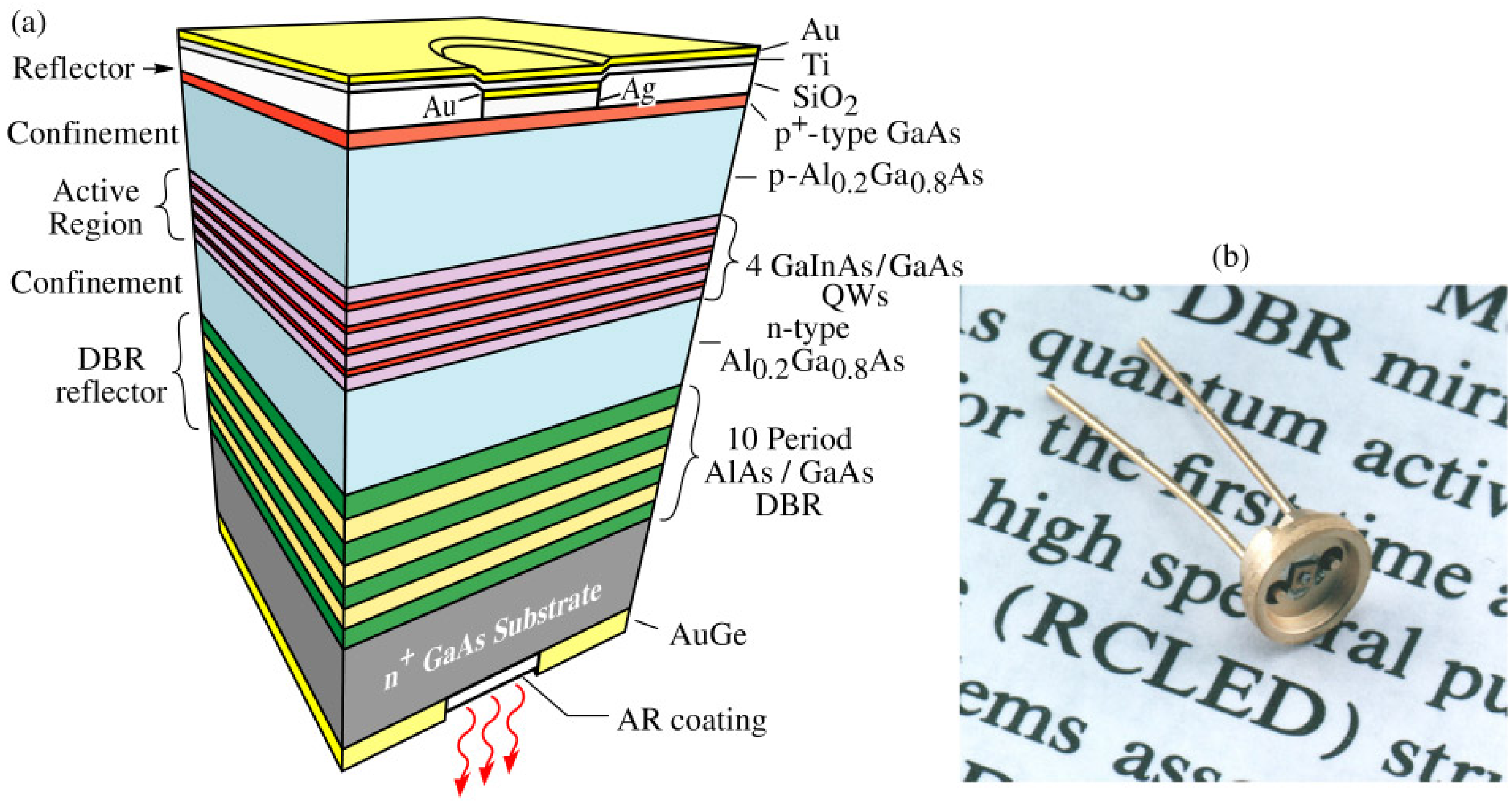

Fig. 10.4. (a) Schematic structure of a substrate-emitting GaInAs / GaAs RCLED consisting of a metal top reflector and a bottom distributed Bragg reflector (DBR). The RCLED emits at 930 nm. The reflectors are an AlAs / GaAs DBR and a Ag top reflector. (b) Picture of the first RCLED (after Schubert *et al.*, 1994).

Cavity mode and RCLED emission

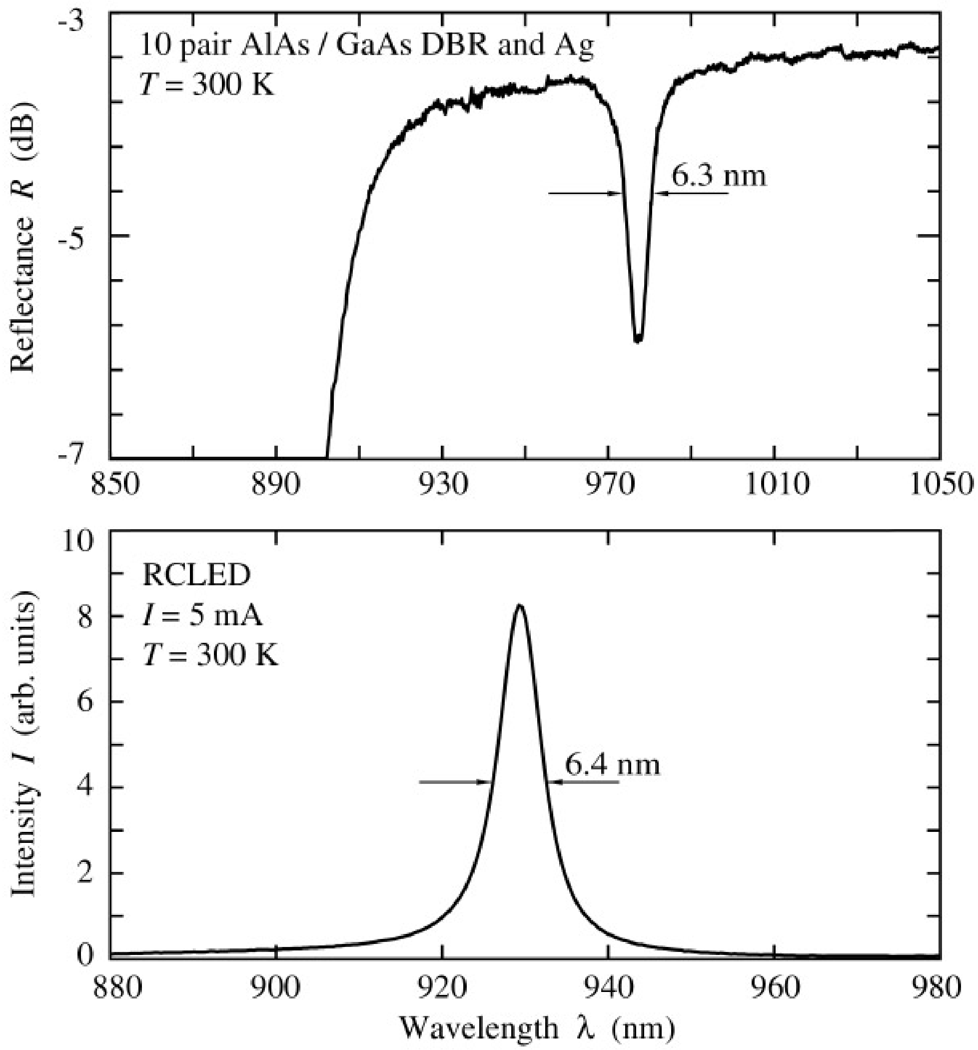

Fig. 10.5. (a) Reflectance of a resonant cavity consisting of a 10 pair AlAs / GaAs distributed Bragg reflector and an Ag reflector. (b) Emission spectrum of a RCLED consisting of a 10 pair AlAs / GaAs distributed Bragg reflector and an Ag reflector (after Schubert *et al.*, 1994).

RCLED spectrum

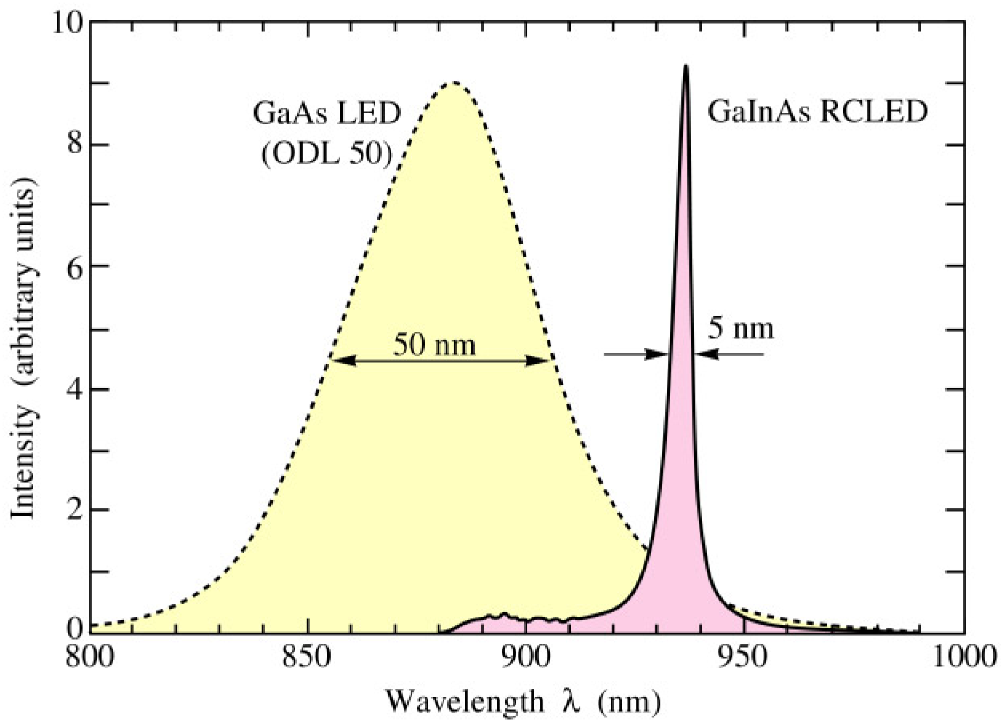

Fig. 10.6. Comparison of the emission spectra of a GaAs LED emitting at 870 nm (AT&T ODL 50 product) and a GaInAs RCLED emitting at 930 nm (after Hunt *et al*., 1993).

RCLED performance

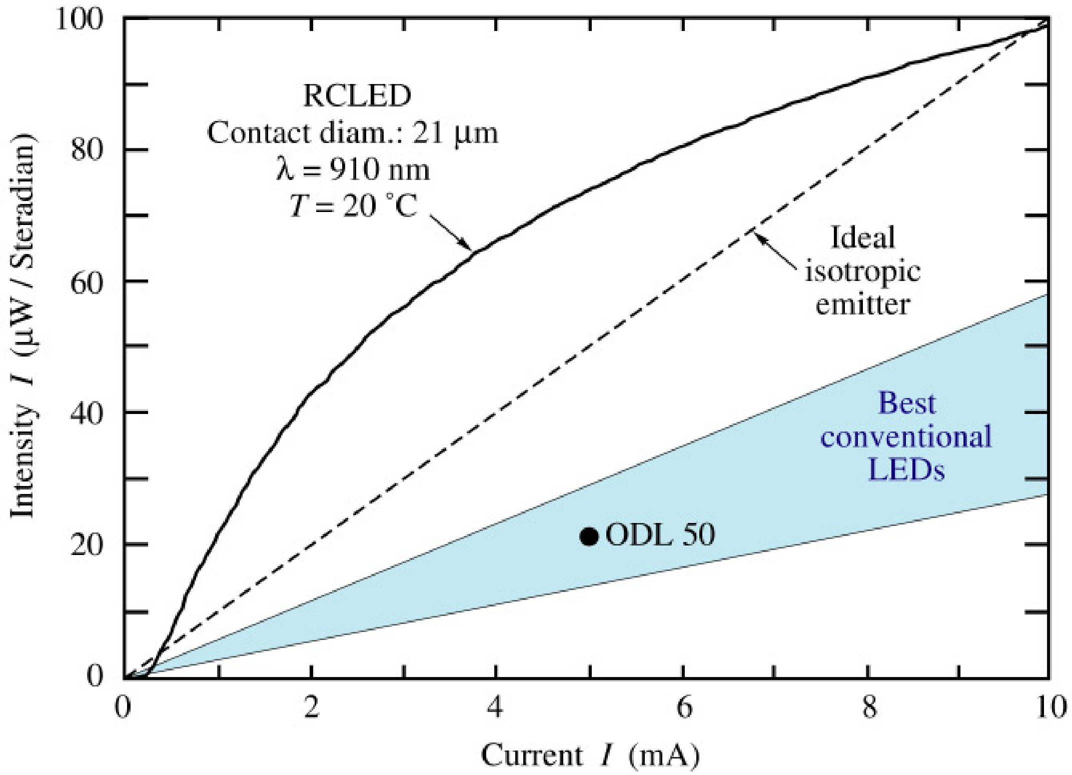

Fig. 10.7. Light-versus-current curves of a GaInAs / GaAs RCLED and of the *ideal isotropic emitter*. The ideal isotropic emitter is a hypothetial device emitting light isotropically with a quantum efficiency of 100 %. The shaded region shows the intensity of the best conventional LEDs. The ODL 50 is a commercial LED product (after Schubert *et al.*, 1994).

Reduced material dispersion with RCLEDs

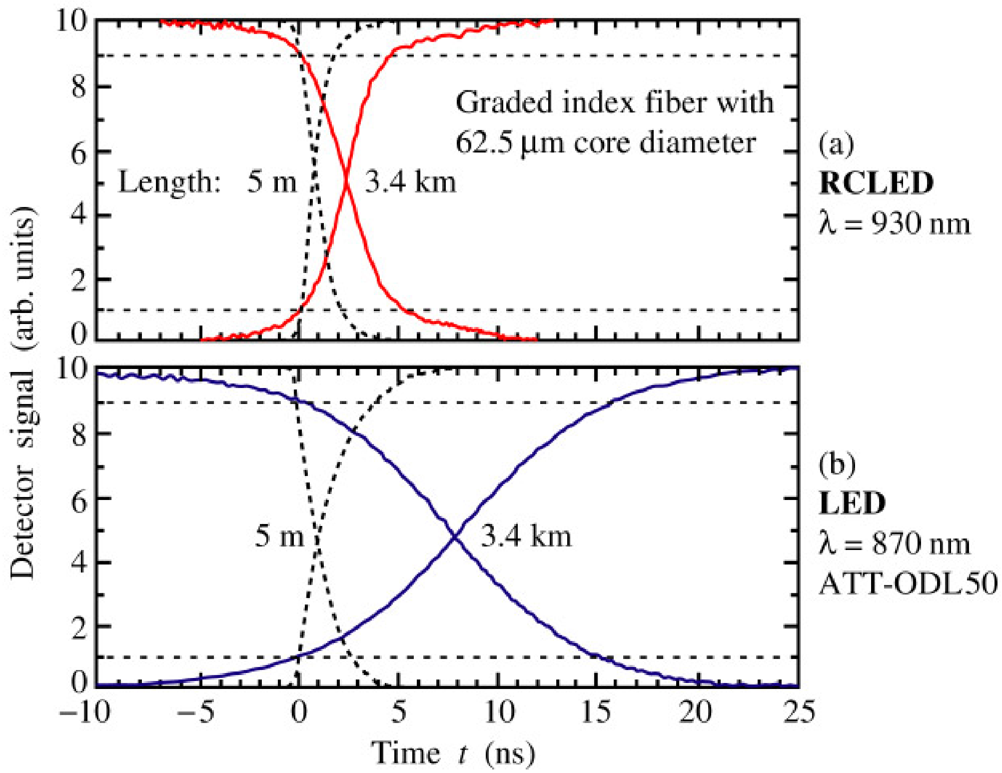

Fig. 10.8. Signal detected at the receiver end of a graded-index multimode fiber with a core diameter of 62.5 μm using an (a) GaInAs RCLED and (b) GaAs LED source. After a short transmission distance of 5 m, no marked difference is found for the two sources. After a transmission distance of 3.4 km, the RCLED exhibits much less pulse broadening than the LED (after Hunt *et al.*, 1993).

650 nm RCLED for plastic optical fiber communications

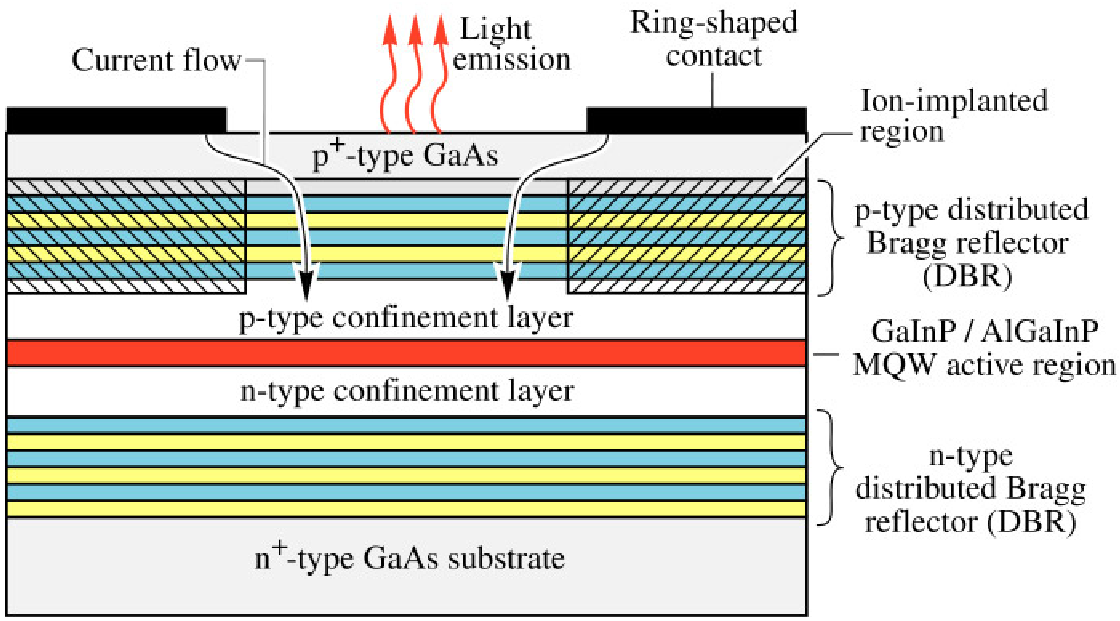

Fig. 10.9. Schematic structure of an GaInP / AlGaInP / GaAs MQW RCLED emitting at 650 nm used for plastic optical fiber applications (after Whitaker , 1999)

Commercial RCLEDs

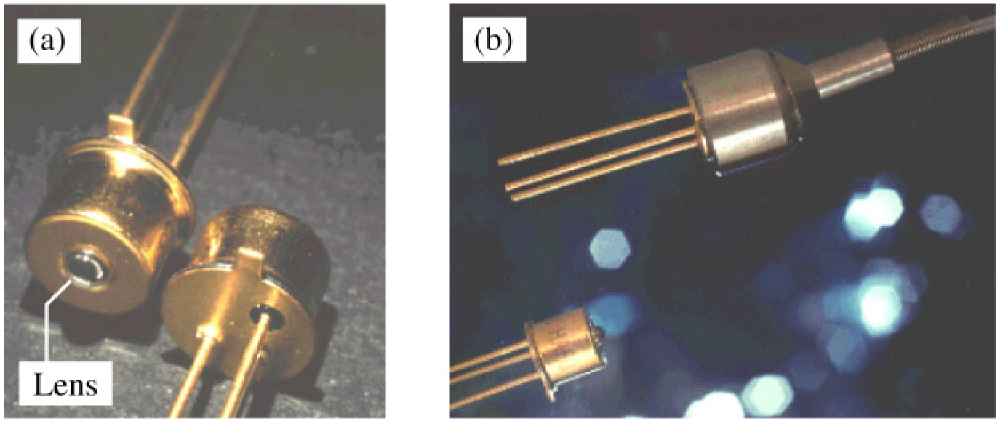

Fig. 10.10. (a) Packaged (TO package) RCLED emitting at 650 nm suited for plastic optical fiber applications. (b) Pig-tailed RCLED (Mitel Corporation, Sweden, 1999).

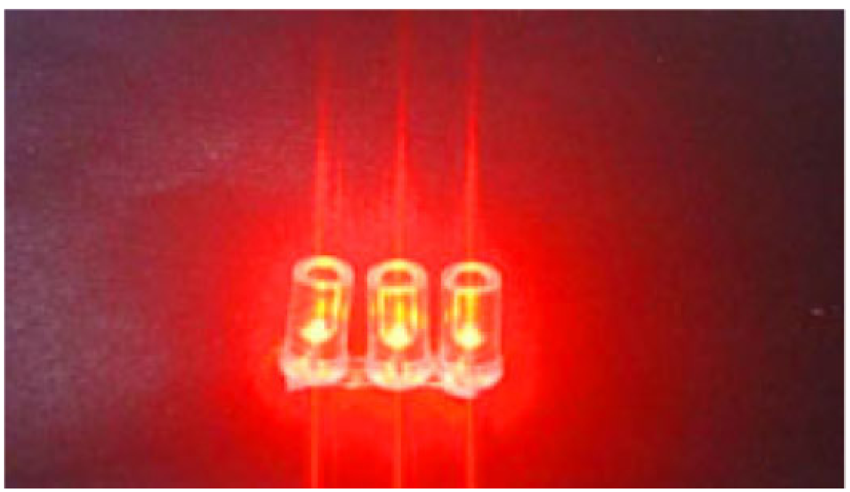

Fig. 10.11. AlGaInP / GaAs RCLEDs emitting at 650 nm. Note the forward-directed emission pattern similar to that of a semiconductor laser (Mitel Corporation, 1999).

RCLEDs for plastic optical fiber (POF) communication

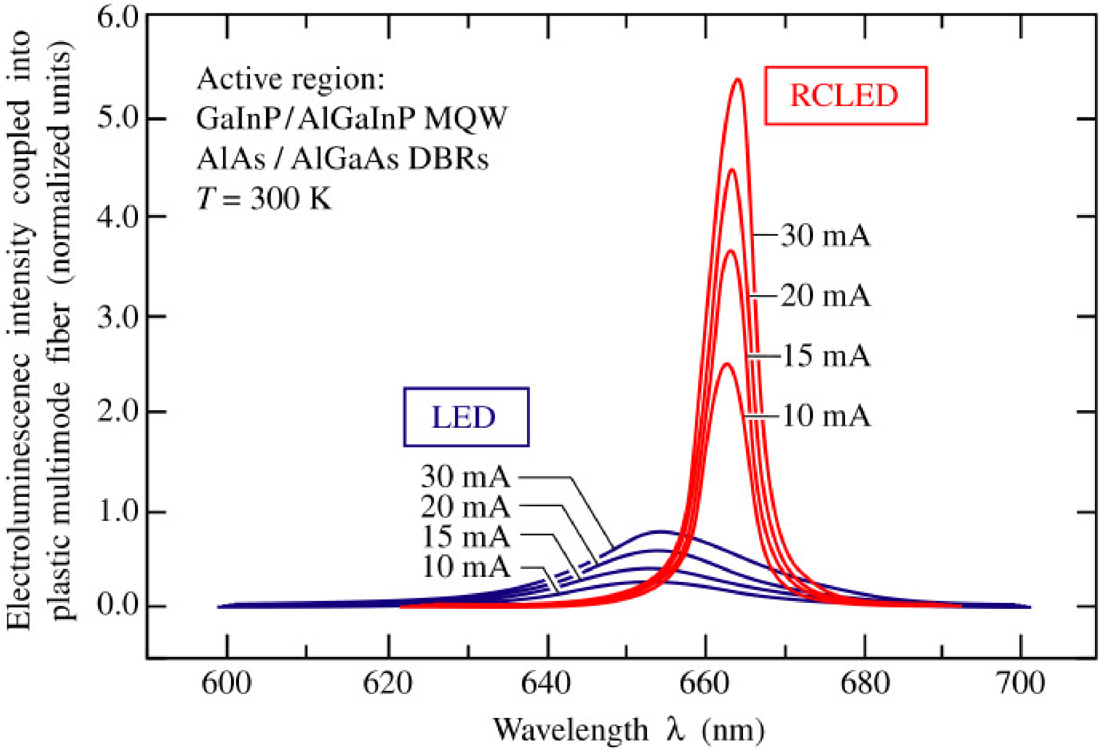

Fig. 10.12. Spectra of light coupled into a plastic optical fiber from an GaInP / AlGaInP MQW RCLED and a conventional GaInP / AlGaInP LED at different drive currents. Note the narrower spectrum and higher coupled power of the RCLED (after Streubel *et al.*, 1998).

11

Human vision

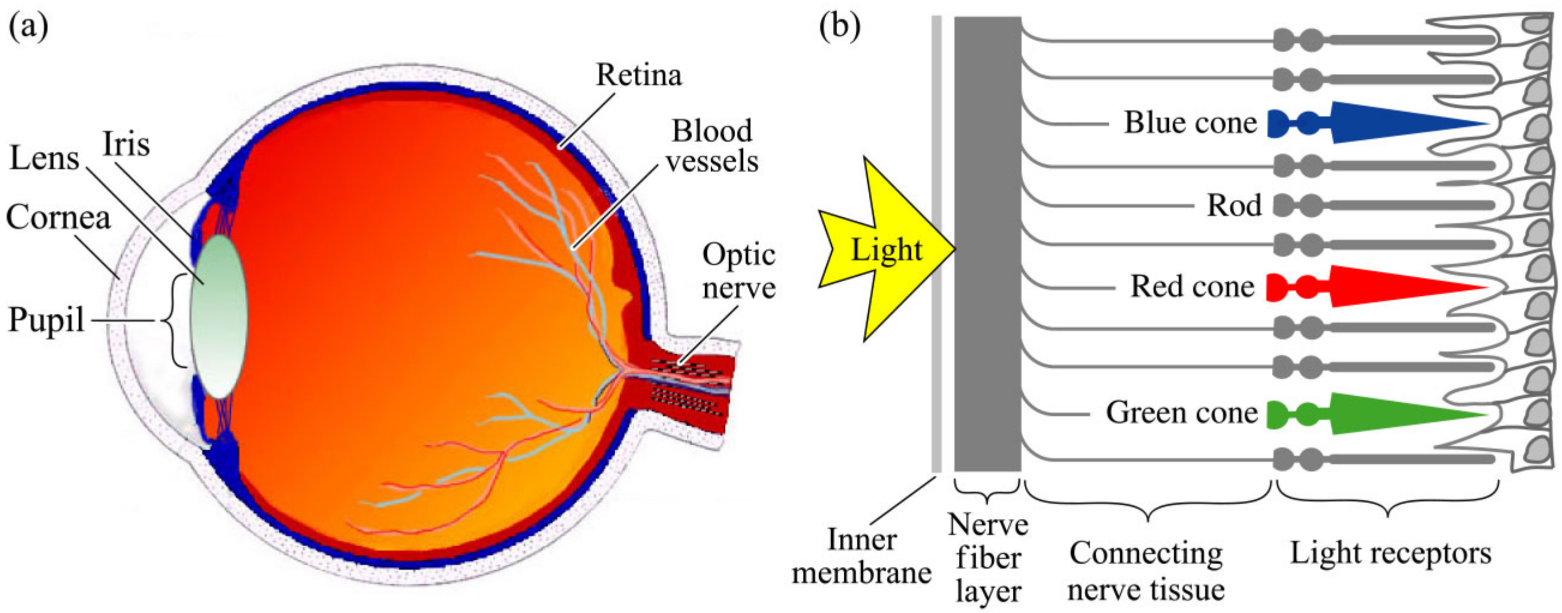

Fig. 11.1. (a) Cross section through human eye. (b) Schematic view of retina including rod and cone light receptors (adopted from Encyclopedia Britannica, 2001).

Cones: Color sensitive
Rods: Color-insensitive
Color perception depends on light level:
• Scotopic vision regime: Low-light-level-vision regime
• Photopic vision regime: High-light-level-vision regime

Sensitivity of cones and rods

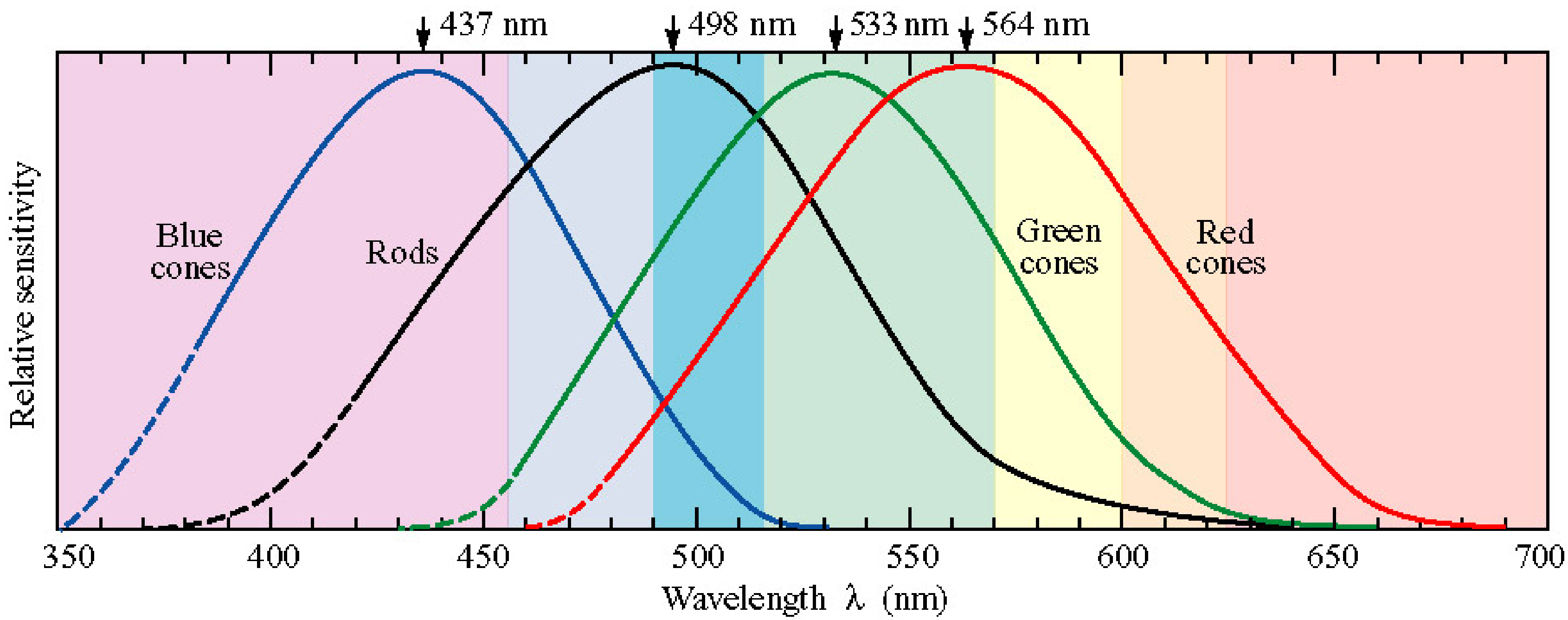

Fig. 11.X. Normalized spectral sensitivity of retinal rod and cone cells of the human eye (adapted from Dowling, 1987).

Eye sensitivity function and luminous efficacy

Visible range:
390 – 720 nm

Among LEDs with same power output, green LEDs are the brightest.

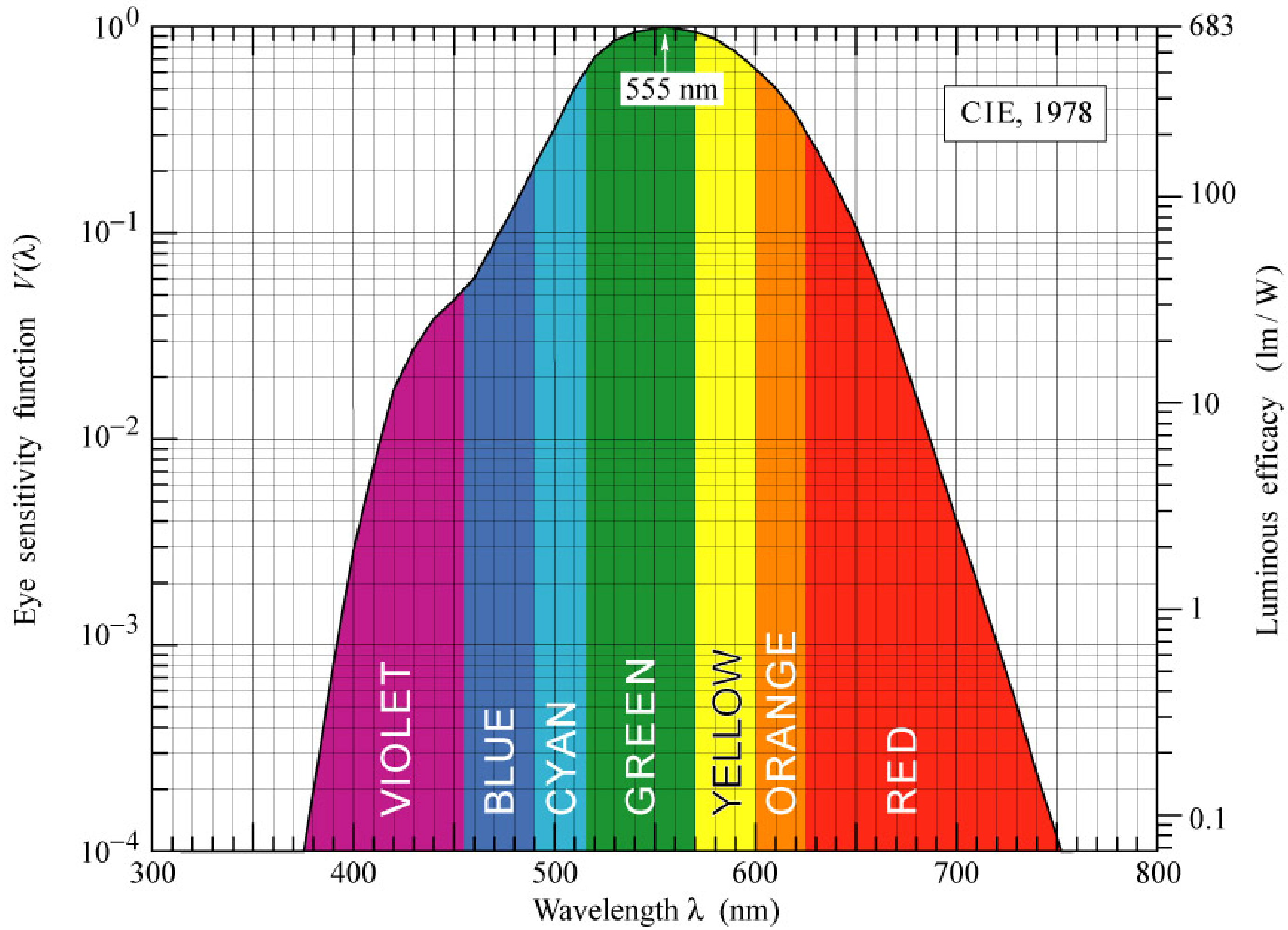

Fig. 11.2. Eye sensitivity function, $V(\lambda)$, (left ordinate) and luminous efficacy, measured in lumens per Watt of optical power (right ordinate). The eye sensitivity is greatest at 555 nm. Also given is a polynomial approximation for $V(\lambda)$ (after 1978 CIE data).

Photopic and scotopic vision regime

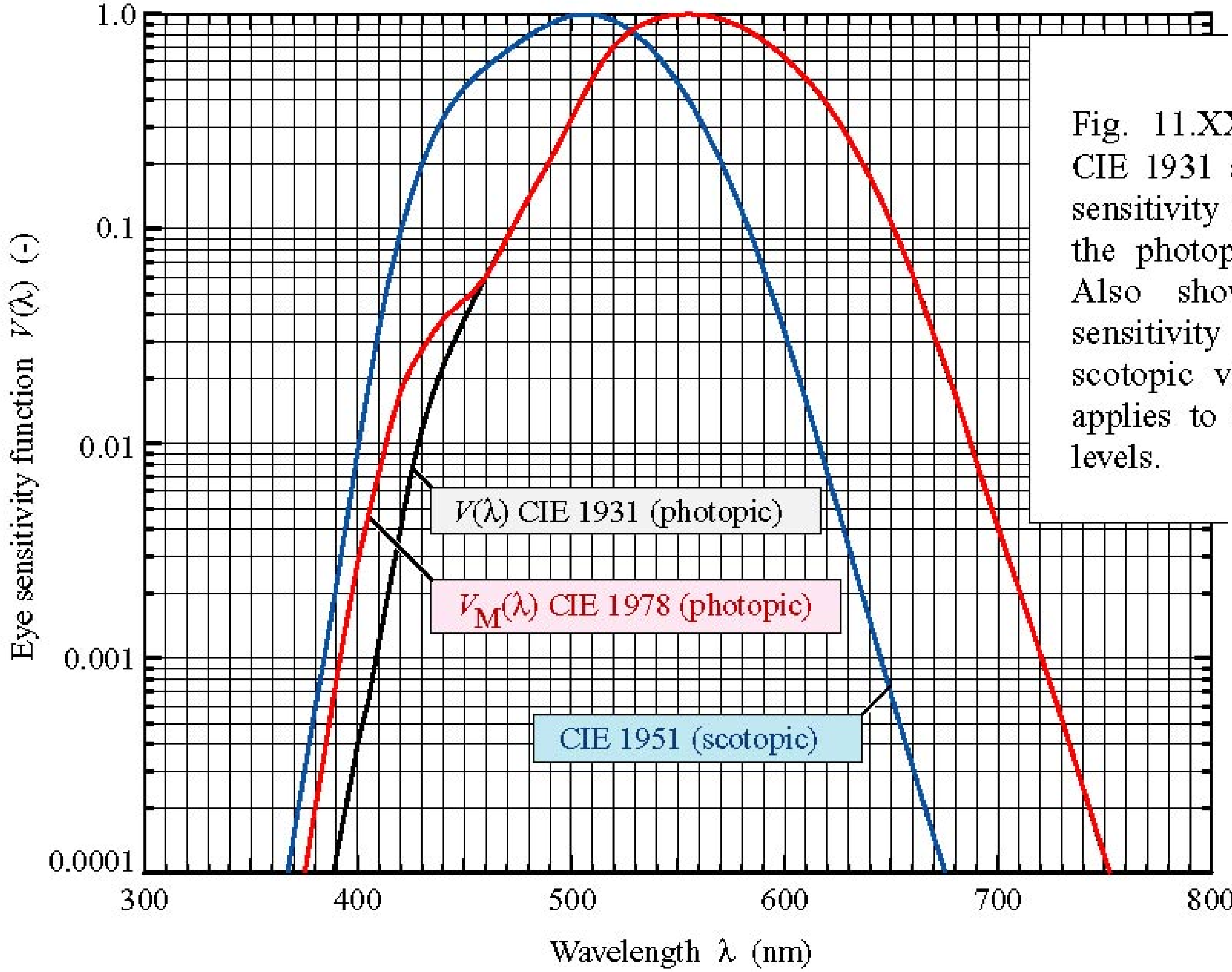

Fig. 11.XX Comparison of CIE 1931 and CIE 1978 eye sensitivity function $V(\lambda)$ for the photopic vision regime. Also shown is the eye sensitivity function for the scotopic vision regime that applies to low ambient light levels.

There are several standards:

Photopic:
CIE 1931
CIE 1978

Scotopic:
CIE 1951

Luminous flux (Unit: lm)

$$\Phi_{\mathrm{lum}} = 683 \frac{\mathrm{lm}}{\mathrm{W}} \int_\lambda V(\lambda)\, P(\lambda)\, \mathrm{d}\lambda$$

Luminous efficacy (Unit: lm / W)

$$\text{Luminous efficacy} = \Phi_{\mathrm{lum}} / P = \left(683 \frac{\mathrm{lm}}{\mathrm{W}} \int_\lambda V(\lambda)\, P(\lambda)\, \mathrm{d}\lambda\right) \Big/ \left(\int_\lambda P(\lambda)\, \mathrm{d}\lambda\right)$$

Luminous efficiency (Unit: lm / W)

$$\text{Luminous efficiency} = \Phi_{\mathrm{lum}} / (IV)$$

Caution:
Some call the “luminous efficacy” the “luminous efficacy of radiation”

Caution:
Some call the “luminous efficiency” the “luminous efficacy of the source”

Color matching functions

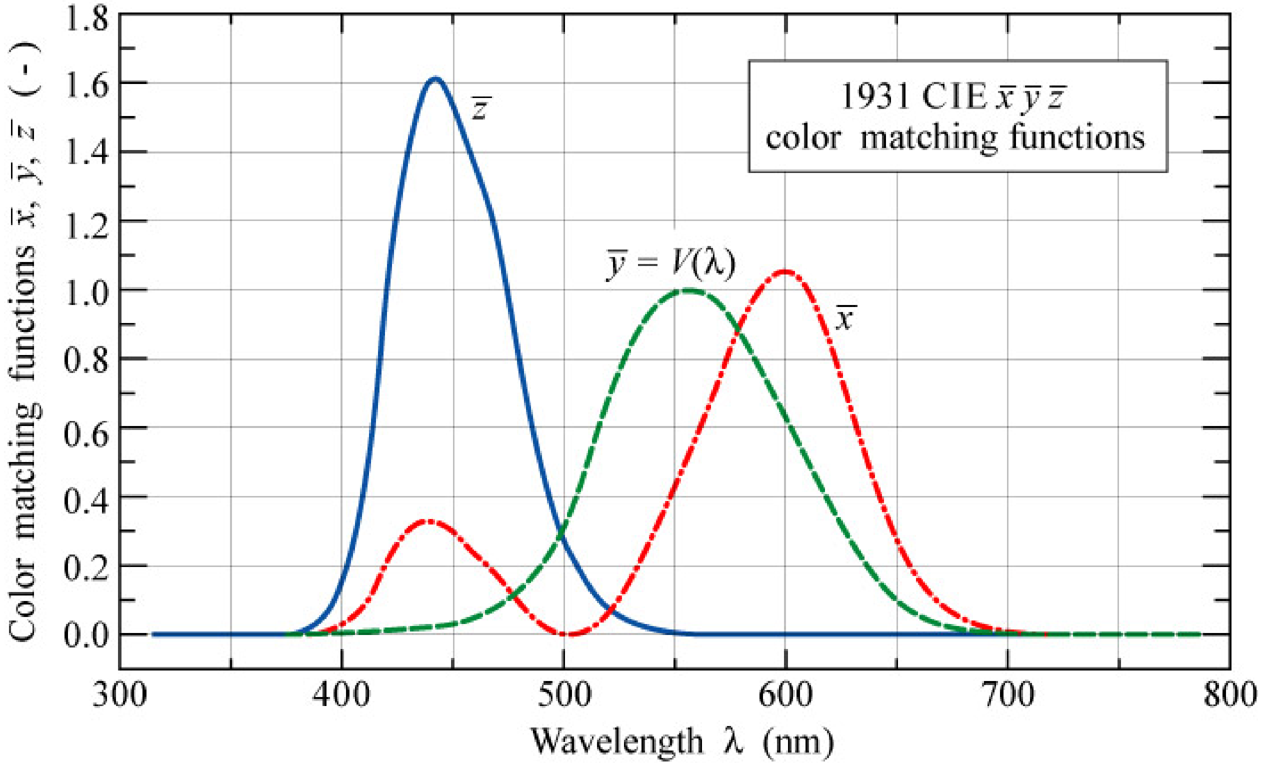

Fig. 11.3. CIE (1931) $\bar{x}\bar{y}\bar{z}$ color matching functions. The $\bar{y}$ color matching function is identical to the eye sensitivity function $V(\lambda)$.

The color matching functions are approximately equal to the spectral sensitivity of the cones

Caution:
There are different standards for the color matching functions

Color matching functions and chromaticity diagram

$$X = \int_\lambda \bar{x}(\lambda)\, P(\lambda)\, \mathrm{d}\lambda$$

$$Y = \int_\lambda \bar{y}(\lambda)\, P(\lambda)\, \mathrm{d}\lambda$$

$$Z = \int_\lambda \bar{z}(\lambda)\, P(\lambda)\, \mathrm{d}\lambda$$

X, *Y*, and *Z* are ***tristimulus values***

Chromaticity coordinates

$$x = \frac{X}{X + Y + Z} \qquad y = \frac{Y}{X + Y + Z}$$

z chromaticity coordinate not needed, since $x + y + z = 1$

Chromaticity diagram

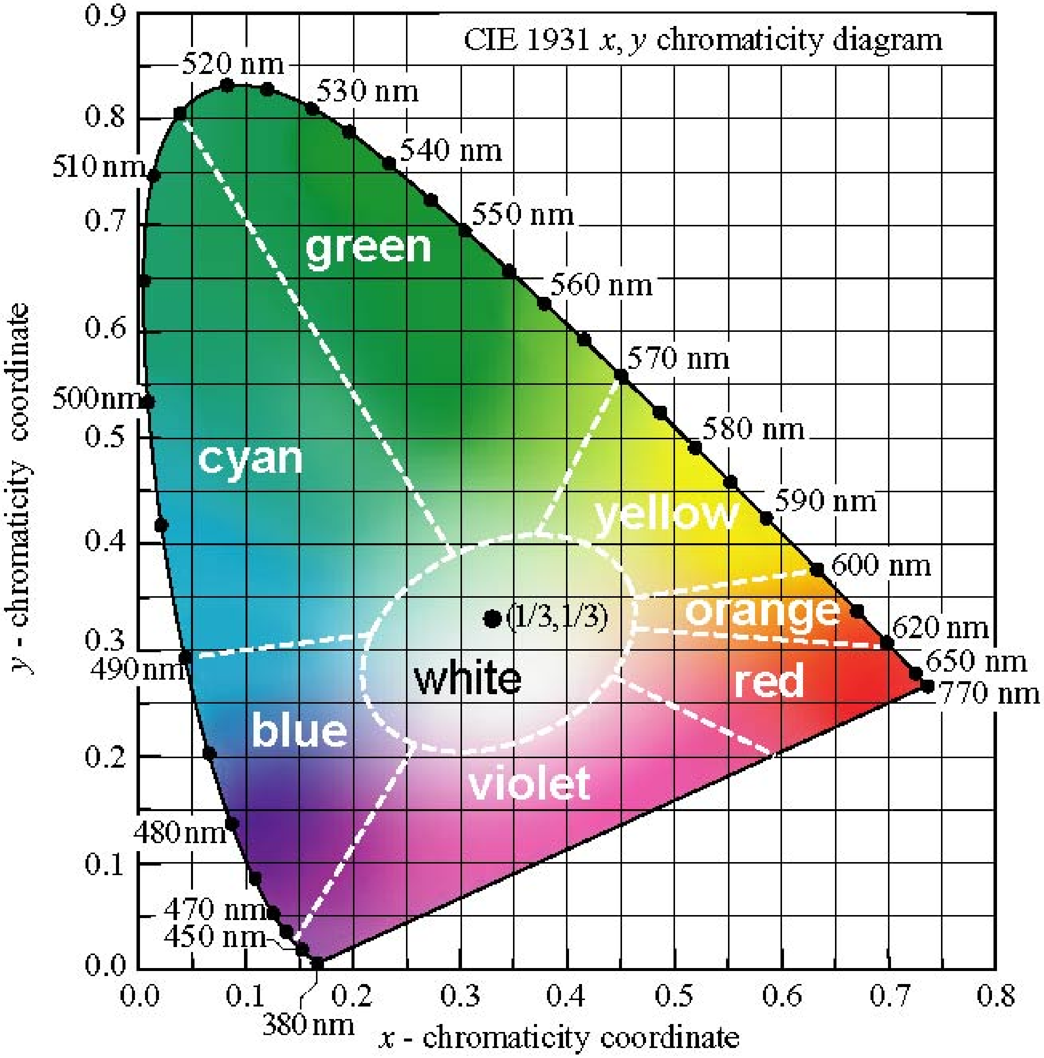

Fig. 11.X. CIE 1931 x, y chromaticity diagram. Monochromatic colors are located on the perimeter. Color saturation decreases towards the center of the diagram. White light is located in the center. Also shown are the regions of distinct colors. The equal-excitation point is located at the center of the chromaticity diagram and has the coordinates $(x, y) = (1/3, 1/3)$

Strictly monochromatic sources are on perimeter

White light is in center

MacAdam ellipses

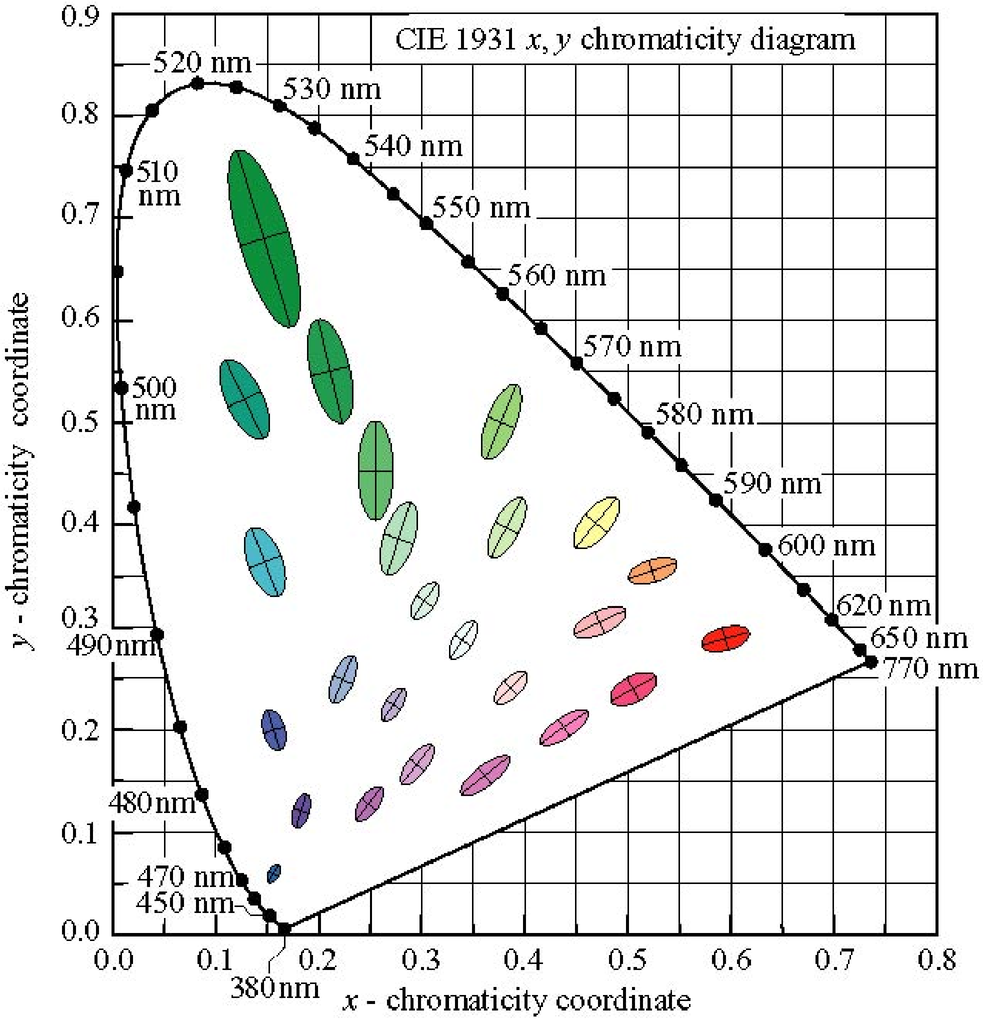

Fig. 11.X. MacAdam ellipses plotted in the CIE 1931 x, y chromaticity diagram. The axes of the plotted ellipses are ten times their actaul lengths (after MacAdam, 1943; Wright, 1943; MacAdam, 1993).

Uniform u' v' chromaticity diagram

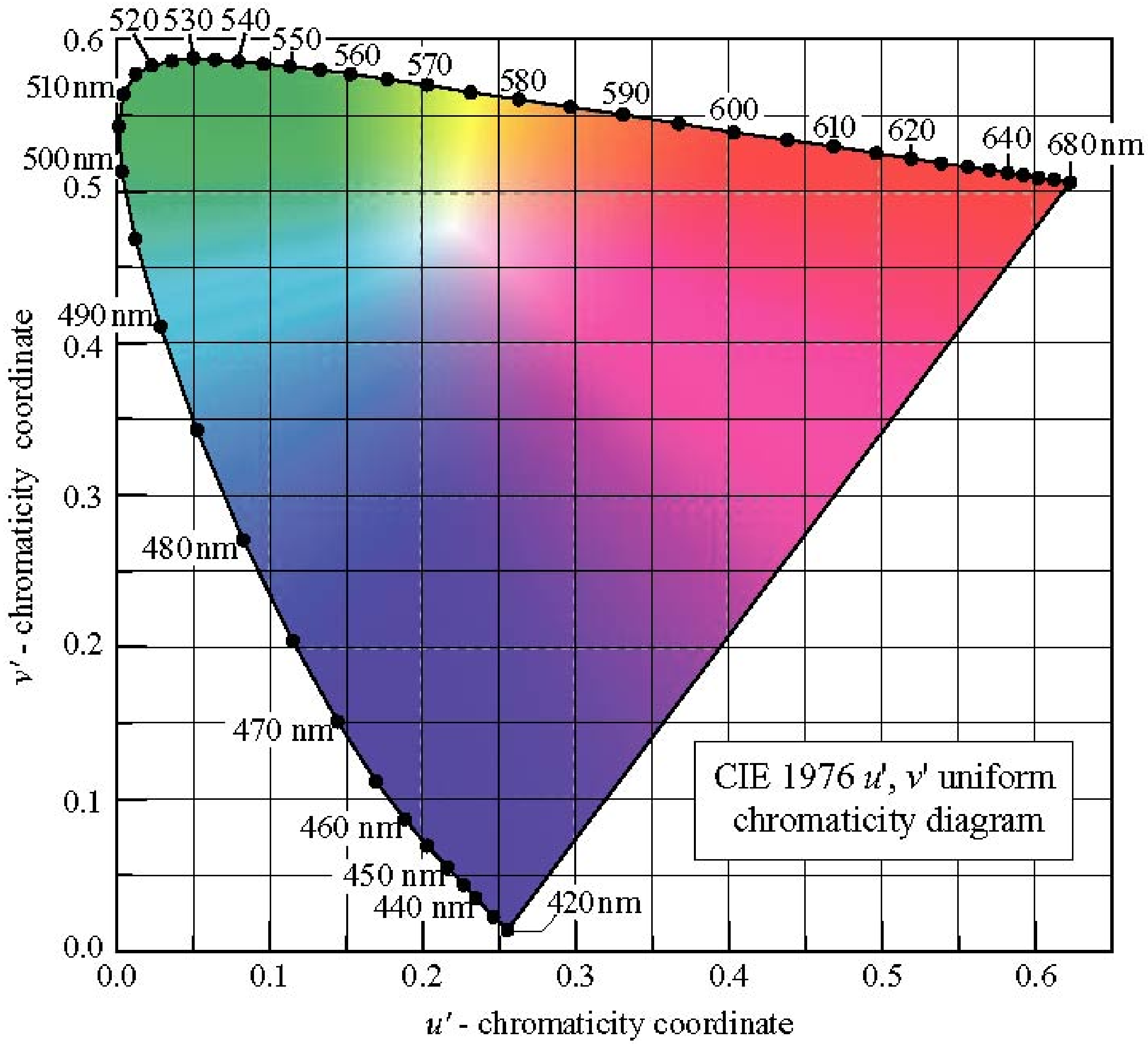

Fig. 11.X. CIE 1976 *u'*, *v'* uniform chromaticity diagram calculated using the CIE 1931 2° observer.

Color difference is proportional to geometric distance

Color purity and dominant wavelength

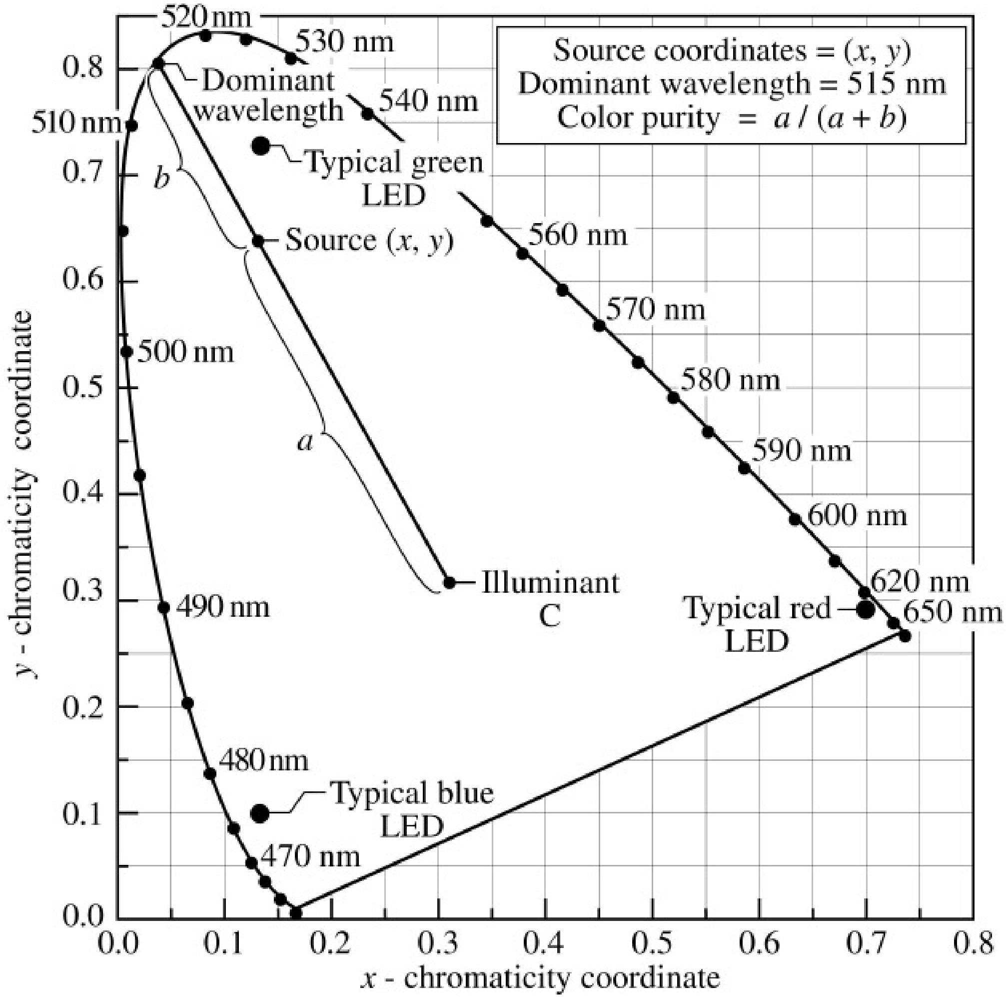

Fig. 11.5. Chromaticity diagram showing the determination of the dominant color and color purity of a light source with chromaticity coordinates (x, y) using the Illuminant C as the white-light reference. Also shown are typical locations of blue, green, and red LEDs.

Caution:

Peak wavelength and dominant wavelength can be different.

Peak wavelength is a quantity used in physics and optics

Dominant wavelength is used by in human vision

LEDs in the chromaticity diagram

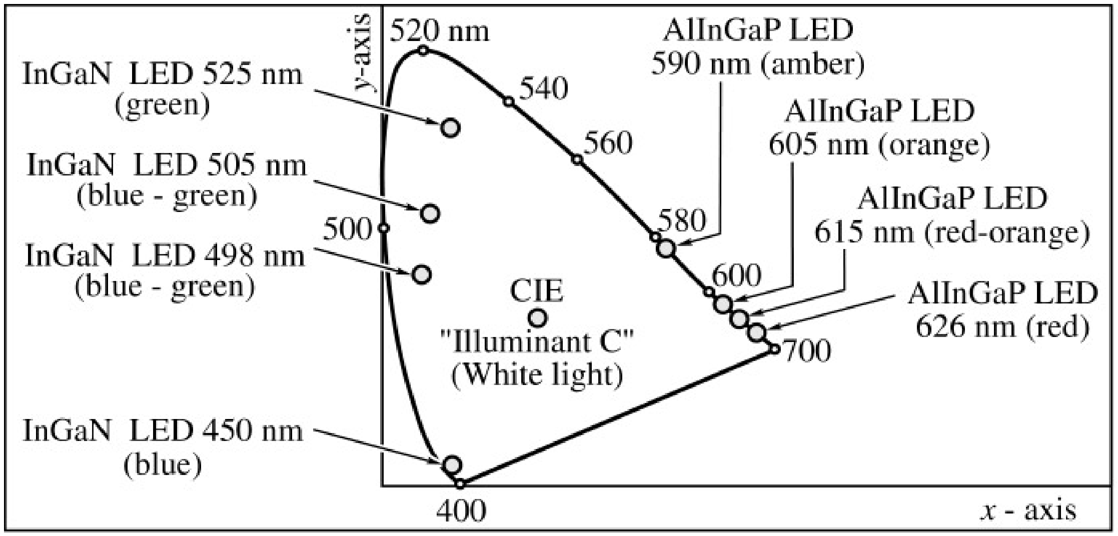

Fig. 11.6. Location of LED light emission on the chromaticity diagram (adopted from Schubert and Miller, 1999).

Note:

Red and blue LEDs are near perimeter

Green LEDs are not at perimeter but are shifted towards center

White illuminants

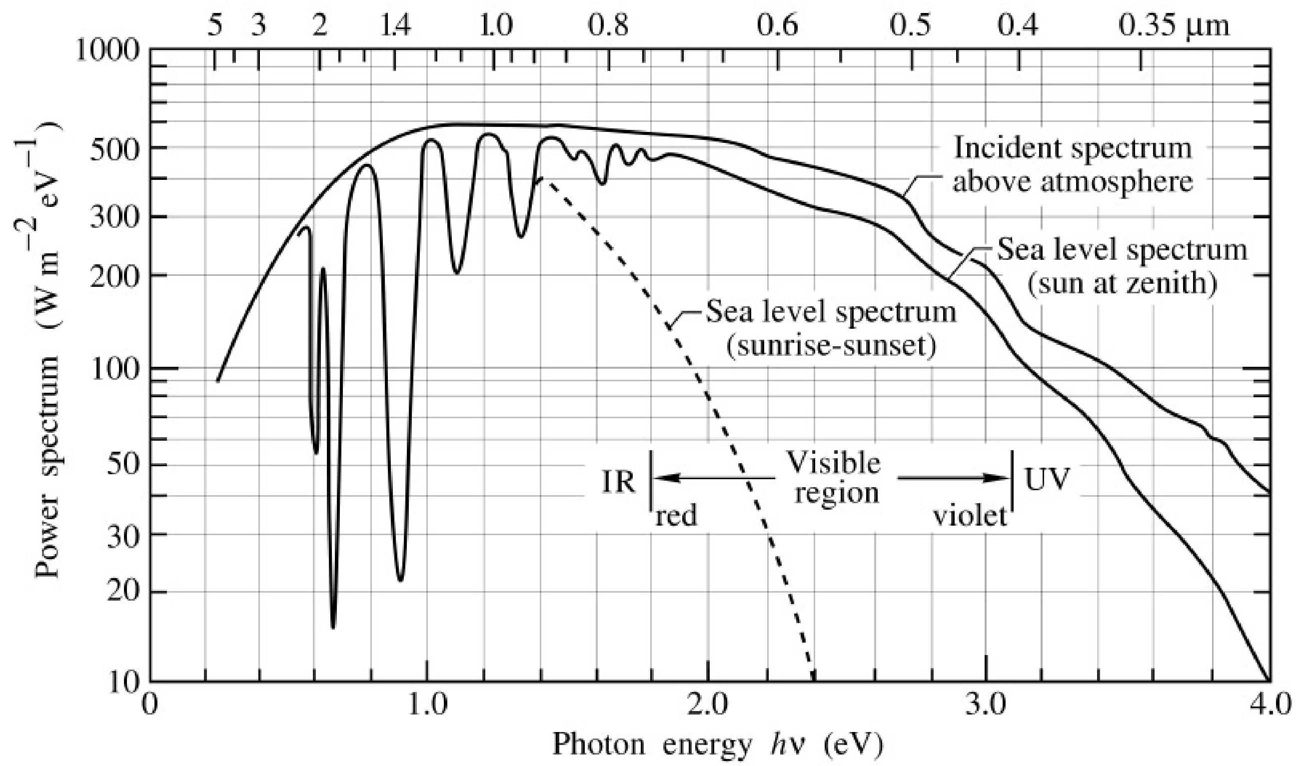

Fig. 11.7. Power spectrum of solar radiation versus photon energy and wavelength for different conditions (adopted from Jackson, 1975).

Caution:
There are many ways to create white light
Sunlight is not a good way to create white light. Why?

Color temperature

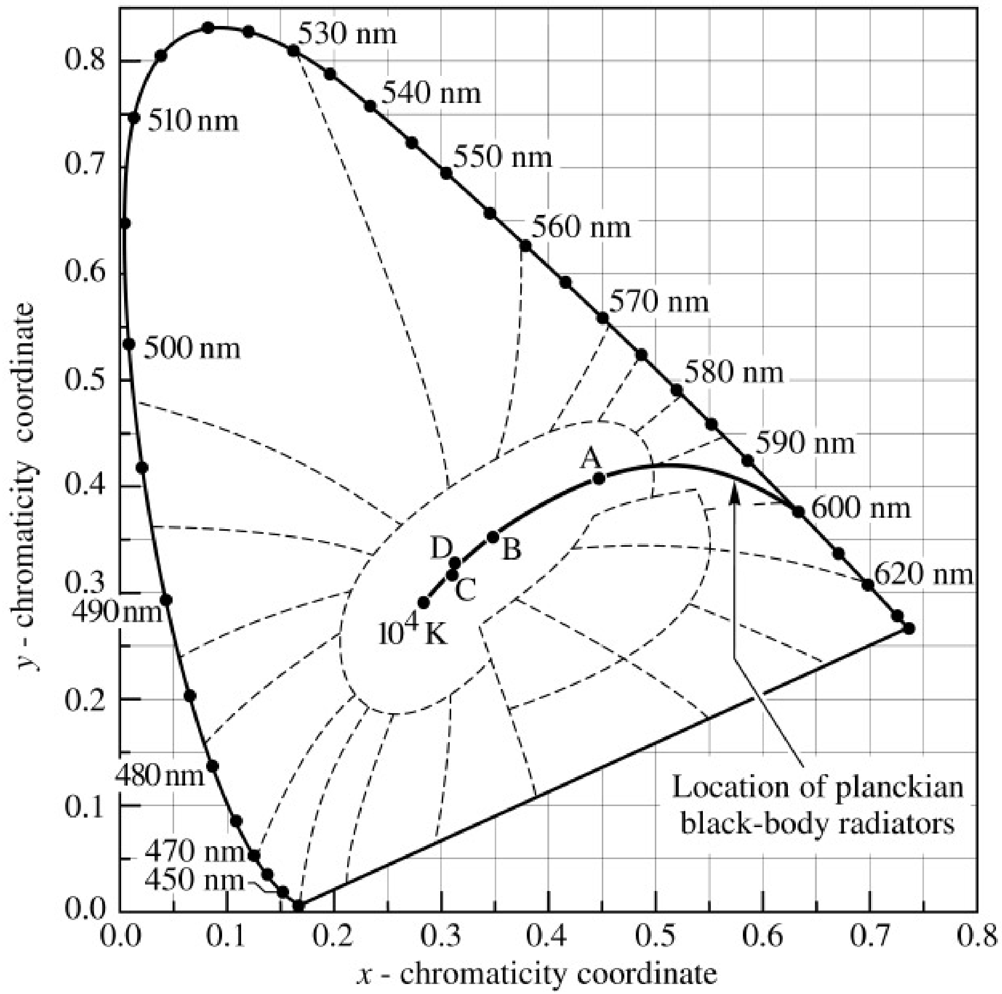

Illuminant A
(x, y) = (0.4476, 0.4074)
(Incandescent source, T = 2856 K)

Illuminant B
(x, y) = (0.3484, 0.3516)
(Direct sunlight, T = 4870 K)

Illuminant C
(x, y) = (0.3101, 0.3162)
(Overcast source, T = 6770 K)

Illuminant D
(x, y) = (0.3128, 0.3292)
(Daylight, T = 6504 K)

Fig. 11.8. Chromaticity diagram showing the standardized white Illuminants A, B, C, and D and their color temperature (after CIE, 1978).

Planckian spectrum or black-body radiation spectrum.
Objects of "low" temperature glow in the red
Objects of "higher" temperature glow yellow or white

Color mixing

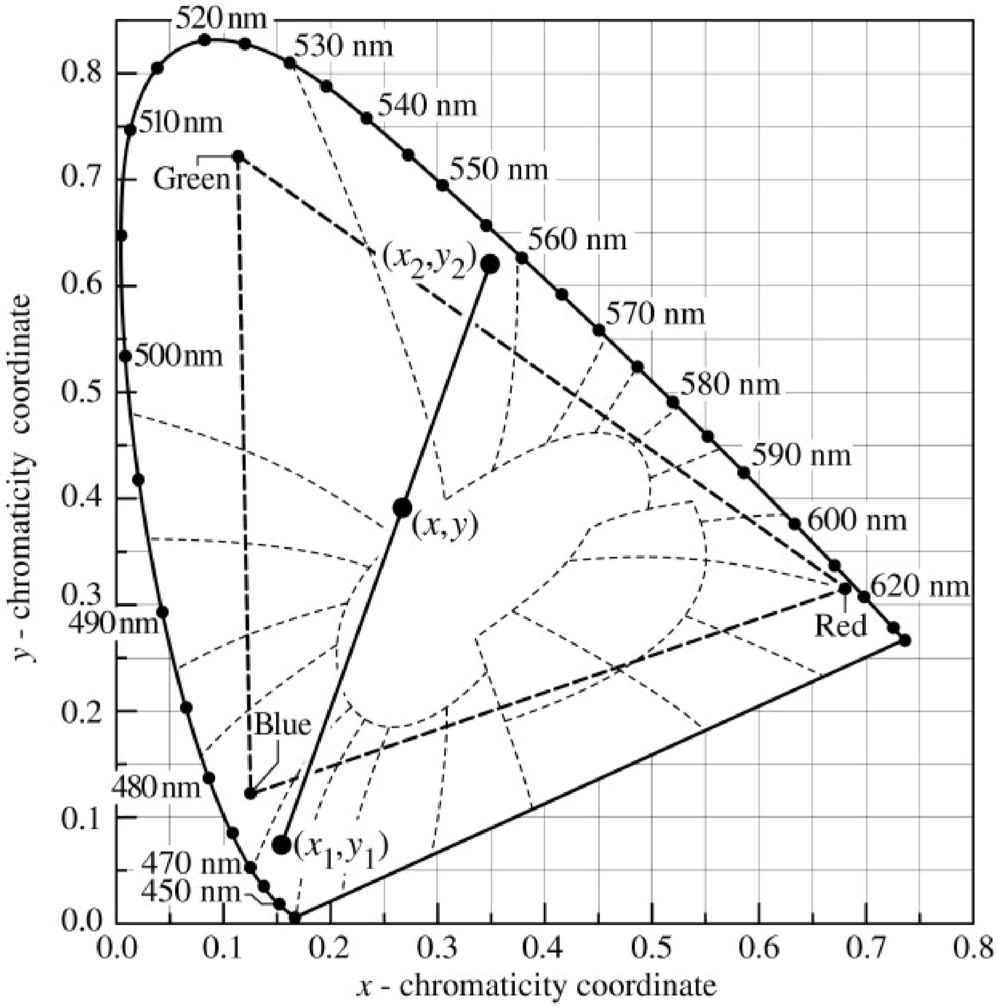

Fig. 11.9. Principle of color mixing illustrated with two light sources with chromaticity coordinates (x_1, y_1) and (x_2, y_2). The resulting color has the coordinates (x, y). Also shown in the area of the chromaticity diagram accessible with the combination of a typical red, green, and blue LED.

- Color gamut
- Gamut of Red-Green-Blue light source has triangular shape
- Area of gamut matters for displays, color printers, etc.

Example of color mixing

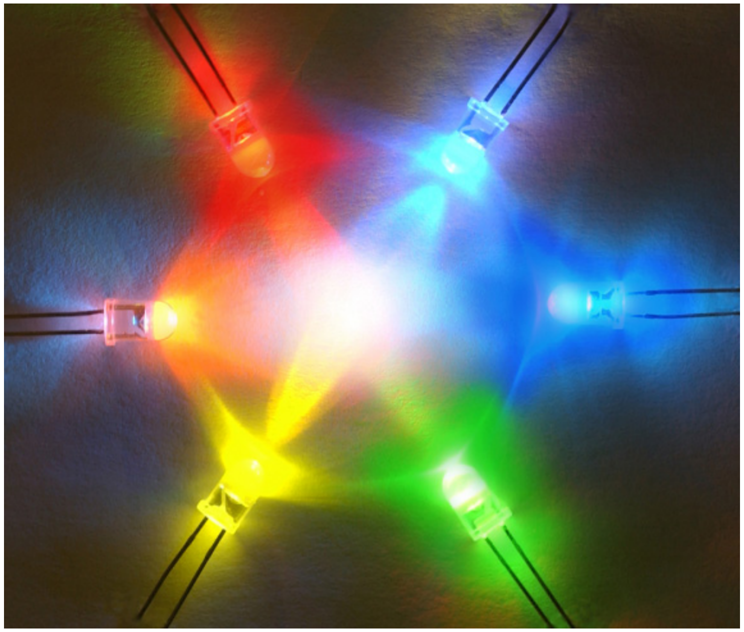

- Color gamut
- Gamut size increases with the number of light sources

Color rendering index (CRI)

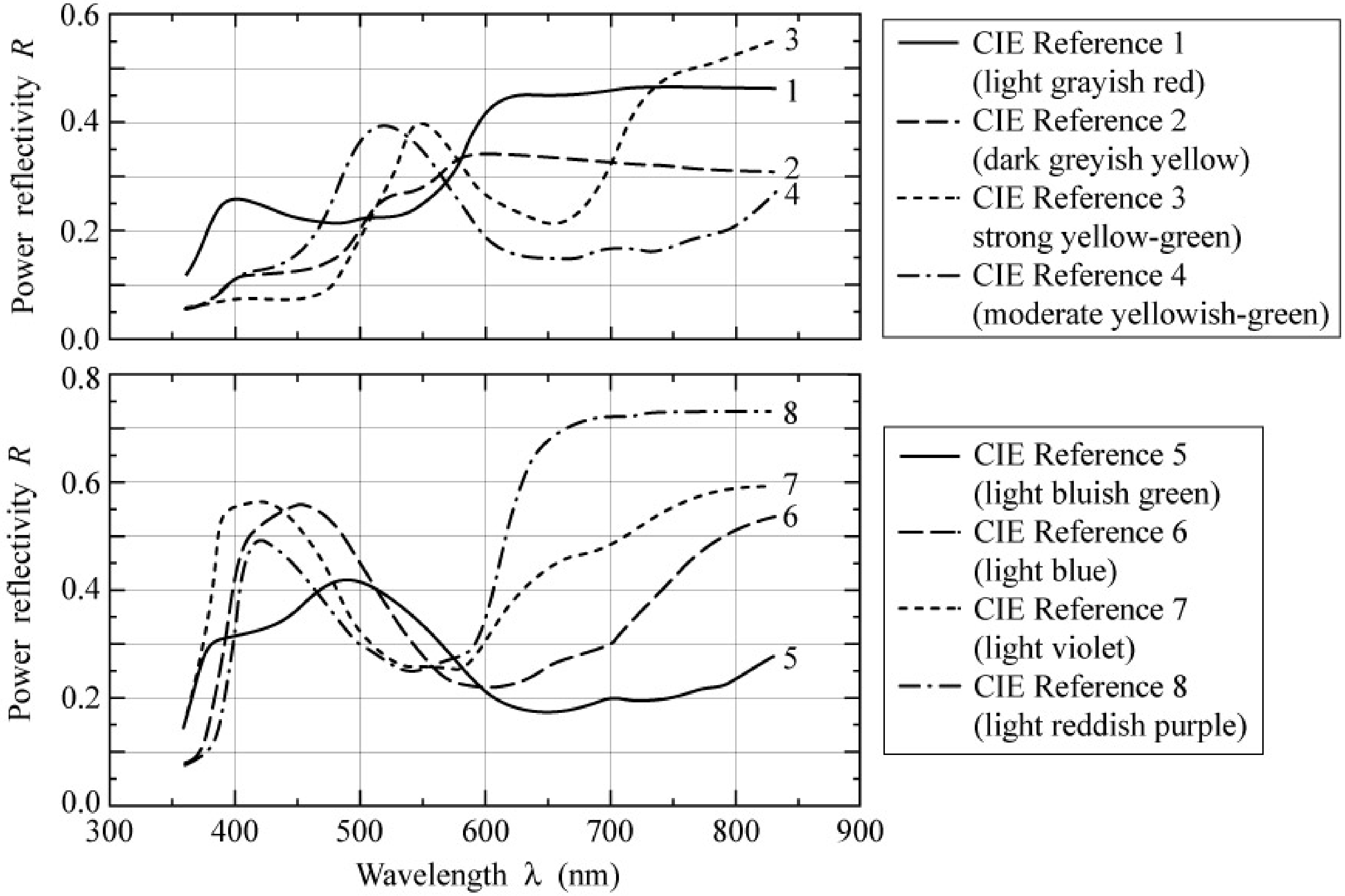

Fig. 11.10. Reflectivity curves of eight sample objects used for the calculation of the general color rendering index (CRI) of light sources used for illumination purposes (after CIE data, 1978).

Color rendering index (CRI)

The reference objects are illuminated with **reference light source**.
As a result, object will have a certain color.

The reference objects are then illuminated with **test light source**
As a result, object will have a certain, but different, color.

The CRI is a measure of the sum of the differences in color.

If color difference is zero, then $CRI = 100$

If color difference is > zero, then $CRI < 100$

Some applications require high and very high CRI. Examples ?

Some applications require low CRI. Examples ?

For some applications, CRI is irrelevant. Examples ?

Caution:
CRI depends on the selection of the reference light source.
Recommended for reference light source: Planckian radiator.

Light source	***Color rendering index***
Sunlight	100
Quartz halogen W filament light	100
W filament incandescent light	100
Fluorescent light	60 – 85
Phosphor-based white LEDs	60 – 85
Trichromatic white light LEDs	60 – 85
Hg vapor light coated with phosphor	50
Na vapor light	40
Hg vapor light	20
Dichromatic white light LEDs	10 – 40
Green monochromatic light	– 50

Table 11.1. Color rendering indices (CRI) of different light sources.

12

White-light LEDs

Generation of white light

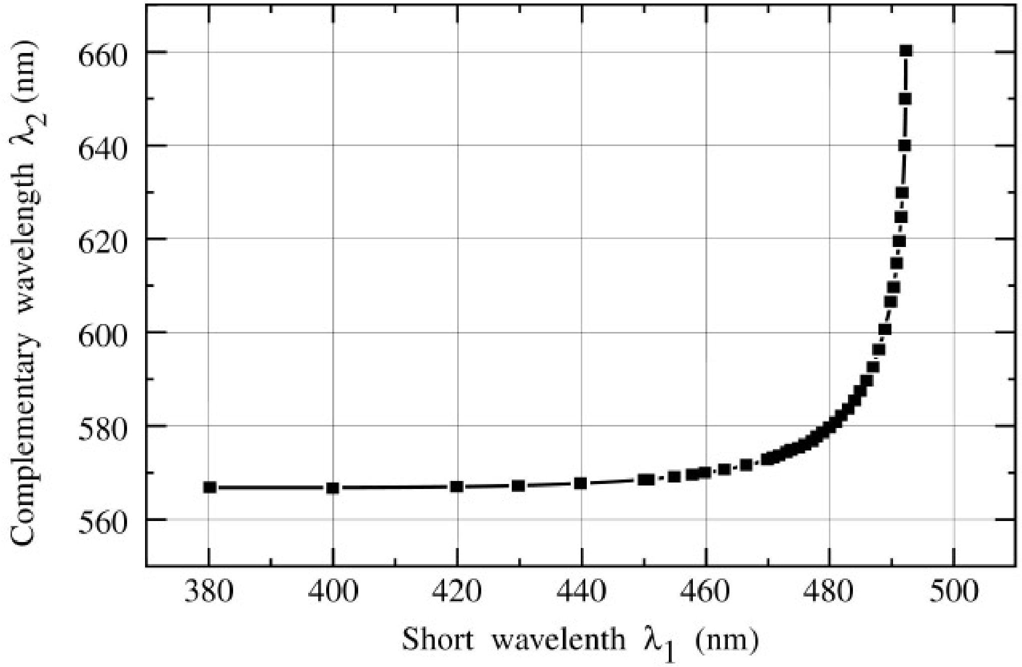

Fig. 12.1. Complementary wavelengths resulting in the perception of white light at a certain power ratio.

Dichromatic white light sources

The most efficient way to create white light is be a dichromatic white light source.

Luminous efficacy > 400 lm / W.

CRI is low.

Suitable for low-CRI sources.

Increasing the CRI is possible, however the luminous efficacy will decrease.

There is a fundamental trade-off between CRI and luminous efficacy.

Creation of white light

- Dichromatic.
- Trichromatic
- Blue source + converter
- UV source + converter

- What about luminous efficacy ?

- What about CRI ?

Converters

- There are different types of converters: Dyes, polymers, phosphors, and semiconductors.

Wavelength converter materials – phosphors

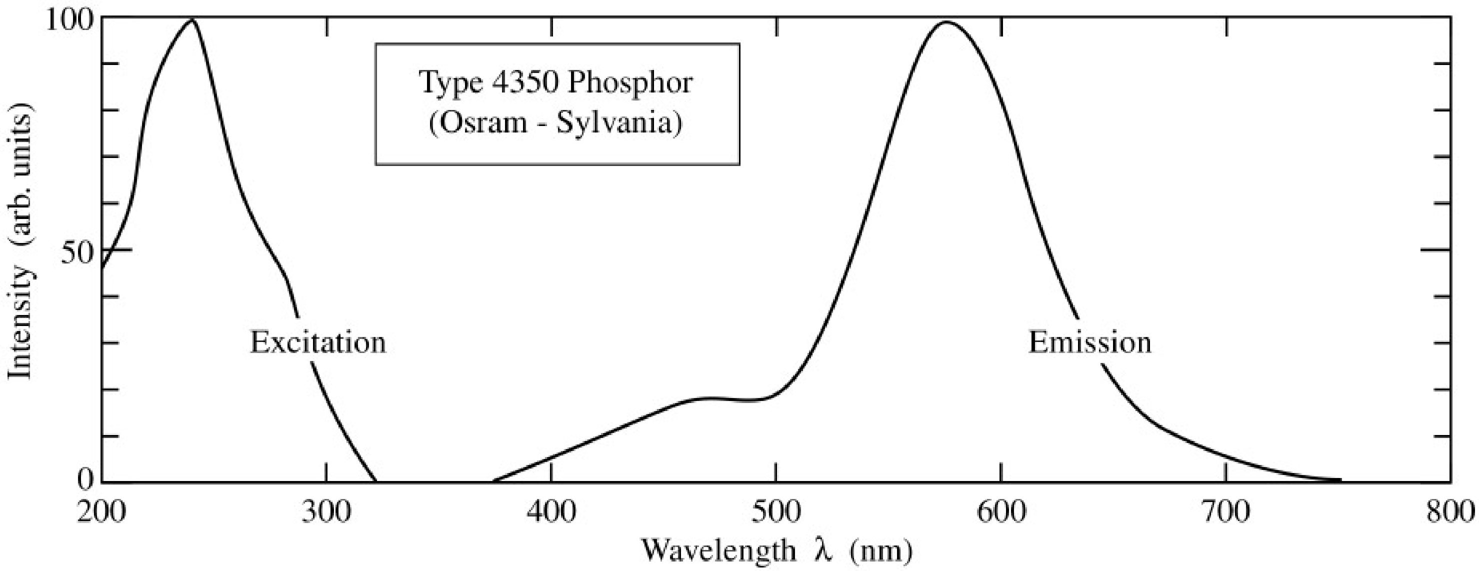

Fig. 12.2. Absorption and emission spectrum of a commercial phosphor (after Osram-Sylvania, 2000).

Wavelength converter materials – dyes

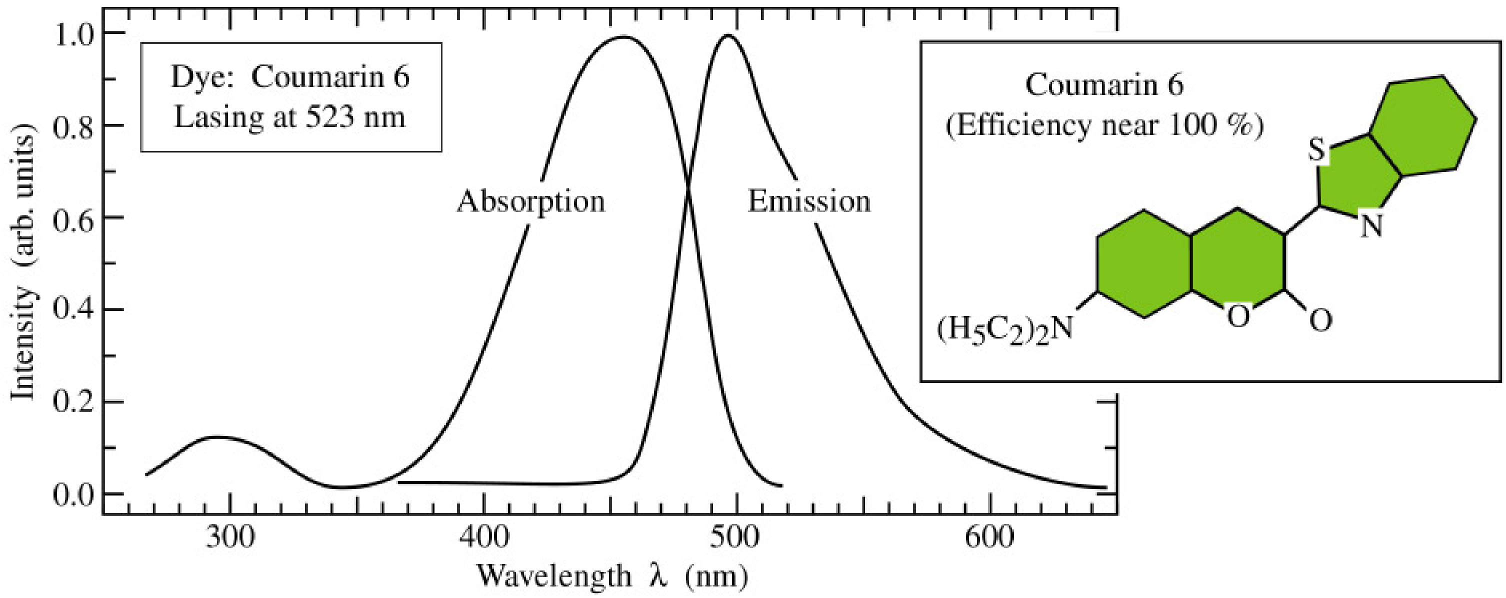

Fig. 12.3. Absorption and emission spectrum of the commercial dye "Coumarin 6". The inset shows the chemical structure of the dye molecule.

Wavelength converter materials – semiconductors

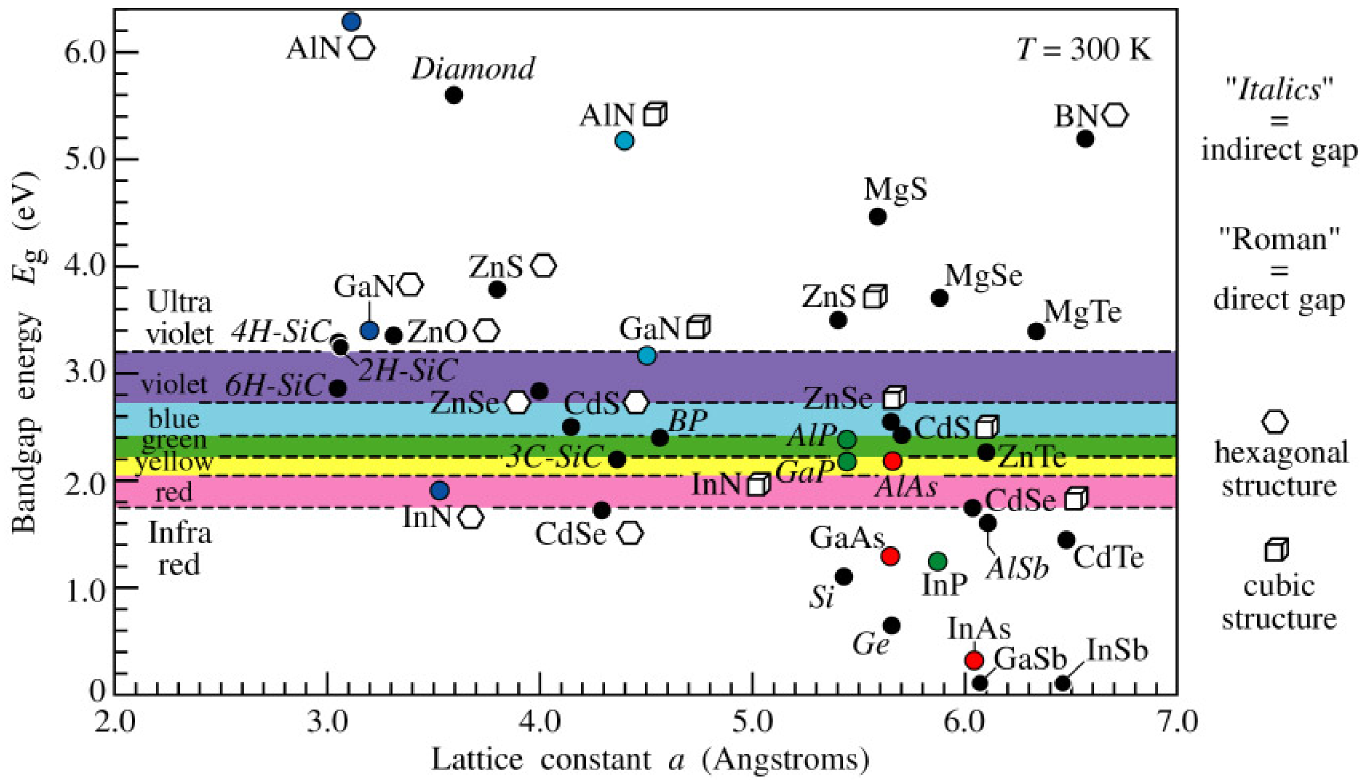

Fig. 12.4. Room-temperature bandgap energy versus lattice constant of common elemental and binary compound semiconductors.

White LEDs based on phosphor converters

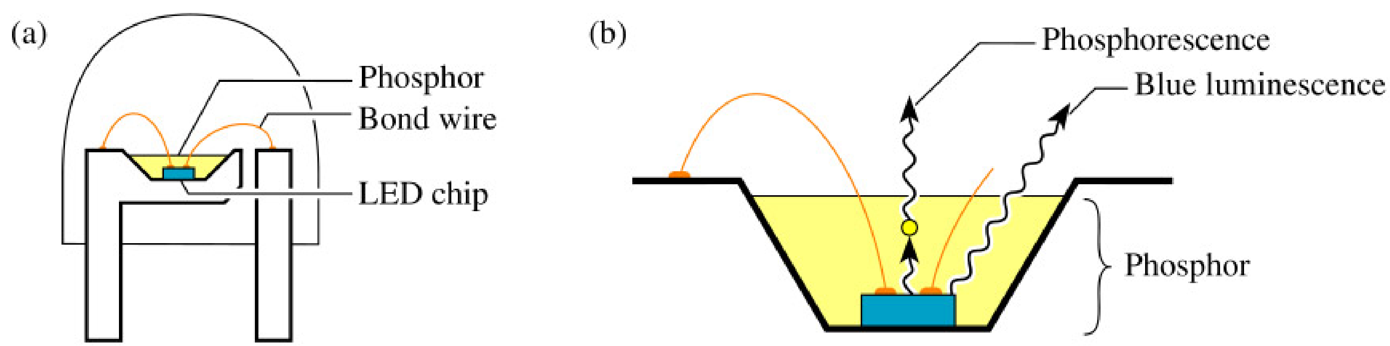

Fig. 12.5. (a) Structure of white LED consisting of a GaInN blue LED chip and a phosphor-containing epoxy encapsulating the semiconductor die. (b) Wavelength-converting phosphorescence and blue luminescence (after Nakamura and Fasol, 1997).

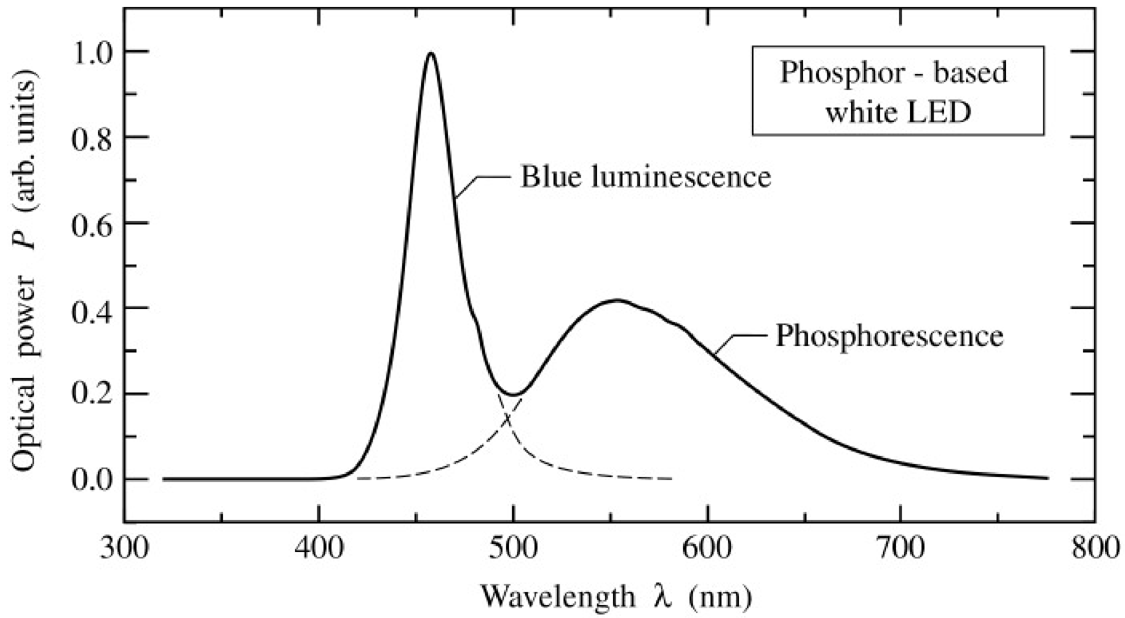

Fig. 12.6. Emission spectrum of a commercial phophor-based white LED manufactured by the Nichia Chemical Industries Corporation (Anan, Tokushima, Japan).

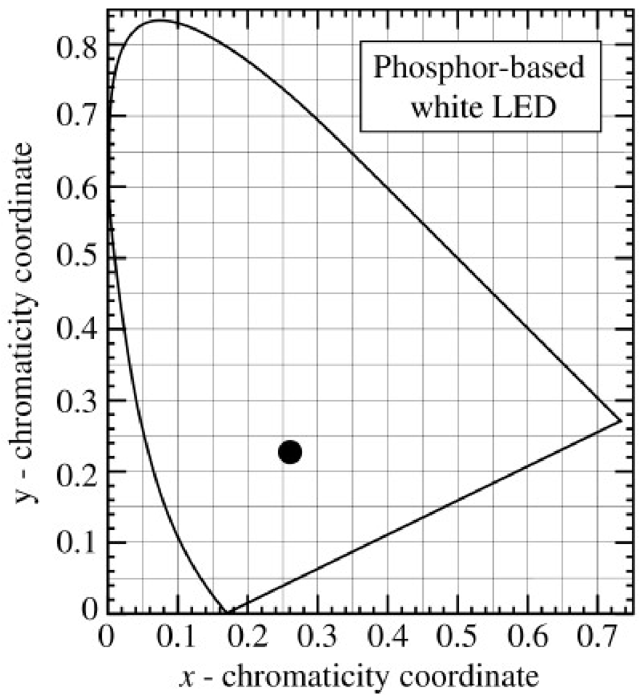

Fig. 12.7. Chromaticity coordinates of a commercial phophor-based white LED manufactured by the Nichia Chemical Industries Corporation (Anan, Tokushima, Japan).

White LEDs based on semiconductor converters (PRS-LED)

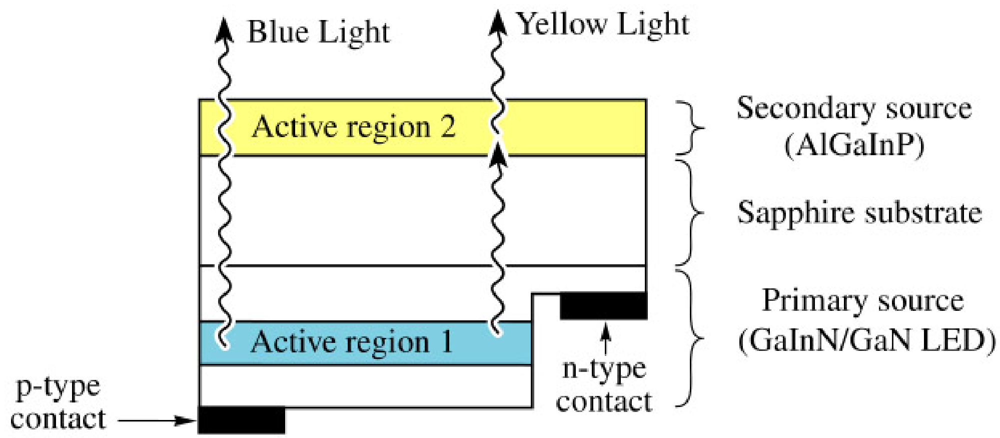

Fig. 12.8. Schematic structure of a photon-recycling semiconductor LED with one current-injected active region (Active region 1) and one optically excited active region (Active region 2) (after Guo *et al.*, 1999).

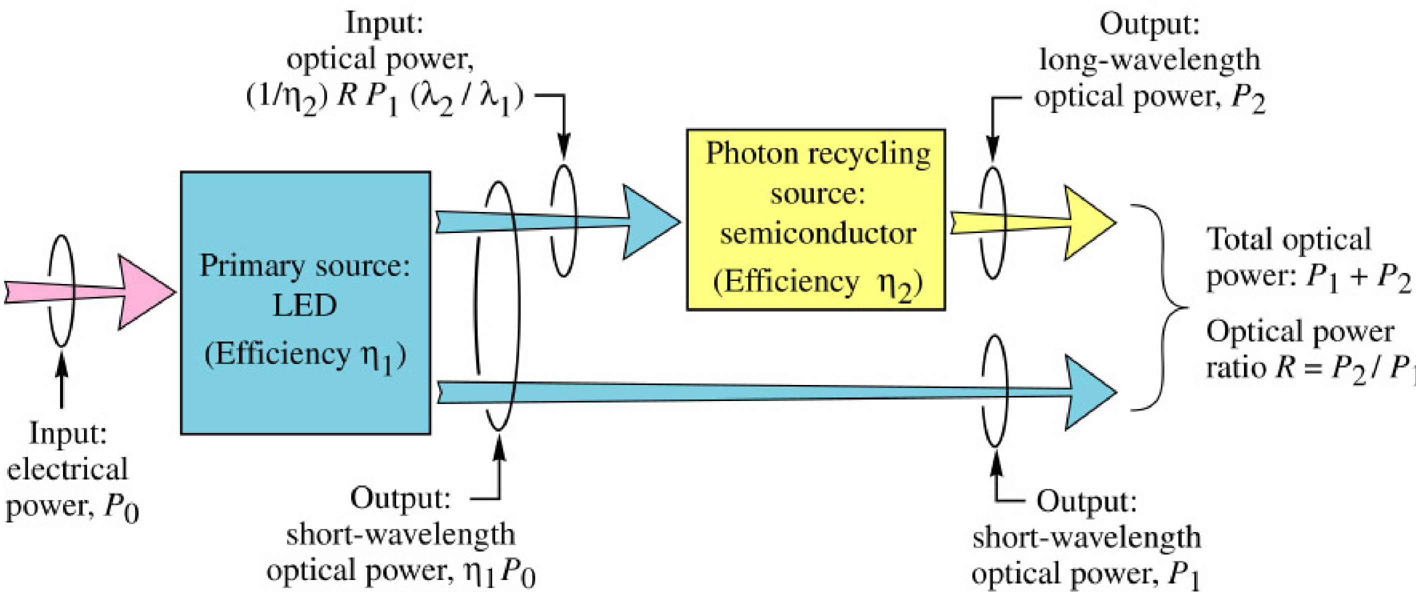

Fig. 12.9. Photon-recycling semiconductor LED power budget with electrical input power P_0 and optical output power P_1 and P_2.

Calculation of power ratio of PRS-LED

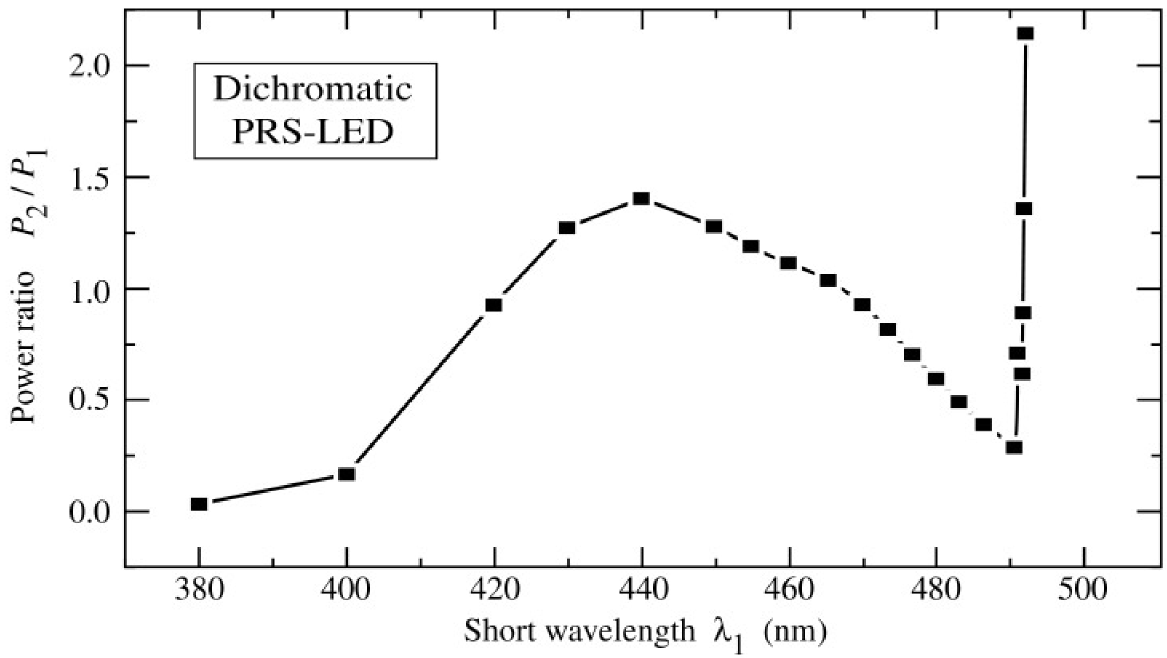

Fig. 12.10. Power ratio between the two optical output powers P_1 and P_2 required to obtain white light emission.

Calculation of luminous performance of PRS-LED

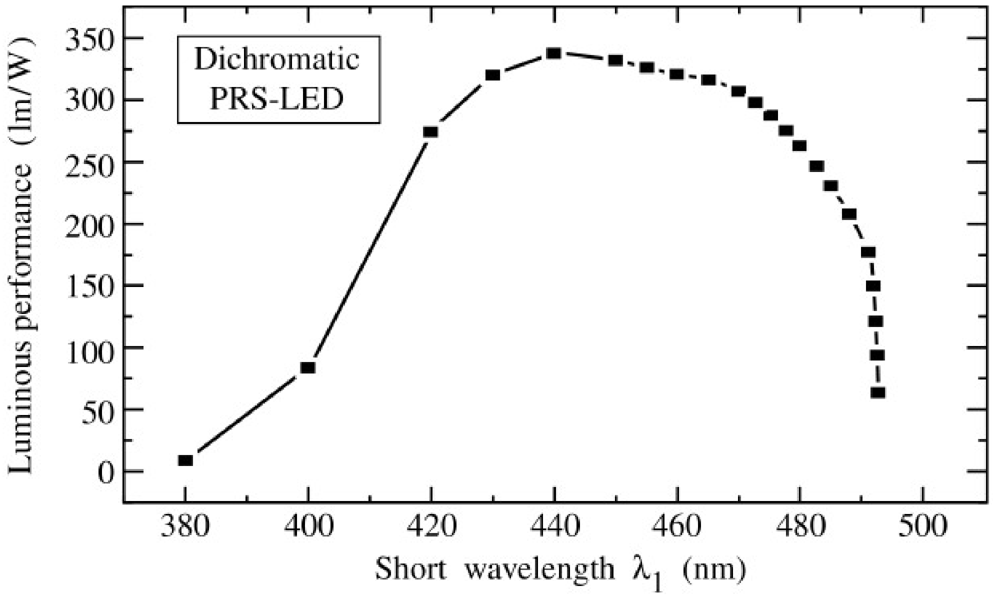

Fig. 12.11. Luminous performance of dichromatic PRS-LED versus the primary emission wavelength.

Spectrum of PRS-LED

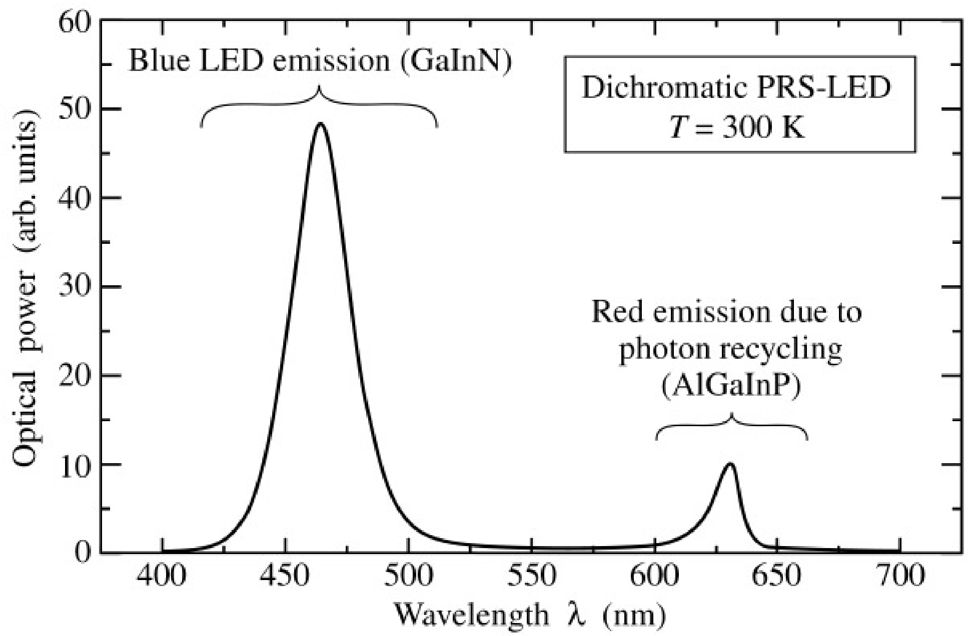

Fig. 12.12. Emission spectrum of dichromatic PRS-LED with current-injected GaInN blue LED primary source and AlGaInP photon recycling wafer (secondary source) emitting in the red.